Publication No. 02-155-243

REMOVAL OF MgO FROM PHOSPHATE PEBBLE BY FLOTATION: PHASE II

FINAL REPORT

Prepared by

UNIVERSITY OF FLORIDA
Gainesville, Florida

under a grant sponsored by

April 2006

The Florida Institute of Phosphate Research was created in 1978 by the Florida Legislature (Chapter 378.101, Florida Statutes) and empowered to conduct research supportive to the responsible development of the state's phosphate resources. The Institute has targeted areas of research responsibility. These are: reclamation alternatives in mining and processing, including wetlands reclamation, phosphogypsum storage areas and phosphatic clay containment areas; methods for more efficient, economical and environmentally balanced phosphate recovery and processing; disposal and utilization of phosphatic clay; and environmental effects involving the health and welfare of the people, including those effects related to radiation and water consumption.

FIPR is located in Polk County, in the heart of the Central Florida phosphate district. The Institute seeks to serve as an information center on phosphate-related topics and welcomes information requests made in person, or by mail, email, or telephone.

Florida Institute of Phosphate Research
1855 West Main Street
Bartow, Florida 33830
(863) 534-7160
Fax: (863) 534-7165
http://www.fipr.state.fl.us

REMOVAL OF MgO FROM PHOSPHATE PEBBLE BY FLOTATION: PHASE II

FINAL REPORT

Hassan El-Shall and Regis Stana
Principal Investigators

with

Ayman El-Midany

Department of Materials Science and Engineering
Engineering Research Center for Particle Science and Technology
UNIVERSITY OF FLORIDA
Gainesville, Florida

Prepared for

FLORIDA INSTITUTE OF PHOSPHATE RESEARCH
1855 West Main Street
Bartow, FL 33830 USA

Project Manager: Patrick Zhang
FIPR Contract Number 02-02-155

April 2006

DISCLAIMER

The contents of this report are reproduced herein as received from the contractor. The report may have been edited as to format in conformance with the FIPR *Style Manual*.

The opinions, findings and conclusions expressed herein are not necessarily those of the Florida Institute of Phosphate Research, nor does mention of company names or products constitute endorsement by the Florida Institute of Phosphate Research.

PERSPECTIVE

Patrick Zhang, Research Director - Beneficiation & Mining

With the depletion of the higher grade, easy-to-process Bone Valley deposits, the central Florida phosphate industry has moved into the lower grade, more dolomitic ore bodies from the Southern Extension. The phosphate deposits in the Southern Extension may be divided into two zones: an upper zone and a lower zone. The upper zone is readily amenable to current beneficiation practice, but the lower zone has a higher dolomite concentration and is difficult to process. Dolomite is generally concentrated in the pebble fraction, typically within the size range of 1 to 20 mm.

Under Phase I of this research (FIPR #00-02-145), it was demonstrated that when surfactant-coated dolomitic phosphate pebbles were immersed in a 3% sulfuric acid solution, effectively all the high MgO particles would float to the surface, leaving the phosphate rock phase that is low in MgO to sink. The best coating agent was found to be polyvinyl alcohol (PVA). The table below summarizes results from two encouraging tests.

Results from Two Phase I Lab Tests

Time	Size, mm		Wt%	Chemical Analysis			Recovery		
				MgO%	CaO%	P_2O_5%	MgO%	CaO%	P_2O_5%
30 min	-4+1.19	Float	16.75	13.62	24.25	0.76	77.84	13.55	0.8
		Sink	83.25	0.78	31.12	18.89	22.16	86.45	99.2
		Balance	100	2.93	29.97	15.73	100	100	100
		Feed	100	3.03	30.38	15.76	100	100	100
60 min	-4+1.19	Float	17.44	13.6	26.17	0.94	78	15.22	1.03
		Sink	82.56	0.81	30.8	19.06	22	84.78	98.97
		Balance	100	3.04	29.99	15.90	100	100	100
		Feed	100	3.03	30.38	15.76	100	100	100

These results justified the Phase II project, which tested different separation techniques and evaluated various parameters. The optimum process was determined to be crushing the rock to 1-2 mm, coating the rock with the PVA solution, treating the coated particles with dilute sulfuric acid, and then separating the apatite and dolomite in a sluice like device. Preliminary economic analysis appeared to be promising, with a chemical consumption cost of less than $2.15, an electrical cost of less than $1.00, and other operating costs of $2.50 per ton of feed. Those costs translate to a total cost of $8.10 per ton of product. However, the practicality of this approach remains to be determined based on larger-scale, continuous testing.

ABSTRACT

Phosphate rock as it is mined in Florida contains an increasing quantity of magnesium. The magnesium is present as discrete particles of dolomite (calcium magnesium carbonate). High magnesium adversely affects both the production of phosphoric acid (lowers phosphate recovery or production rate) and acts as a diluent in the final fertilizer products. Therefore, this study was initiated to investigate a novel reactive flotation (RF) technology to separate dolomite from dolomitic phosphate ores. Research results suggested that polyvinyl alcohol (PVA) could be used to coat phosphate rock containing a high concentration of magnesium. This coated rock was then placed in a 3% sulfuric acid solution where CO_2 was generated on the surface of the dolomite. The bubbles of gas remained attached to the dolomite and floated it to the surface. Typically the remaining rock contained over 90%of the phosphate and had an MgO concentration of less than 1%. Spray coating gave PVA consumptions as low as 1 pound per ton.

Several separation techniques were tested and a sluice like device was found to give the best separation results. The chemical consumption cost was estimated to be less than $2.15 per ton of feed with an electrical cost of less than $1.00 per ton of feed. Other operating costs, including depreciation, should add no more than $2.50 per ton of feed. With typically over 70% of the feed tons being recovered as product, this represents a product rock cost of $8.10/ton. This is comparable to current typical flotation costs (to recover less than 1 mm size phosphate particles) of >$10.00/ton of product. Nevertheless, more work is still needed to optimize this separation process and to further evaluate its economics.

ACKNOWLEDGMENTS

The authors wish to express their appreciation to IMC Phosphates and Cargill for providing the high magnesium phosphate rock sample used in this study. The authors also wish to express their appreciation to Jacobs Engineering of Lakeland for the use of their screw-dewatering device for some of the test work.

TABLE OF CONTENTS

PERSPECTIVE iii

ABSTRACT v

ACKNOWLEDGMENTS vi

EXECUTIVE SUMMARY 1
INTRODUCTION 3
EXPERIMENTAL PLANS/PROCEDURES 7

Optimization Flotation Studies 7

Central Composite Design 8
Flotation Procedures for Screening and Central Composite Designs 9
Factorial Design for Conditioning (Coating) with PVA Before Flotation 9
Flotation Procedure for Conditioning (Coating) Statistical Designs 10
Chemical Analysis 10
Density and Surface Area Determination 11
PVA Preparation 11
Spectrophotometric Determination of PVA 12
Static (Equilibrium Surface Tension) 12
Dynamic Surface Tension (DST) 12
Dynamic Surface Tension Setup 13
Contact Angle 14
Measurement of Contact Angle 15
Surface Characterization by FTIR 15
Zeta Potential Measurements 15
Adsorption 16
Adsorption Kinetics 16

Pilot Scale Experiments 16

Size Reduction 16
Coulter Size Analyzer 17

Separation Devices 17

Spiral Concentrator 17
Shaking Table 18
Floatex - Density Separator 19
The Sluice 20

TABLE OF CONTENTS (CONT.)

Sluice Experimental Procedure 21
Dissolution Kinetic Experiments 21

Experimental Results 22

Screening Statistical Design 22
Central Composite Design 26
Efforts to Reduce the PVA Consumption 28
Experimental Design of the PVA Conditioning (Coating) Step 29
Saturation Experiment 31
Pilot Scale Testing 31
Tests Using Pond Water 33
Screw Classifier 34

Adsorption Mechanisms 34

Work of Adhesion 35
Surface Tension 36
Contact Angle 38
Work of Adhesion 39
Adsorption Study 40
Specific Surface Area Measurements (BET Method) 41
Pore Size Distribution 41
Zeta Potential 42
Zeta Potential of Minerals in Supernatant Solutions 45
Zeta Potential in the Presence of PVA 46
Infrared (FTIR) 48
Kinetics of Adsorption 50
Adsorption Isotherm 52
Calculation of PVA Adsorption and Parking Area 55
Adsorbed Layer Thickness 56
Factors Affecting Adsorption 57
Effects of pH 57
Effects of pH on Apatite 58
Effects of pH on Dolomite 58
Desorption 58
Desorption in Acidic Solution 60
Adsorption in Supernatants 60
Reactive Flotation Kinetics 60
Chemical Analysis of Samples Used in the Kinetic Study 62
Effect of the Particle Size 62
Formation of an Insulating Layer 63
Effect of PVA Coating 63

TABLE OF CONTENTS (CONT.)

Bubble Formation and Growth 64
Modeling of Bubble Formation and Dolomite-Particle Separation 65
Blockage of the Acid Model 65
Disappearance of Active Sites Model 68
Estimation of CO_2 Required to Float the Dolomite Particles 70
Change in Density 71
Dynamic Surface Tension 73

Process Economics 75

CONCLUSIONS 77
REFERENCES 79
FOR ADDITIONAL READING 87

LIST OF FIGURES

Figure **Page**

1. Schematic of Five-Level, Rotatable Central Composite Design 8
2. Characteristic Bubble Pressure Versus Time Curve in MBP to Determine Dynamic Surface Tension....13
3. Setup for the Measurement of Dynamic Surface Tension by Means of the Maximum Bubble Pressure Method 14
4. Contact Angle and Its Relationship with Surface Tension 14
5. Contact Angle Measuring Apparatus....15
6. Disc Pulverizer....17
7. Spiral Concentrator 18
8. Shaking Table and Schematic of Its Principle of Particle Separation 19
9. Floatex – Density Separator....20
10. Schematic Diagram for the Separation of Dolomite from Phosphate in a Sluice....21

11a. Contour Plot for Different Factors Affecting RF....22
11b. Contour Plot for Different Factors Affecting RF....23
12a. Contour Plot for the Effects of Different Factors on MgO % in Concentrate 24
12b. Contour Plot for the Effects of Different Factors on MgO % in Concentrate 25
13a. Effect of PVA Dosage and Acid Concentration on MgO Recovery % in Floated Fraction at Different Particle Size....26
13b. Effect of PVA Dosage and Acid Concentration on MgO Recovery % in Floated Fraction at Different Particle Sizes....27
14a. Effect of PVA Dosage and Acid Concentration on MgO % in Unfloated Fraction at Different Particle Sizes....27
14b. Effect of PVA Dosage and Acid Concentration on MgO % in Unfloated Fraction at Different Particle Sizes....28

15. Cube Graph for MgO % and MgO Recovery %....30
16. Screw Dewatering Device....34
17. Contact Angle and Interfacial Surface Tension at Solid/Liquid/Gas Interface 36
18. Structural Formula for PVA: (A) Partially Hydrolyzed; (B) Fully Hydrolyzed....37
19. Equilibrium Surface Tension for Aqueous PVA Solutions at 23° C....37
20. PVA Crystal Structure; the Dotted Lines Indicate Hydrogen Bonds 38
21. Static Contact Angle Variation with the PVA Concentration 39
22. Work of Adhesion as a Function of PVA Concentration on Dolomite and Apatite Substrates 40
23. Cumulative Pore Size Distribution for Apatite Sample....41
24. Cumulative Pore Size Distribution for Dolomite Sample....42
25. Zeta Potential of Dolomite and Apatite Samples....43
26. Zeta Potential of Dolomite in Absence and Presence of Polymer....43
27. Zeta Potential of Dolomite in Absence and Presence of Polymer....44

LIST OF FIGURES (CONT.)

Figure **Page**

28. Effect of Polymer on the Shear Plane Position (a) Without Polymer, (b) After Polymer Adsorption....44
29. Zeta Potential of Apatite and Apatite in Dolomite Supernatant....45
30. Zeta Potential of Dolomite and Dolomite in Apatite Supernatant....46
31. Zeta Potential of Dolomite in Apatite Supernatant Before and After PVA Adsorption....47
32. Zeta Potential of Apatite in Dolomite Supernatant Before and After PVA Adsorption....47
33. Infrared Spectra (FTIR) of Polyvinyl Alcohol (PVA)....48
34. Infrared Spectra (FTIR) of (a) Dolomite Alone, and (b) Dolomite/PVA System....49
35. Infrared Spectra (FTIR) of (a) Apatite Alone, and (b) Apatite/PVA System....50
36. Kinetics of PVA Adsorption on Dolomite and Apatite (Initial PVA Concentration 6.7×10^{-7} M, pH 7, 2×10^{-3} M KNO_3 and 23° C)....52
37. Adsorption Isotherm of PVA on Dolomite at 23° C....54
38. Adsorption Isotherm of PVA on Apatite at 23° C....54
39. Polymer Conformation Change with Increasing Concentration: (a) Conformation of a Single Molecule; (b) Conformation of More than One Molecule....56
40. Effect of pH on Adsorption of PVA on Apatite and Dolomite....57
41. Desorption of PVA from the Apatite Surface....59
42. Desorption of PVA from the Dolomite Surface....59
43. Adsorption Isotherm of Apatite in Dolomite Supernatant Solution, and Dolomite in Apatite Supernatant Solution....60
44. Bubble Formation Mechanism....61
45. Schematic Diagram of Reaction Kinetics of the RF Process....61
46. Dissolution Kinetics of Different Particle Sizes in Terms of Calcium Ions in a 3% Sulfuric Acid Solution at 23° C....62
47. Dissolution Kinetics of Different Particle Sizes in Terms of Magnesium Ions in 3% Sulfuric Acid Solution at 23° C....63
48. Dissolution Kinetics of Coated and Uncoated 0.2-0.3 mm Dolomite Particles in a 3% Sulfuric Acid Solution at 23° C....64
49. Growth of Bubbles with Time on the Dolomite Particle Surface (50 X)....65
50. Acid Blockage Model Fitting to 1-2 mm Experimental Data....67
51. Acid Blockage Model Fitting to 0.25-0.35 mm Experimental Data....67
52. Active Sites Disappearance Model Fitting to 1-2 mm Data....69
53. Active Sites Disappearance Model Fitting to 0.25-0.35 mm Data....69
54. Sequence of Calculating the Particle Density and Membrane Elasticity....72
55. Density Changes for Different Particle Sizes....73

LIST OF FIGURES (CONT.)

Figure **Page**

56. Dynamic Surface Tension of PVA Concentration at Different CO_2 Flow Rates 74
57. Elasticity of PVA Membrane in Terms of PVA Concentration at Different CO_2 Flow Rates 75

LIST OF TABLES

Figure **Page**

1. First Example of Rock Quality from Hand Separation....3
2. Second Example of Rock Quality from Hand Separation 4
3. Experimental Plackett-Burman Design for 11 Variables....7
4. Plackett-Burman Variables Used in the Reactive Flotation Study 8
5. Levels of Various Variables Used in the Central Composite Design....9
6. Rotatable Central Composite Design with Five Levels and Three Variables 9
7. Factorial Design for Conditioning (Coating) with PVA....10
8. Variable Levels Used for Conditioning (Coating) with PVA....10
9. Wave Lengths Used for ICP Analysis 11
10. Average Molecular Weight and Degree of Hydrolysis of PVA Samples....11
11. Comparison of Two Different Coating Methods and Their Effects on MgO Removal Using Sluice as a Separation Device 30
12. Effect of Saturated Acid on the Reactive Flotation (RF)....31
13. Analysis of Floated Fractions Using Different Separation Devices 31
14. Separation Results of -16+200 Mesh Size Fraction....32
15. Separation Results of -35+200 Mesh Size Fraction....32
16. Separation Results of -2+1mm Fraction 33
17. Separation Results of -16+200 Mesh Size Fraction....33
18. Separation Results of -35+200 Mesh Size Fraction....33
19. Chemical Analysis of the Samples Used in Adsorption Tests....40
20. Fitting Parameters of 2nd Order Kinetic Model 51
21. Chemical Analysis of the Samples Used in Kinetic Tests....62
22. Acid-Blockage Model Parameters 68
23. Active Sites Disappearance Parameters....70

EXECUTIVE SUMMARY

Separation of dolomitic limestone impurities from apatite has become increasingly important especially with the depletion of current high-grade phosphate deposits. Phosphoric acid production from phosphate rock dictates that the phosphate feed to the chemical plants contain no more than 1% MgO, and generally the MgO must be below 0.6% to produce on grade DAP.

The presence of higher MgO content in the phosphate rock is reported to increase the viscosity of the phosphoric acid, resulting in higher pumping cost, lower filtration rates, increased phosphate losses, and reduction in the nutrient concentration in fertilizer products. Since the MgO source is mostly dolomite (mixture of calcium and magnesium carbonate), it also increases the gypsum generation rate per ton of P_2O_5.

Most of MgO exists as liberated dolomite particles and is amenable to removal by physical separation processes. Several attempts in the past have been made to remove dolomite from apatite, however, none of these processes produces a phosphate rock with less than 1% MgO on a commercial scale.

While there are several processes under investigation that do a better job of removing the magnesium, they require grinding of the pebble size rock (which contains the bulk of the dolomite) to a fine degree and generally require several unit operations.

It is well known that the dolomite particles generate CO_2 when exposed to acid solution. If the generated CO_2 is contained around the particle by the use of a good surfactant or coating agent, then (as demonstrated in FIPR Research Project 00-02-145) the dolomite will be selectively floated and separated from the phosphate rock. While this may not be possible with large size pebbles, it will work with the smaller sized pebble as well as with crushed (not ground) oversized pebbles.

For this product to be used commercially, a process must be developed to achieve the separation in an economical manner. The purpose of this study was to further define the process to determine the economics. Multiple tests were conducted to optimize the process with respect to coating concentration, coating molecular weight, coating method, drying time, flotation acid concentration, rock size etc. as well as separation equipment type. Other tests were conducted to determine the mechanism of preferential PVA attachment to the dolomite.

The tests demonstrated that a PVA consumption of 1 pound per ton could be achieved when using a spray coating technique, the acid solution could be used for flotation even after saturation with calcium, and the PVA remaining on the treated rock would not have any adverse effect on the reactivity of the rock in the phosphoric acid reactor.

A sluice or sluice like device was found to be more effective in making the separation than a spiral concentrator, shaker table or Floatex density separator.

The optimum process was determined to be crushing the rock to 1-2 mm, spray coating the rock with the PVA solution, and then separating the apatite and dolomite in a sluice like device. The chemical consumption cost was estimated to be less than $2.15 per ton of feed with an electrical cost of less than $1.00 per ton of feed. Other operating costs, including depreciation, should add no more than $2.50 per ton of feed. With typically over 70% of the feed tons being recovered as product, this represents a product rock cost of $8.10/ton. This compares to current typical flotation costs (to recover less than 1 mm size phosphate particles) of >$10.00/ton of product.

INTRODUCTION

As phosphate-mining operations continue to move south in Central Florida, there is an increase in the MgO content of the rock. This MgO increases the difficulty in processing the rock (lowers the P_2O_5 recovery) and makes it difficult to make DAP grade. In fact, much of the higher MgO rock is simply left in the ground, as there is no economical method for removing it from the rock. At present, the only method ever commercialized, heavy media separation, is sitting idle due at least partially to its relatively high operating cost and poor performance. The heavy media product typically contained 1% or above of MgO and less than half the BPL tons. The high MgO rock is now either discarded or blended off with lower MgO rock. The separation coefficient (phosphate in sink/phosphate in float times MgO in sink/MgO in float) is estimated to be about 4 for this process.

Over the years, FIPR and the industry have looked at a number of methods for removal of the MgO. They include selective flotation, flocculation, grinding and screening, and partial acidification (Jacobs 1995; Laird 1997; El-Shall 1994; Smith and others 1997). All flotation methods required that the rock be first ground to concentrate size material prior to the flotation. While some of these have shown promise in the laboratory, none have been commercialized to date, generally due to either a complex flow sheet, poor economics or low BPL recovery. The most promising process evaluated to date is the CLDRI process. Its separation coefficient is about 20.

In general, when high MgO is encountered in the phosphate matrix, most of it is contained in the pebble fraction and the -150 mesh fraction (Hanna and Anazia 1990). The concentrate fraction typically contains less than 1% MgO, even if the pebble contains over 5% MgO. In addition, the MgO is contained mostly in granules of dolomite. Very little of the MgO is contained in the particles of apatite rock.

In fact the particles of dolomite and apatite rock can be separated by hand, simply based on the color and texture of the particles. From a presentation made at the 1997 phosphate conference (Stana 1997), the data in Tables 1 and 2 were presented.

Table 1. First Example of Rock Quality from Hand Separation.

	Initial Rock	Rock Fraction	Dolomite Fraction	% in Rock
BPL	55.65	66.92	49.16	49.8
Al_2O_3	0.69	0.70	0.68	42.9
Fe_2O_3	0.67	0.51	0.78	32.3
MgO	4.05	0.46	6.67	4.8
CaO/P_2O_5	1.80	1.49	2.03	
Wt%		37.7	62.3	

Table 2. Second Example of Rock Quality from Hand Separation.

	Initial Rock	Rock Fraction	Dolomitic Fraction	% in Rock
BPL	50.15	68.91	36.46	58.0
Al_2O_3	0.91	0.82	0.98	37.9
Fe_2O_3	0.93	0.59	1.17	26.9
MgO	5.06	0.52	8.37	4.3
CaO/P_2O_5	1.95	1.49	2.28	
Wt%		33.9	66.1	

This clearly demonstrates that it is possible to physically separate the high MgO rock into a fraction that contains an acceptable quantity of MgO and as much as half the phosphate of the initial rock.

Separation of dolomitic limestone impurities from apatite has become increasingly important especially with the depletion of current high-grade phosphate deposits. Phosphoric acid production from phosphate rock dictates that the phosphate fed to the chemical plants contain no more than 1% MgO, and generally the MgO must be below 0.6% to produce on grade DAP.

The presence of higher MgO content is reported to increase the viscosity of the phosphoric acid, resulting in higher pumping cost, lower filtration rates, increase phosphate losses, and also the reduction in the nutrient concentration in fertilizer products. Since the MgO source is mostly dolomite (mixture of calcium and magnesium carbonate), it also increases the sulfuric acid consumption and the gypsum generation rate per ton of P_2O_5. It is well known that the dolomite particles generate CO_2 when exposed to acid solution. If the generated CO_2 is contained around the particle by the use of a good surfactant or coating agent, then the dolomite will be selectively floated and separated from the phosphate rock. While this may not be possible with large size pebbles, it should work with the smaller sized pebble and the crushed (not ground) oversized pebble.

This technique for separation was explored in a previous FIPR funded project (FIPR Project Number 00-02-145). The major objectives of that project were to conduct a bench scale investigation to develop a new process for the removal of MgO from phosphate pebble without grinding the pebble. The new methodology separated the dolomite from phosphate pebble by flotation through the use of a surfactant to capture the gas generated by the reaction of the dolomite with acid. The investigation included:

(1) Testing different types of surfactants (anionic, cationic, non-ionic, and polymers)
(2) Testing different acid types (sulfuric, nitric, hydrochloric, and acetic acids)
(3) Testing different acid concentrations
(4) Establishing a procedure for such flotation tests
(5) Determining the phosphate rock particle size suitable for flotation

(6) Investigating the effect of operating variables
(7) Testing the flotation of dolomite using pond water
(8) Testing the flotation of dolomite under dynamic conditions

In the study, preliminary tests were conducted to test different surfactant types and dosages, different acid type and concentration, and different particle sizes. Initial tests were conducted in beakers using discrete dolomite particles dipped or coated with a surfactant or surfactant system. Observations were then made as to the rate and adherence of generated gas to the particles, the time required to float the particle to the surface and the long-term stability of the floated particles.

In the initial screening tests, conducted with a variety of surfactants, it was observed that the performance of anionic surfactants were better than non-ionic surfactants The non-ionic surfactants were better than cationic surfactants. Cationic surfactants were essentially ineffective. However, even the best performing anionic surfactants could not float particles above 4 mm in size or keep the floated particles at the surface for more than a few minutes.

After additional tests with a wide variety of coating agents and coating systems, polyvinyl alcohol was found to be the most effective. While it did require a higher acid concentration (3% sulfuric) to work effectively, it could float particles up to 8 mm in size and maintain the floated particles at the surface for very long periods of time.

Tests were also conducted with various screen fractions of a high MgO pebble rock. The batch tests were conducted in a 5-gallon bucket and the floated material removed from the top of the bucket after time periods up to 24 hrs. The floated fractions contained 11-16% MgO and 3-5% P_2O_5, the fraction that did not float contained less than 1.5% MgO and over 20% P_2O_5. While these tests did demonstrate a separation coefficient (phosphate in sink/phosphate in float times MgO in sink/MgO in float) in excess of 50, the non-floating fraction contained a lower quantity of phosphate than expected. Further analytical tests were conducted with the non-floated rock that had been in contact with the 3% sulfuric acid for 24 hrs and it was found that it contained a significant quantity of gypsum. After correcting for the dilution effect of the gypsum, the non-floated rock contained 62-65 BPL which is consistent with rock containing 1.2-1.7% MgO.

Based on encouraging results obtained in FIPR Project Number 00-02-145, a Phase II proposal was submitted to further develop this process. The proposal was funded and this two-year project was started in May 2003. The overall goal of this project was to develop a continuous reactive flotation (RF) process for making the separation and determine the economics of the process.

EXPERIMENTAL PLANS/PROCEDURES

OPTIMIZATION FLOTATION STUDIES

In this study, screening and central composite statistical experimental designs were used to determine the effect of various factors on the removal of MgO and its recovery. The Plackett-Burman design was used to screen out which of the seven factors being considered were the most statistically significant. This design is a tool that helps determine which factors made the greatest impact on the MgO removal. A central composite design was used to determine if there were any interactions between the three most significant factors determined from the Plackett-Burman design.

The variables examined in the screening stage were acid concentration (1% and 3%), polyvinyl alcohol (PVA) concentration in the coating solution (1% and 3%), the PVA molecular weight (60,000 and 150,000), the degree of hydrolysis (88%-99%) of the PVA, particle size (-0.5 mm and 5-9 mm), and drying time of the coating (0 and 2 hrs). The levels were chosen according to the exploratory test results from Phase I of this project. The Plackett-Burman design used for this study had 11 factors and 12 experimental runs (Tables 3 and 4). MgO percentage was determined using chemical analysis. Chemical analyses were performed using wet chemical methods, acid attack (digestion) method as described later.

Table 3. Experimental Plackett-Burman Design for 11 Variables.

Run No.	Variable Levels										
	1	2	3	4	5	6	7	8	9	10	11
1	-	-	+	+	+	-	+	+	-	+	-
2	+	-	+	-	-	-	+	+	+	-	+
3	-	-	-	-	-	-	-	-	-	-	-
4	+	+	+	-	+	+	-	+	-	-	-
5	+	-	+	+	-	+	-	-	-	+	+
6	+	-	-	-	+	+	+	-	+	+	-
7	+	+	-	+	-	-	-	+	+	+	-
8	+	+	-	+	+	-	+	-	-	-	+
9	-	+	+	+	-	+	+	-	+	-	-
10	-	-	-	+	+	+	-	+	+	-	+
11	-	+	-	-	-	+	+	+	-	+	+
12	-	+	+	-	+	-	-	-	+	+	+

Table 4. Plackett-Burman Variables Used in the Reactive Flotation Study.

Variables	Low Level (-)	High Level (+)
Acid concentration	1%	3%
PVA concentration	1%	3%
Dummy*		
Dummy		
PVA M.W.	60,000	150,000
Degree of hydrolysis	88%	99%
Time of drying	0	2 Hrs.
Dummy		
Particle size	-0.5 mm	5-9 mm
Dummy		
Dummy		

*Dummy variables are used to calculate the variance of the experimental runs.

Central Composite Design

A central composite design (CCD) was used to further investigate the three most significant factors (acid concentration, PVA concentration, and particle size) determined from the screening design. Five levels were used. The central composite experimental design having 17 experimental runs is illustrated in Figure 1 and in Tables 5 and 6. For each run, the products were chemically analyzed as mentioned above and the MgO percentage and MgO removal recovery were calculated for all the experimental runs. The computer program, Design expert® (SAS Institute, Inc.), was used to perform the statistical analysis for the central composite design. The data was analyzed by fitting the response variables to a second order polynomial model.

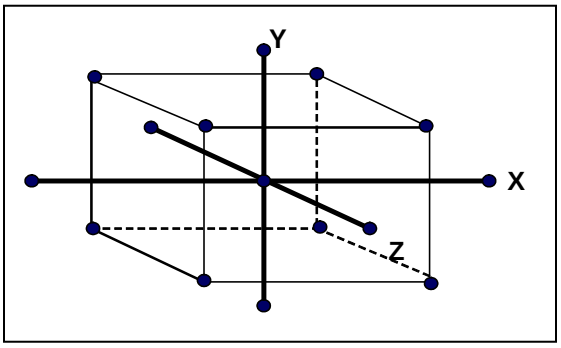

Note: The X, Y, and Z axes represent the 3 variables: sulfuric acid concentration, PVA concentration, and particle size. The circles represent each experimental run.

Figure 1. Schematic of Five-Level, Rotatable Central Composite Design.

Table 5. Levels of Various Variables Used in the Central Composite Design.

Variables	-1.68	-1	0	+1	+1.68
Acid conc. (%)	0.32	1	2	3	3.68
3% PVA, ml (lb/t)	0.1(0.6)	0.3 (2)	0.6(4)	0.9(6)	1.1(6.6)
Particle size, mm	-0.5	0.5-1	1-2	2-5	5-9

Flotation Procedures for Screening and Central Composite Designs

Using 300 ml of 3% H_2SO_4 in a 400 ml beaker, particles were pre-coated by spraying 3% PVA solution (using a mist delivery nozzle) then added to the acidic solution. The experiment was left for five minutes. Dolomite floated to the surface, which was separated by decantation on a screen. The products (floated and unfloated fractions) were dried, weighed, and chemically analyzed.

Table 6. Rotatable Central Composite Design with Five Levels and Three Variables.

Run No.	Acid Conc.	PVA %	Particle Size
1	-1	-1	-1
2	-1	-1	+1
3	-1	+1	-1
4	-1	+1	+1
5	+1	-1	-1
6	+1	-1	+1
7	+1	+1	-1
8	+1	+1	+1
9	-1.68	0	0
10	+1.68	0	0
11	0	-1.68	0
12	0	+1.68	0
13	0	0	-1.68
14	0	0	+1.68
15	0	0	0
16	0	0	0
17	0	0	0

Factorial Design for Conditioning (Coating) with PVA Before Flotation

This design was used to study the factors affecting the conditioning (coating) step with PVA, which is a promising step for reducing PVA consumption. Tables 7 and 8 show the design and levels used.

Table 7. Factorial Design for Conditioning (Coating) with PVA.

Run No.	PVA Concentration (%)	Pulp Density (S/L Ratio)	Conditioning Time (min)
1	-1	-1	-1
2	-1	-1	+1
3	-1	+1	-1
4	-1	+1	+1
5	+1	-1	-1
6	+1	-1	+1
7	+1	+1	-1
8	+1	+1	+1
9	0	0	0
10	0	0	0
11	0	0	0

Table 8. Variable Levels Used for Conditioning (Coating) with PVA.

Variables	-1	0	+1
PVA concentration (%)	0.25	0.625	1
Pulp density	30%	50%	70%
Conditioning time (min)	2	11	20

Flotation Procedure for Conditioning (Coating) Statistical Designs

Fifty gm of ore were added to 1% PVA solution in a 600 ml beaker according to a specific solid/liquid ratio. The slurry was mixed for the required time at 300 rpm (using a 2.5 cm magnetic bar). After the conditioning time elapsed, the solids were screened. The solids were then used for flotation in acidic solution and the filtrate solution was collected for PVA analysis to determine the PVA residual concentration.

Chemical Analysis

About 0.5 gm of the dried and ground representative sample were digested in 50 ml of aqua regia by boiling on a hotplate until the reaction was complete. After cooling, this solution was filtered through a Whatman 42 filter paper into 1000 ml volumetric flask. The filter paper and residue were then washed at least five times to remove all the traces of dissolved salts and acid.

The filtrate was diluted with distilled water and thoroughly mixed and the concentrations were measured using an Inductively Coupled Plasma (ICP) emission spectrometer (Perkin Elmer Optima 3200RL Optical Emission Spectroscopy, Norwalk, CT). The ICP was calibrated using AFPC rock check No.22.

Standard sample concentrations were measured from time to time in the course of the analyses to check the accuracy of the calibration curve. Five replicates were taken and averaged for each element. The wavelengths used are given in Table 9.

Table 9. Wave Lengths Used for ICP Analysis.

Element	Wave Lengths (nm)
Ca	315.887, 317.933, 393.366, and 396.847
Mg	279.077, 285.213, and 279.553
P	213.617, and 214.914
Fe	238.204, 239.562, 259.939, and 234.349
Al	308.215

Density and Surface Area Determination

Densities of powders were measured using a Quanta Chrome ultrapycnometer. The specific surface area (m^2/g) of dolomite and apatite particles was determined using a Quanta Chrome NOVA 1200 instrument. (Quantachrome Corp., Boynton Beach, FL). The analysis was performed using a five-point BET (0.10, 0.15, 0.20, 0.25, 0.30) using Nitrogen gas. The particles were outgassed at 60°C for 24 hours before analysis.

PVA Preparation

PVA was supplied by Celanese Chemicals Co., USA. Different PVA types with various ranges of molecular weights and degree of hydrolysis were used in the screening factorial design. These are given in Table 10.

Table 10. Average Molecular Weight and Degree of Hydrolysis of PVA Samples.

Type	Average Molecular Wt.	Degree of Hydrolysis (%)
Celvol 165	150000	99
Celvol 540	150000	88
Celvol 305	60000	99
Celvol 203	60000	88

PVA flakes were gradually dissolved in deionized water at 90 ^{o}C with continuous mixing by magnetic stirrer and heated at 90 °C for two hours to produce different PVA concentrations (0.5, 1, 2, 3, and 4%). Once Celvol 165 was found to give the best performance, it was used for all subsequent tests.

Spectrophotometric Determination of PVA

PVA solution of a certain concentration was treated with 25 ml of 4% boric acid solution and 2 ml of iodine solution (prepared from 1.27g of iodine and 25 g of KI/l) in that order. The resulting solution was diluted to 100 ml and kept at 25°C and its absorbance measured at 690 nm against a blank solution containing the same amount of boric acid and iodine solution. Beer's law applies in the concentration range of 0-40 mg of PVA/l of solution. (Finch 1992).

Absorbance spectra were taken using ultraviolet/visible spectrophotometer (UV-Vis spectrophotometer, Perkin-Elmer Lambda 800). All spectra were taken at room temperature.

Static (Equilibrium Surface Tension)

Equilibrium surface tension was measured for freshly prepared solutions by the Wilhelmy plate method at room temperature. The platinum plate was always cleaned and heated to a red/orange color with a Bunsen burner before use.

Dynamic Surface Tension (DST)

Since the equilibrium surface tension is not reached in many dynamic interfacial processes, the DST must be studied. The DST can be measured by drop weight (Miller and others 1993), oscillating jet (Thomas and Hall 1975), capillary wave (Kelvin 1871), growing drop technique (MacLeod and Radke 1993), and the maximum bubble pressure method (Mysels 1986; Ross and others 1992). The maximum bubble pressure (MBP) technique is the most commonly used technique for the measurement of DST and has been applied to a variety of surfactant solutions (Fainerman and others 1994; Tamura and others 1995). For pure water, a newly formed interface should have a surface tension approaching 72 mN/m, the equilibrium value as measured by, for example, the Wilhelmy plate static surface tension method. The physical principle behind the MBP measurement is the Laplace pressure—the pressure inside a curved liquid interface is higher than the ambient. This excess pressure (P) can be calculated from the Laplace equation (Adamson and Gast 1997).

$$P = \frac{2\gamma}{r} + \rho gh$$

where γ is the surface tension, r is the radius of curvature of the bubble, ρ is the liquid density, g is the gravitational constant and h is the depth of the bubble in the liquid. The first term expresses the Laplace pressure due to the curved gas/liquid interface and the second term is the hydrostatic pressure due to the liquid height above the forming bubble. The first term will vary during the life cycle of the bubble while the second term will remain constant. Figure 2 shows the typical cycle of a bubble and the resulting pressure within the capillary. After a bubble breaks off from the capillary tip, the pressure is the

lowest. As more gas flows into the capillary, the pressure builds up as the gas is pushed out of the capillary and the radius of curvature at the tip decreases. During this expansion process, surfactant is populating the new interface and acting to lower the surface tension. At the point of minimum interface radius of curvature, where a hemisphere of gas is formed at the capillary tip, the pressure reaches maximum. Both the minimum radius of curvature and the surface tension, as described by the Laplace equation, govern the maximum pressure experienced. On the incremental addition of gas, the bubble expands out of the capillary tip and the radius of curvature gradually increases. This results in a drop in the Laplace pressure and a resulting rapid expansion of the bubble. At some point, the bubble breaks off from the capillary tip and the whole process starts again.

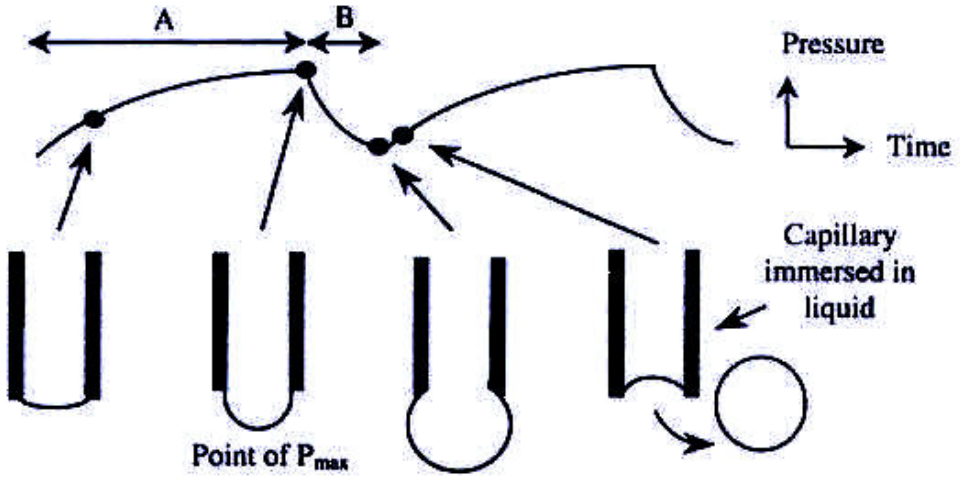

Figure 2. Characteristic Bubble Pressure Versus Time Curve in MBP to Determine Dynamic Surface Tension.

Dynamic Surface Tension Setup

The maximum bubble pressure apparatus was constructed using a differential pressure transducer purchased from Omega Engineering, Inc. (Stanford, CT), with a sensitivity of 0 to 10 in (25 cm) H_2O (0 to 2500 Pa). A #23 steel needle was used as a capillary, with nominal 0.025 in (0.64 mm) external diameter, 0.013 in (0.33 mm) internal diameter, and a flush cut tip. The capillary diameter was chosen so that the various resistance of water to bubble growth could be ignored. Such internal and viscous effects are a potential source of error in these measurements and need to be taken into consideration (Garrett and Ward 1989). All measurements were conducted with the capillary tip 1 cm beneath the liquid surface. CO_2 gas was used as the bubbling gas to simulate the gas produced in the reaction of acid with dolomite and an oscilloscope connected to the pressure transducer was used to determine the bubble frequency and the dynamic surface tension. A schematic diagram of the setup is shown in Figure 3.

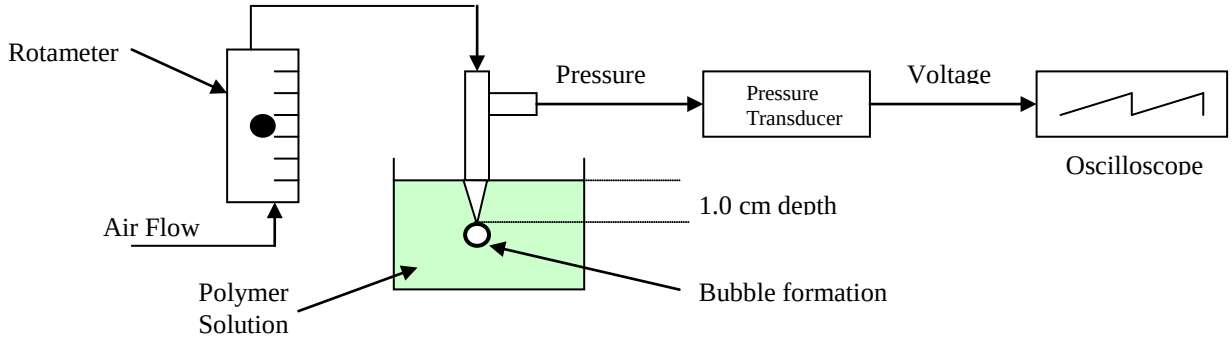

Figure 3. Setup for the Measurement of Dynamic Surface Tension by Means of the Maximum Bubble Pressure Method.

Contact Angle

The contact angle was formed at a point on the line of contact of three phases, of which at least two are condensed phases, by the tangents to the curves obtained by intersecting a plane perpendicular to the line of contact with each of three phases. One of the phases must be a liquid, another phase may be solid or liquid and the third phase may be gas or liquid.

In other words, the contact angle is the angle included between the tangent plane to the surface of the liquid and the tangent plane to the surface of the solid, at any point along their line of contact. The surface tension of the solid will favor spreading of the liquid, but this is opposed by the solid-liquid interfacial tension and the vector of the surface tension of the liquid in the plane of the solid surface.

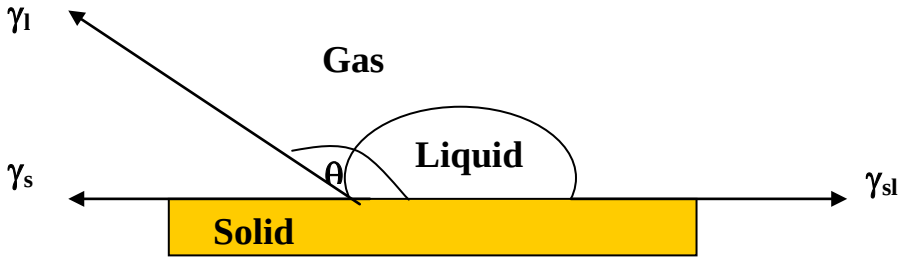

Figure 4. Contact Angle and Its Relationship with Surface Tension.

Equilibrium wetting properties of liquids and solutions can be interpreted in terms of the balance of surface tensions, illustrated in Figure 4 and described by the following equation:

$$\gamma_{sg} - \gamma_{sl} = \gamma_{lg} \cos \theta$$

Measurement of Contact Angle

The contact angle goniometer (see Figure 5) is a device mounted on the optical bench to examine a single liquid drop or gas bubble resting on the smooth, planar, solid substrate. The drop/bubble is illuminated from the rear to form a silhouette, which is viewed through a telescope connected to a computer. The image of the drop/bubble appears on the computer monitor by which the brightness and contrast, focusing and amount of illumination can be adjusted. After adjusting the image, the contact angle can be measured.

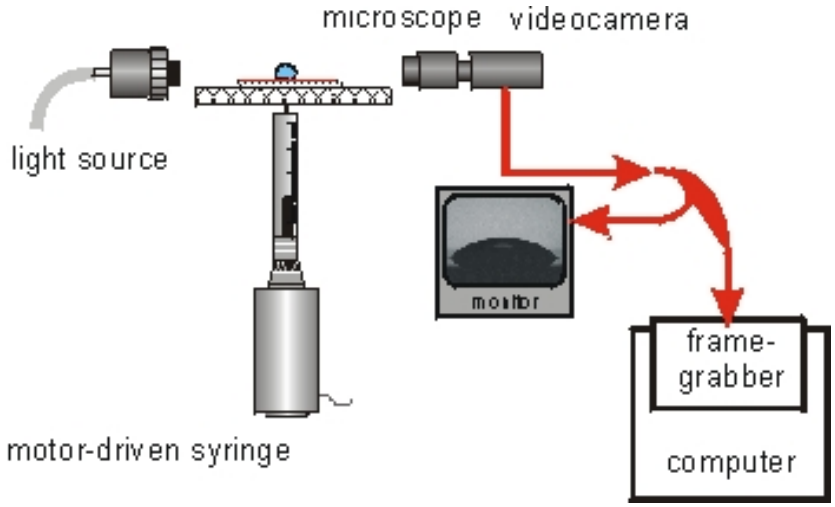

Figure 5. Contact Angle Measuring Apparatus.

Surface Characterization by FTIR

The spectrometer used for FTIR was a Magna-IR760 spectrometer by Nicolet in transmission setting.

As for the spectra recorded in transmission mode, KBr pellets were prepared for the background measurements. Additional pellets were prepared by mixing about 1 mg of filtered powder with 50 mg of KBr. Transmission spectra were recorded using a DTGS detector, with 128 scans and 4 cm^{-1} resolution.

Zeta Potential Measurements

In the zeta potential measurement tests, 1 g of ground mineral samples was added into a 250 ml beaker in which 100 ml 0.003 M KNO_3 solutions were added. The suspension was conditioned for 3 min during which the pH was adjusted, followed by 5 min of conditioning after adding the polymer. It was then allowed to settle for 3 min, and about 10 ml of the supernatant was transferred into a standard curette for zeta potential

measurement using a Brookhaven ZetaPlus Zeta Potential Analyzer. Solution temperature was maintained at 25 °C. Ten measurements were taken and the average was reported as the measured zeta potential.

Adsorption

These studies were carried out at 25°C using a 0.5 gm mineral sample in a 50 ml solution having the desired PVA concentration and the ionic strength fixed at 3×10^{-3} M using KNO_3. One set of experiments was performed first to determine the effect of conditioning time at a fixed pH (pH 7) and PVA concentration of 100 ppm (3.33×10^{-8} M). Another set of experiments was then carried out as a function of pH at the same PVA concentration. Adsorption isotherm was also determined for PVA/dolomite, PVA/apatite, PVA/dolomite/apatite supernatant, PVA/apatite/dolomite supernatant systems at pH 7 and 3×10^{-3} M KNO_3 as an ionic strength.

After the conditioning step, the suspensions were centrifuged at 3000 rpm for 5 min using a IEC-Medispin centrifuge (Model 120). Then, a volume of the clear solution was withdrawn for measurement of the PVA residual concentration.

Adsorption Kinetics

In adsorption kinetic experiments, a 0.5 gm of dolomite or apatite were added to 100 ppm (3.33×10^{-8} M) PVA solution to a 30 ml screw-capped bottle at room temperature using Wrist Hand Shaker for a given recorded time (0.05, 0.083, 0.0166, 0.25, 0.5, 1, 2, 4, 6, 8, 10, 16, 20, 24 hr). After that, the contents of each bottle were allowed to settle, followed by a centrifugation step using an IEC-Medispin centrifuge (Model 120). The amount of PVA adsorbed was determined by the difference between the initial and final concentrations measured spectrophotometrically with a Uv-vis spectrophotometer (UV-Vis spectrophotometer, Perkin-Elmer Lambda 800). These experiments were used to establish the equilibrium time for adsorption of PVA on dolomite and apatite. This equilibrium time was used as contact time in adsorption isotherm experiments.

PILOT SCALE EXPERIMENTS

Size Reduction

The 8" Disc Pulverizer, as shown in Figure 6, was used for grinding the feed samples for the separation tests. Grinding was performed between two 8" wide, replaceable abrasion-resistant discs. During operation, one disc remains stationary while the other revolves as the feed material passes between the discs. Both the pulverizer and motor are mounted on a 32" × 40" steel plate.

The 8" grinding discs can be adjusted and locked into position to obtain optimal particle size. The entire grinding chamber is accessible for easy cleaning and greater sample recovery (Mular 1980).

Figure 6. Disc Pulverizer.

Coulter Size Analyzer

The Beckman Coulter LS 230 Enhanced Laser Diffraction Analyzer was used in this study to determine the particle size. The laser diffraction method of measuring particle size takes advantage of an optical principle, which dictates that small particles in the path of a light beam scatter the light in characteristic, symmetrical pattern, which can be viewed on a screen. Given a certain pattern of scattered light intensity as a function of angle to the axis of the incident beam (flux pattern), the distribution of particle sizes can be deduced.

The Beckman Coulter LS 230 Enhanced Laser Diffraction Analyzer uses a patented technique for the characterization of sub-micron particles. PIDS or polarization Intensity Differential scattering is unique to the Beckman Coulter LS 230 and provides exceptional performance extending the size measurement down to 0.04 μm.

SEPARATION DEVICES

Spiral Concentrator

The spiral concentrator, Figure 7, is one of the relatively modern, high capacity, low cost units developed for the inexpensive pre-concentration of low value ores. The spiral is a unique device in its approach to separation and recovery. The first beach sand operation to use spiral was in Florida.

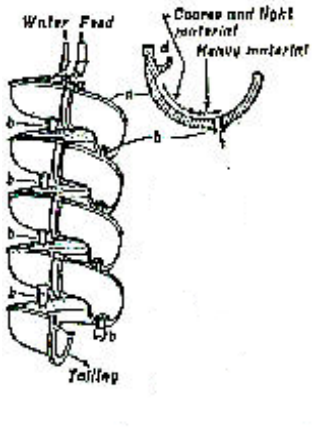

Figure 7. Spiral Concentrator.

The spiral operation starts when the feed is introduced through the feed box, which reduces its velocity and establishes the flow pattern. As the pulp flows around the helix of the spiral concentrator, stratification occurs in a vertical plane. The result is that, in the vertical plane, the heavier particles proceed to the lower velocity zones near the trough surface, while the lights tend to stratify above them in the higher velocity zone.

The helical twist of the spiral concentrator causes not only a flowing film velocity gradient to be set in a vertical plane, but also a radial, or centrifugal, velocity gradient related to the other, in a horizontal plane. The difference in centrifugal forces acting upon the varying stream components causes a cross-sectional rotation to develop. The portion of the stream nearest the surface moves outward to the point of maximum stream velocity; from there it moves down into the stream near the spiral surface. It then follows the spiral surface inward to the inner margin of the stream. This cross-sectional rotation of the stream serves to shift the heavy minerals inward toward the collecting ports and the light, faster-flowing but slower-settling mineral components of the streams are thus shifted laterally in opposite direction so that one is separated from the other (Burt 1984).

Shaking Table

This wet concentrating table is a rectangular or rhomboid shaped riffled-deck operated in, essentially, a horizontal plane. A drive mechanism imparts a differential motion to the deck along its long axis while water flows by gravity along the short axis. The separation that occurs on a concentrating table is the result of numerous mineral-processing principles simultaneously acting on the material feed to the table. These principles include flowing-film concentration, hindered settling, consolidation trickling, and asymmetrical acceleration (Deurbrock and Agey 1985). Wills (1992) also gives detailed descriptions of each of these principles.

Operationally, slurry of solids and water is fed to the upper edge of the sloping table. As the suspended material moves across the table, it is caught and forms pools behind the longitudinal riffles. The differential shaking action of the table causes size

classification and specific gravity stratification. This causes similar particles to arrange themselves vertically according to size (Deurbrock and Agey 1985). A schematic of a shaking table with the idealized size and specific gravity stratification is illustrated in Figure 8.

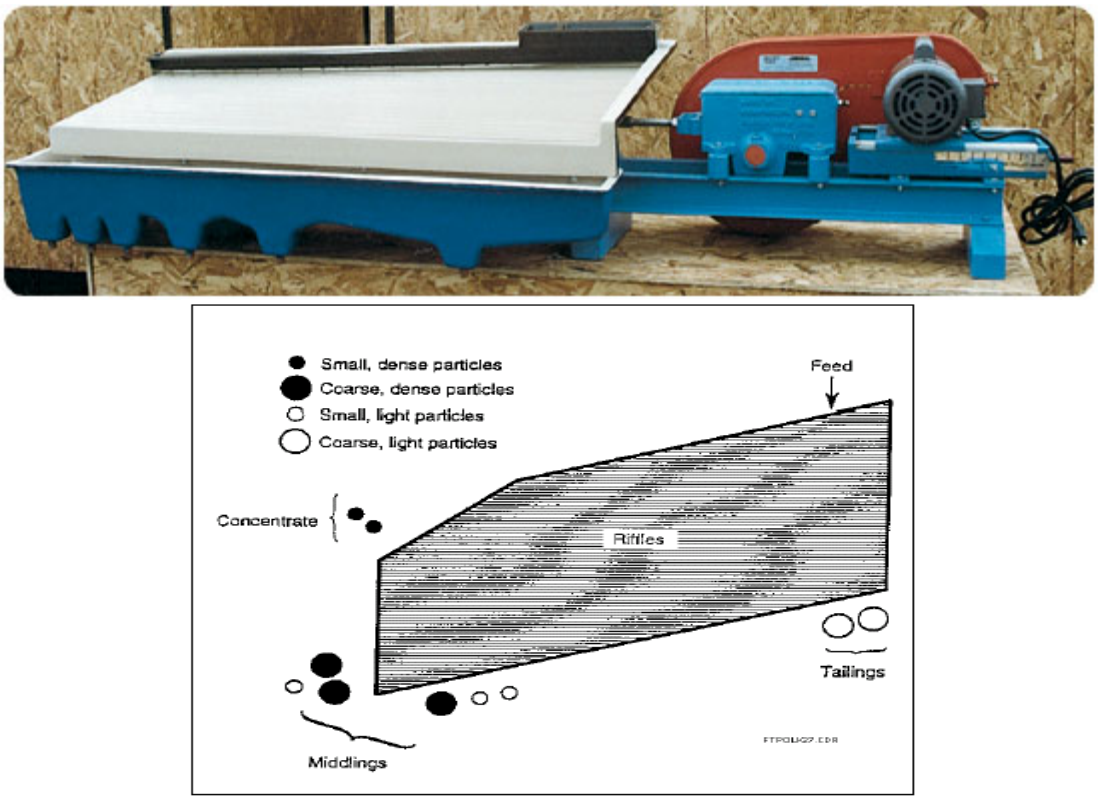

Figure 8. Shaking Table and Schematic of Its Principle of Particle Separation.

The effectiveness and speed of the separation is dependent on the table's operational factors. These factors include: the size and shape of the particles, the difference in specific gravity of individual particles, the size consistency of the feed, the water and slurry flow rates, and the mechanical settings of the shaker table (Deurbrock and Agey 1985).

Floatex - Density Separator

The Floatex Density Separator is a hindered-bed classifier that consists of an upper square tank and a lower conical section (Figure 9). The Floatex can be divided into three main zones:

(1) The upper zone (zone A) above the feed inlet,

(2) The intermediate zone (zone B) between the feed inlet and teeter water addition point, and

(3) The lower section (zone C) below the teeter water addition point.

Feed slurry is introduced to the Floatex tangentially through a centralized feed well that extends to approximately one third of the length of the main tank. Fluidizing (teeter water) is introduced over the entire cross-sectional area at the base of the teeter chamber through evenly spaced water distribution pipes. As the feed enters the main separation zone it expands into a teetered or fluidized bed as a result of the rising current of water. The teeter water flow rate is dependent upon a) feed particle size distribution, b) density and c) the desired cut-point for the separation. The separation takes place in zone B and the separated lighter/finer particles and the coarser/heavier particles leave the separator through zone A and zone C, respectively. The separator is equipped with a pressure sensor mounted in zone B above the teeter water pipes as well as an underflow discharge control valve. The pressure, sensed by a level sensor, is transmitted to the underflow control valve using a specific-gravity set-point controller. This instrumentation helps in maintaining a constant height of the teeter bed and a steady discharge of the underflow (Venkatraman and others 2000).

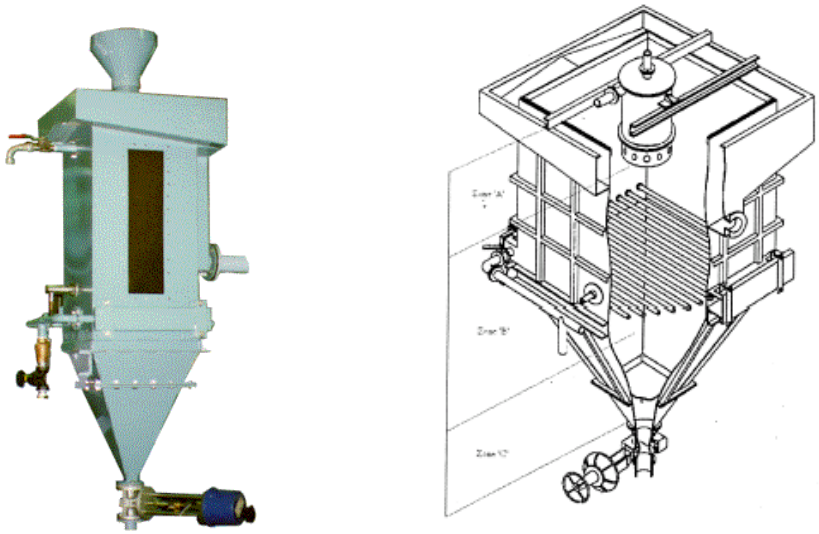

Figure 9. Floatex – Density Separator.

The Sluice

The pre-conditioned material is introduced into a feed box, which contains 3% sulfuric acid. The reaction of sulfuric acid with particles starts forming bubbles around the dolomite particles in the feed box and creating the required density difference for the separation in that device. The particles soon enter the moving stream and, because of the bubbles on the dolomite particles, they settle at lower rate and float to the surface. When the enough bubbles are formed, they are carried away until they reach the lip of the

trough and are discharged with liquid overflow. Since the phosphate particles do not produce CO_2 and have no bubbles at their surfaces, they are collected at the bottom of the trough. A schematic diagram for the sluice used in this study and its separation principle is illustrated in Figure 10.

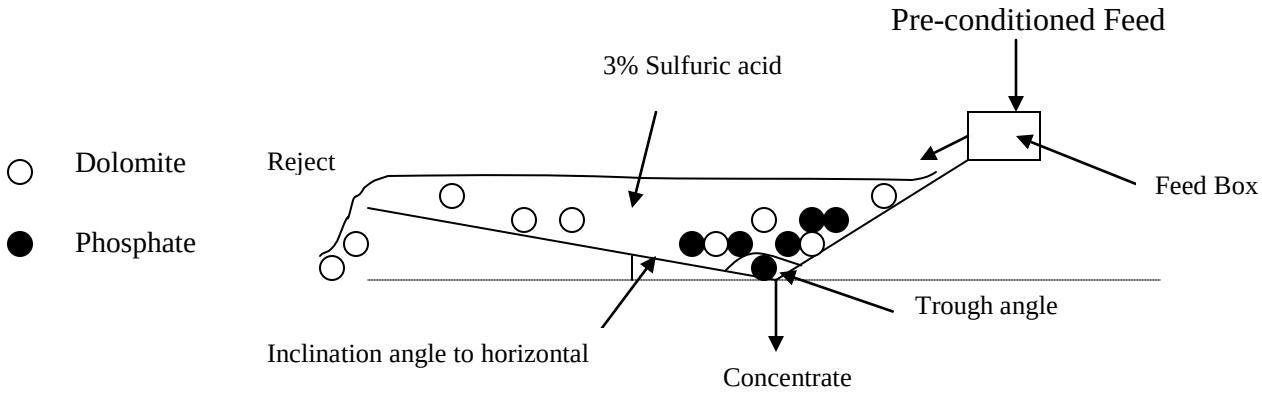

Figure 10. Schematic Diagram for the Separation of Dolomite from Phosphate in a Sluice.

Sluice Experimental Procedure

In a 1% polyvinyl alcohol solution, 250 gm of ore (a mixture of dolomite and phosphate) of particle size 1-2 mm were conditioned for 5 minutes, then screened to separate the solids from PVA solution. The screened solution was analyzed to determine the actual PVA consumption by depletion method. Alternatively, the material was sprayed with the equivalent amount of PVA and was tumbled in a plastic jar to attain a good coating. After that, the coated solids were poured into sluice feed box in which the sulfuric acid and consequent reaction started to generate CO_2 bubbles. The particles moved through the sluice at flow rate of 125 ml/sec (2 GPM). The floated fraction, dolomite, was collected on 0.5 mm screen and the sink fraction, phosphate, was collected in the sluice trough. The floated and sink products were analyzed for MgO, P_2O_5, CaO, and I.R.

Dissolution Kinetic Experiments

Dolomite specimens (1-2 mm and 0.2-0.3 mm), both uncoated and coated with PVA, were added to 2000 ml aqueous medium (3% H_2SO_4) at 23 ± 0.5°C to carry out 120 min static dissolution tests. After a definite time interval, solution samples were collected periodically and concentrations of Mg^{2+} and Ca^{2+} were determined with ICP.

The relations of concentration, C, with time, t was plotted to explore the dissolution kinetics of the dissolution process.

EXPERIMENTAL RESULTS

Screening Statistical Design

MgO recovery is affected by the acid concentration and PVA concentration in the coating solution, as shown in Figure 11, which represents the contour plot for the effects of these factors. It can be observed in Figure 11 that the MgO recovery changes from almost 0% to more than 37% as the PVA and acid concentrations increase from 1 to 3%. Increasing the PVA molecular weight also increases MgO recovery, while the degree of hydrolysis and drying time have a very slight effect on recovery. However, particle size inversely affects MgO recovery, which decreases with increasing particle size. The confidence interval is within 95%, i.e., the effects are statistically significant at the 95% level. The standard deviation and R-Squared for both of them are 1.15, 0.9999 and 0.058, 0.9998, respectively.

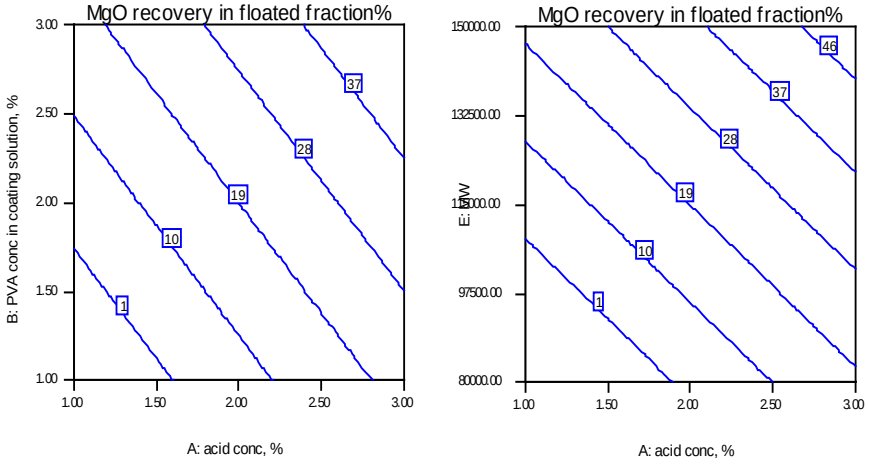

(a) (b)

Note: (a) (MW = 115000, D.H. = 93.5%, Drying time = 1 hrs, Particle size= 4.75 mm); (b) (PVA Conc.=2%, D.H. = 93.5%, Drying time = 1 hrs, Particle size= 4.75 mm).

Figure 11a. Contour Plot for Different Factors Affecting RF.

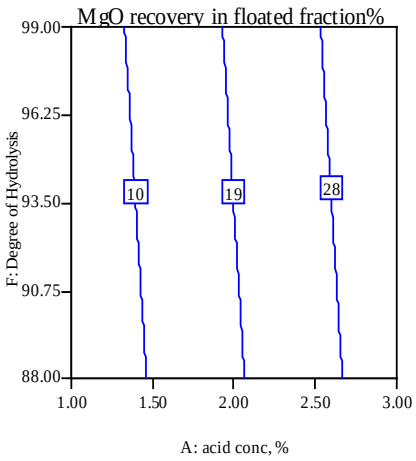

(c)

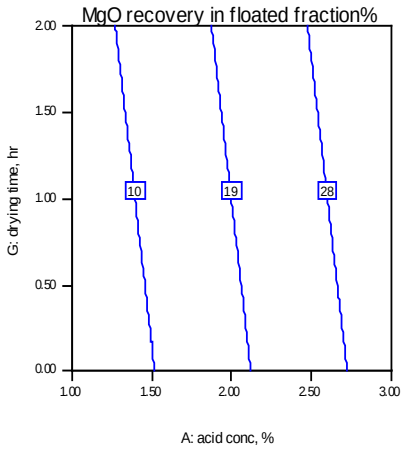

(d)

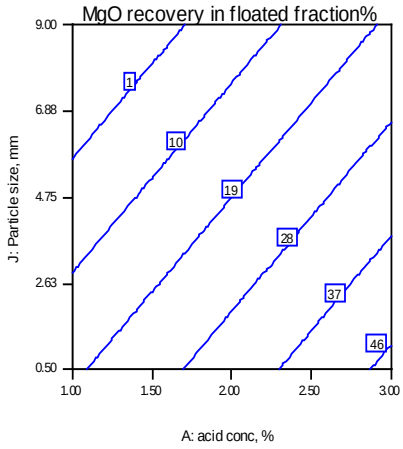

(e)

Note: (c) (PVA Conc.=2%, MW = 115000, Drying time = 1 hrs, Particle size= 4.75 mm); (d) (PVA Conc.=2%, MW = 115000, D.H. = 93.5%, Particle size= 4.75 mm); (e) (PVA Conc.=2%, MW = 115000, D.H. = 93.5%, Drying time = 1 hrs).

Figure 11b. Contour Plot for Different Factors Affecting RF.

On the other hand, MgO% in the concentrate (sink fraction) indicates that the main factors affecting this process are PVA concentration in the coating solution, acid concentration, and particle size, as can be observed from Figure 12.

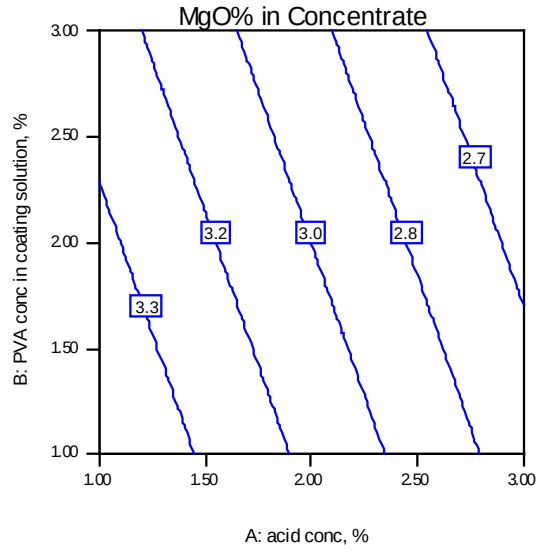

(a)

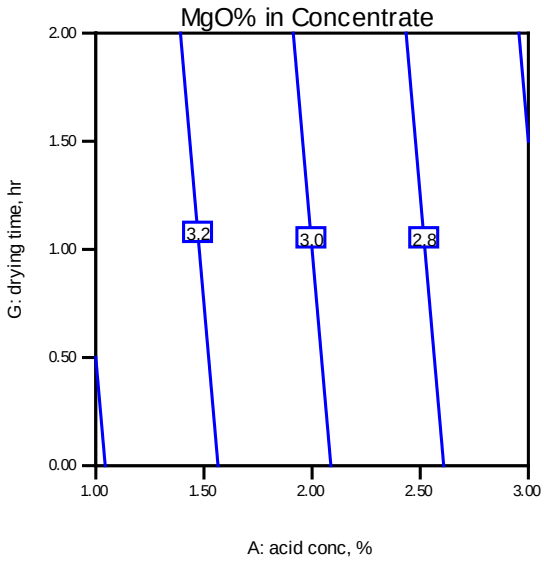

(b)

Note: (a) (MW = 115000, D.H. = 93.5%, Drying time = 1 hrs, Particle size= 4.75 mm);
(b) (PVA Conc.=2%, D.H. = 93.5%, Drying time = 1 hrs, Particle size= 4.75 mm).

Figure 12a. Contour Plot for the Effects of Different Factors on MgO % in Concentrate.

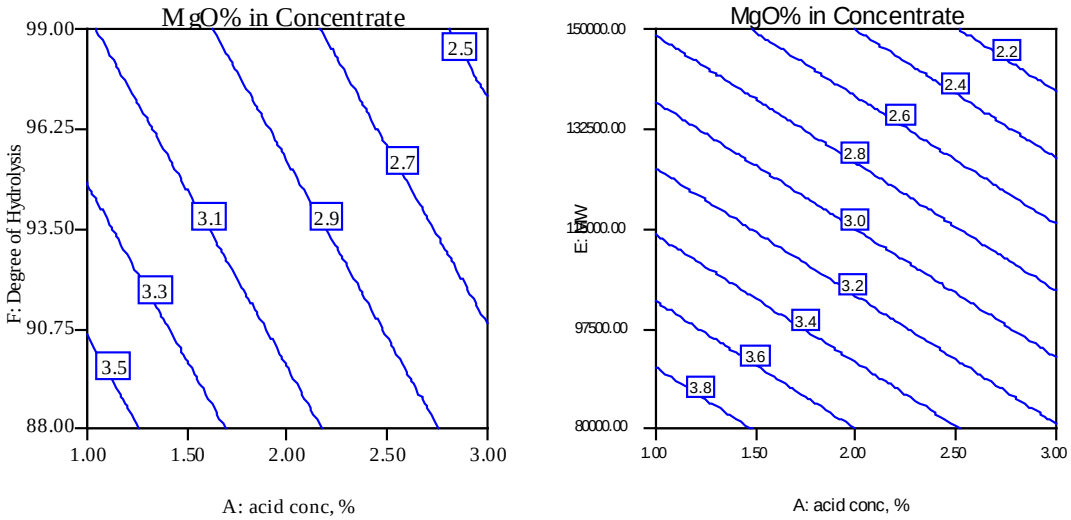

(c) (d)

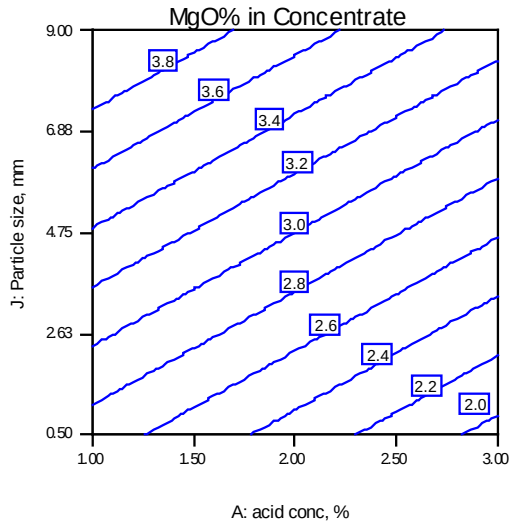

(e)

Note: (c) (PVA Conc.=2%, MW = 115000, Drying time = 1 hrs, Particle size= 4.75 mm); (d) (PVA Conc.=2%, MW = 115000, D.H. = 93.5%, Particle size= 4.75 mm); (e) (PVA Conc.=2%, MW = 115000, D.H. = 93.5%, Drying time = 1 hrs).

Figure 12b. Contour Plot for the Effects of Different Factors on MgO % in Concentrate.

Central Composite Design

Central composite design (CDD) results of dolomite flotation experiments are given in Figures 13-14 in terms of MgO recovery % in floated fraction and MgO % in sink (nonfloat) fraction respectively. The confidence interval is within 95%. In other words, the effects are statistically significant at the 95% level. The standard deviation and R-Squared for both of them are 13, 0.9287 and 0.36, 0.9287, respectively.

It was indicated, from these figures, that the % MgO recovery and MgO concentration in concentrate are greatly and positively affected by increasing either acid concentration or PVA dosage, i.e., % MgO recovery increases from 30 to more than 90% and MgO concentration in the concentrate decreases from more than 2.1 to 0.6 respectively. However, particle size negatively affects the % MgO recovery and MgO concentration in concentrate. With increasing particle size the % MgO recovery decreases. At the maximum acid concentration and PVA dosage, it decreases from 90 to 75% and % MgO concentration in the concentrate increases from 0.6 to 1.1%.

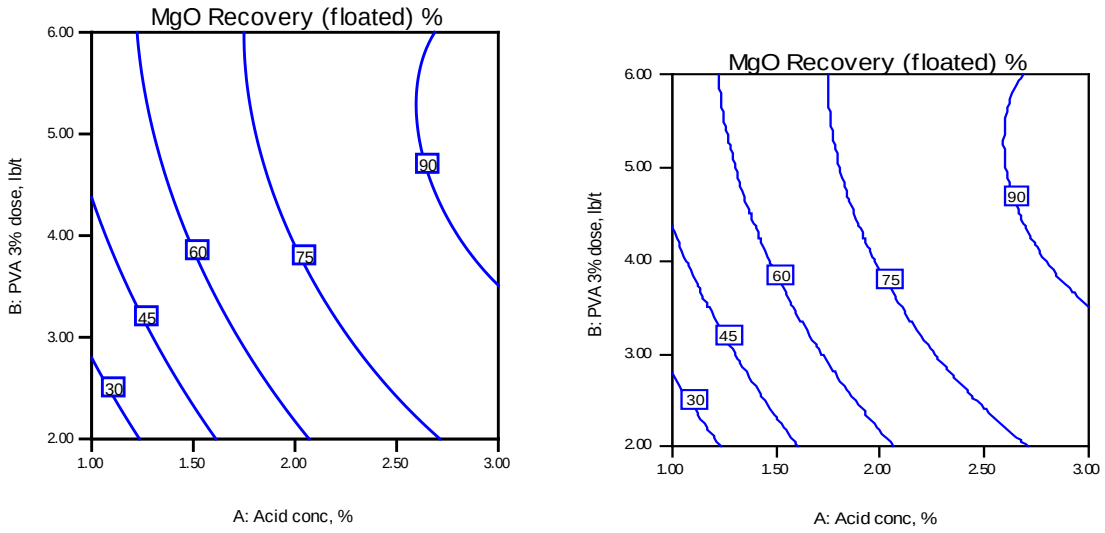

(a) (b)

Note: (a) Particle size = -0.5 mm; (b) Particle size = 1-2 mm.

Figure 13a. Effect of PVA Dosage and Acid Concentration on MgO Recovery % in Floated Fraction at Different Particle Size.

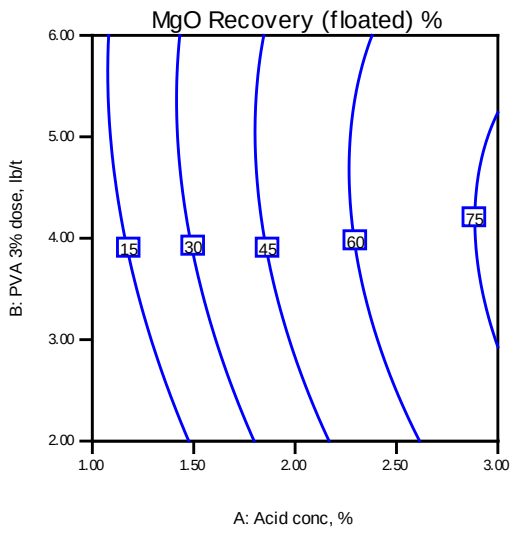

(c)

Note: (c) Particle size = 5-9 mm.

Figure 13b. Effect of PVA Dosage and Acid Concentration on MgO Recovery % in Floated Fraction at Different Particle Sizes.

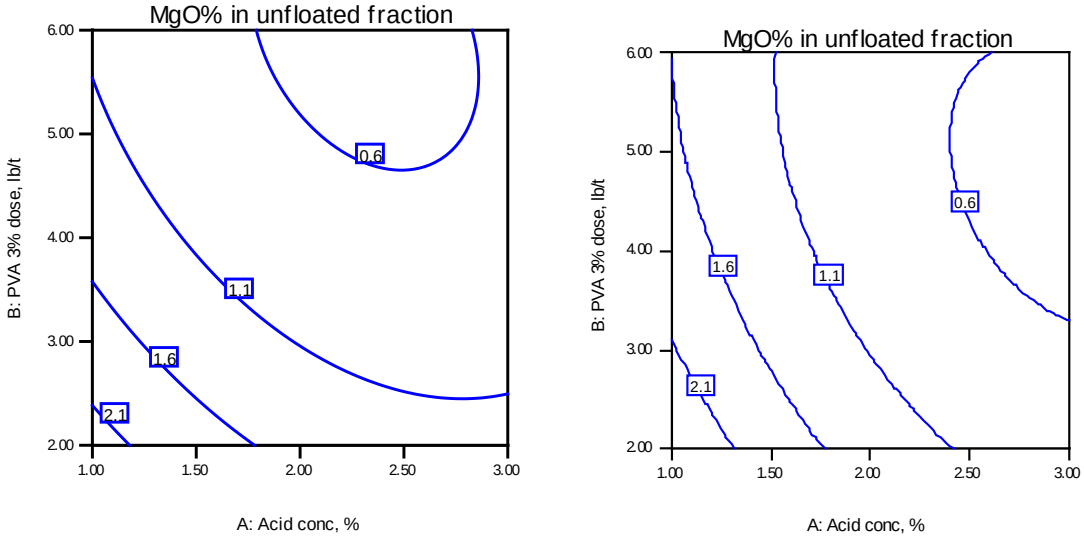

(a) (b)

Note: (a) Particle size = -0.5 mm; (b) Particle size = 1-2 mm.

Figure 14a. Effect of PVA Dosage and Acid Concentration on MgO % in Unfloated Fraction at Different Particle Sizes.

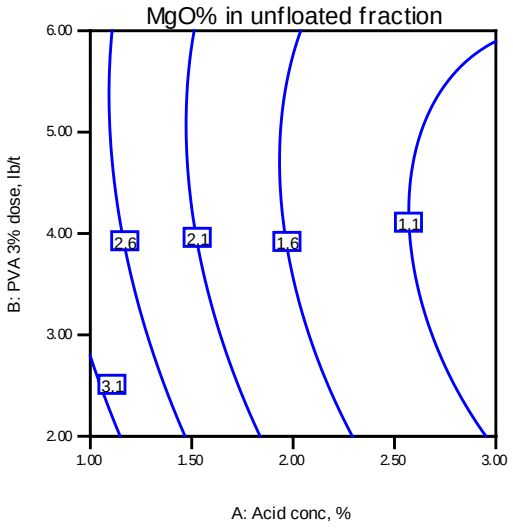

(c)

Note: (c) Particle size = 5-9 mm.

Figure 14b. Effect of PVA Dosage and Acid Concentration on MgO % in Unfloated Fraction at Different Particle Sizes.

It can be seen from these results that the PVA consumption is high (about 4.5 lb/t), which is economically unfeasible, to get a concentrate containing < 1% MgO with high recovery >90%. Therefore, further study is needed to reduce that consumption as discussed in the following section.

Efforts to Reduce the PVA Consumption

As mentioned above, the goal of this study is to develop a cost effective process. Therefore, reduction of PVA consumption can improve the economics of the process. In this regard several tests were conducted, as summarized below:

- Using compounds compatible with PVA such as starch and cellulose. It was found that the presence of these compounds negatively affected the stability of the bubbles at the interface.

- Only using fine rock particles (-40 mesh) with different PVA (1, 2, 3%) and acid concentrations (1, 2, 3%). It was found that the 3% PVA and 3% acid were needed, which are the same conditions as before and in addition the reaction was too fast due to the high surface area of the small particles.

- PVA + Drimax (spreading agent): to spread the PVA on the particle surface in order to reduce the amount needed to cover the particles. The results of these experiments indicates that there is an interaction between the PVA and

Drimax that prevented the formation of stable bubbles at the particle/solution interface.

- PVA + Boric acid: from the literature (Finch 1992, 1973), boric acid and borax are used in PVA cross-linking. Using the boric acid (5% of PVA) does slightly reduce the PVA consumption due to polymer cross linking but further experiments were not conducted because of toxicity of boric acid and environmental concerns.

- PVA + Na_2SO_4: sulfate ions lead to coagulation of the PVA according to literature (Finch 1992, 1973). However, the coagulation was not enough to float the dolomite particle at low PVA concentration.

- Conditioning of the rock particles with PVA and screening it (or filtering it) to recover the excess PVA. This approach was the most promising one since the consumption of PVA was reduced to 1 lb/t from 4-6 lb/t in the previous coating procedure. In this process, the conditioning step (with about 1% PVA) is followed by a filtration step. The PVA consumption was then calculated from the net consumption.

It was also found that the full coverage of the particle with PVA is not needed since the formation of some bubbles may be enough to create the density difference needed to float the particles. If a sluice or spiral is used, the lighter dolomite particles will follow the flowing liquid stream. In this manner, the dolomite particle will separate from the non floating phosphate.

Experimental Design of the PVA Conditioning (Coating) Step

These tests were conducted to optimize a coating methodology similar to the conditioning technique used for mixing reagents with ores before flotation. A statistical design with three factors, i.e. conditioning time, PVA concentration, and pulp density was used. The results shown in Figure 15 suggest that the PVA concentration is the main factor followed by the conditioning time while the pulp density (solid liquid ratio) has a slight effect on % MgO in the concentrate and % MgO recovery in floated fraction. Perhaps the most important conclusion from these tests is that the PVA consumption could be reduced to 1-2 lb/t instead of 4-6 lb/t as was obtained in the previous experiments.

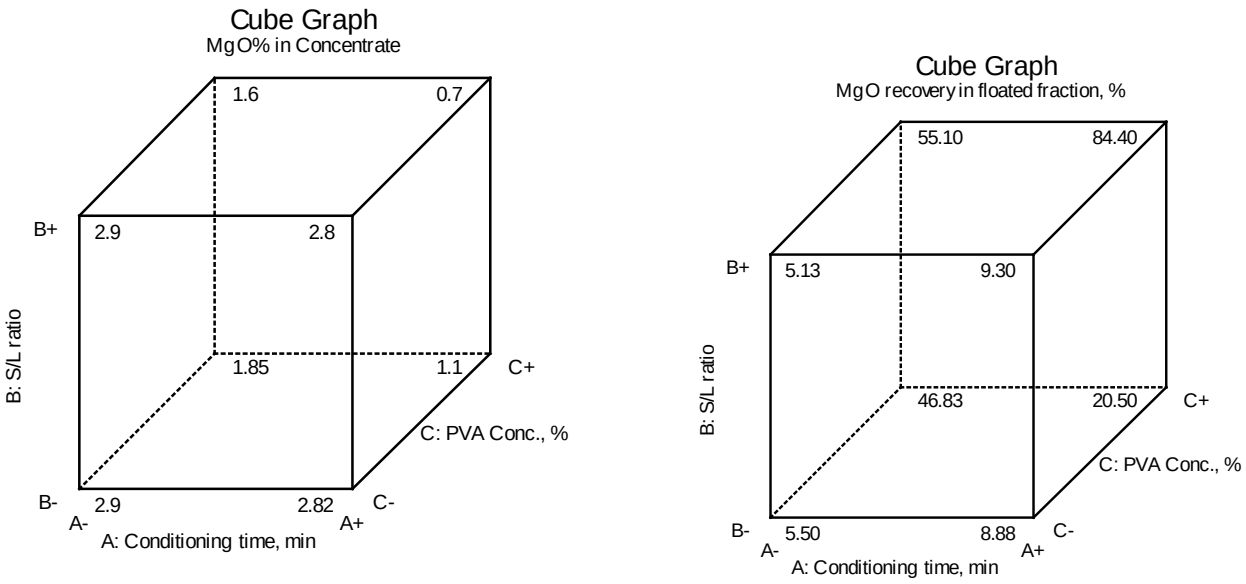

Figure 15. Cube Graph for MgO % and MgO Recovery %.

It was shown that the PVA consumption could be reduced to 1 lb/t on lab scale. Testing of the reactive flotation process using a simple sluice was conducted on pilot scale. Starting from the point that the formation of the bubbles on the dolomite surface creates a density difference between dolomite and phosphate particles. Therefore, the gravity separators are the promising techniques to do this separation.

In that regard, two tests were run using the sluice under two different coating conditions. The first was spraying the particles with 3% PVA solution before adding the particles to the sluice and the second was conditioning the particles in 1% PVA solution and screening the particles to remove the excess PVA solution to reuse it (the PVA consumption is estimated to be 0.8 lb/t), then adding the particles to the sluice. The results of these two tests are given in Table 11. From these results, it can be seen that by applying the optimum conditions, the reactive flotation process can reduce the MgO % to less than 1% with high recovery. In the rest of this work, the fundamental interpretations of what are observed experimentally were carried out.

Table 11. Comparison of Two Different Coating Methods and Their Effects on MgO Removal Using Sluice as a Separation Device.

Sample	Coating				Conditioning			
	Wt%	MgO%	P_2O_5%	CaO%	Wt%	MgO%	P_2O_5%	CaO%
Float	20.74	12.3	2.9	32.82	20	12.41	2.85	33.55
Sink	79.26	0.65	22.3	38.33	80	0.68	21.90	37.93
Calc. Feed	100	3.06	18.27	37.19	100	3.03	18.09	37.05
Feed	100	3.04	18.13	37.45	100	3.04	18.13	37.45

Saturation Experiment

In commercial application of this process, it is envisioned that acidic solution will be recycled to the flotation circuit for multiple usage. Thus, it is anticipated that the solution will be eventually saturated with calcium. In order to test effect of calcium saturation on the reactive flotation performance, this saturation test was performed. The experiment was carried out by adding $CaCO_3$ to 3% sulfuric-acid solution to saturate the solution with calcium sulfate. Formation of $CaSO_4$ precipitate indicated that the solution was saturated. It was found that 1.78gm/l of $CaCO_3$ would cause the precipitate to form. Flotation tests were then run in this saturated solution is an indication of reaching saturation Table 12 shows the results of these experiments. Interestingly, the data suggest that saturation of the acid does not significantly affect performance of the reactive flotation process.

Table 12. Effect of Saturated Acid on the Reactive Flotation (RF).

Sample	Before Saturation			After Saturation		
	Wt%	MgO%	P_2O_5%	Wt%	MgO%	P_2O_5%
Float	22.1	11.1	4.2	21.3	10.95	4.15
Sink	77.9	0.8	21.1	78.7	0.85	21.2

Pilot Scale Testing

In order to scale up this process, several pilot scale tests were conducted using various gravity separation techniques kindly supplied by Outokumpu Technology Inc. It should be noted here that no attempt was made to optimize the operating conditions in any of these runs. The goal was to explore the potential of performing the reactive flotation process in any of these techniques for dolomite separation.

The results obtained from devices such as the spiral concentrator, shaking table, Floatex density separator, and a sluice are shown in Table 13 in terms of the MgO%, P_2O_5%, and CaO% in the floated fractions.

Table 13. Analysis of Floated Fractions Using Different Separation Devices.

Device	MgO%	P_2O_5%	CaO%
Spiral	2.1	12.1	22.36
Shaking table	2.23	11.63	20.22
Floatex	10.6	4.11	33.83
Sluice float	12.3	2.90	32.82

The Floatex-density separator shows a high MgO% in the float, which is close to the best result, 12.3, using the sluice. However, the reason behind the lower recovery in

that device is the long vertical distance (30-40 in) that particles have to travel through in comparison to the sluice which is only one inch deep.

Also, the unsuccessful separation results in either spiral or shaking table are due to the short residence time and high stream velocity. The short residence time does not allow the reaction to form the required number of bubbles. Furthermore, the high stream velocity, especially in the spiral, prevents the formation of stable bubbles due to high shear rate.

More testing of the sluice was conducted to study effect of feed size distribution and the use of pond water as an acidic medium instead of sulfuric acid solution as discussed below.

Two sluice tests were run using two different particle size distributions. Spraying the particles with 1% PVA solution (1 lb/t) before adding the particles to the sluice was the coating method used in these experiments. The separation results of these two size fractions are given in Tables 14 and 15.

Table 14. Separation Results of -16+200 Mesh Size Fraction.

Sample	Wt %	MgO %	P_2O_5 %	CaO %	Recovery		
					MgO %	P_2O_5 %	CaO %
Float	42.45	2.4	12.2	20.95	52.53	33.11	38.56
Sink	57.55	1.6	18.18	24.63	47.47	66.89	61.44
Calc. Feed	100	1.94	15.64	23.07	100	100	100
Feed	100	1.99	15.52	23.21	100	100	100

Table 15. Separation Results of -35+200 Mesh Size Fraction.

Sample	Wt %	MgO %	P_2O_5 %	CaO %	Recovery		
					MgO %	P_2O_5 %	CaO %
Float	40.01	2.17	11.50	17.29	49.95	27.60	40.94
Sink	59.99	1.45	20.12	16.64	50.05	72.40	59.06
Calc. Feed	100	1.74	16.67	16.90	100	100	100
Feed	100	1.81	16.52	16.95	100	100	100

The results show that the weight % floated is almost the same in both cases. In addition, the MgO % in the concentrate did not go below 1.45. This may be due to flocculation of small particles that increased its entrapment in the float fraction. This is also reflected in the high P_2O_5 in the float fraction and low P_2O_5 concentrate recovery.

Tests Using Pond Water

IMC New Wales pond water was used as a separating medium in order to reduce the consumption of sulfuric acid. Different size fractions were also tested using this water. The results are listed in Tables 16-18.

Table 16. Separation Results of -2+1mm Fraction.

Sample	Wt%	MgO%	P_2O_5%	CaO%	Recovery		
					MgO%	P_2O_5%	CaO%
Float	17.48	8.4	5.76	35.25	48.36	5.55	16.36
Sink	82.52	1.9	20.78	38.17	51.64	94.45	83.64
Calc. Feed	100	3.04	18.15	37.66	100	100	100
Feed	100	2.99	18.20	37.39	100	100	100

Table 17. Separation Results of -16+200 Mesh Size Fraction.

Sample	Wt%	MgO%	P_2O_5%	CaO%	Recovery		
					MgO%	P_2O_5%	CaO%
Float	39.80	2.25	12.30	20.60	46.67	30.65	35.43
Sink	60.20	1.7	17.94	24.82	53.33	69.35	64.57
Calc. Feed	100	1.92	15.70	23.14	100	100	100
Feed	100	1.99	15.52	23.21	100	100	100

Table 18. Separation Results of -35+200 Mesh Size Fraction.

Sample	Wt%	MgO%	P_2O_5%	CaO%	Recovery		
					MgO%	P_2O_5%	CaO%
Float	30.27	1.93	12.45	16.07	34.37	23.14	28.59
Sink	69.73	1.60	17.95	17.42	65.63	76.86	71.41
Calc. Feed	100	1.70	16.29	17.01	100	100	100
Feed	100	1.81	16.52	16.95	100	100	100

The results show that as the size decreased from -2+1 mm to -1000+80 micron, the wt % floated increased. Once again, this may be due to polymer flocculation of the small particles, leading to their entrapment in the float fraction. In this case also, it is reflected in the high P_2O_5 in the float fraction and low P_2O_5 recovery.

Generally, in the case of pond water, the weight % floated is lower than that floated in presence of 3% sulfuric acid. This is attributed to the difference in reactivity between the pond water and the 3% sulfuric acid solution.

Screw Classifier

The loadings in the sluice possibly could be increased significantly by continuous removal of both the float and sink fractions of the rock. A screw classifier was borrowed from Jacobs Engineering of Lakeland to test this concept. The device is shown in Figure 16. It has an inclined screw or auger-type shaft that continuously removes any material that settles at the bottom of the hopper while liquid overflowing at the top continuously removes any floating (unsettled) material. In this application, the sink fraction is removed by the screw rotating shaft and the overflow carries the floated dolomite. Unfortunately, the screw could only operate at one fixed speed, which was fast for this application.

Figure 16. Screw Dewatering Device.

Nevertheless, a series of tests were conducted with this device. In all cases, the removal from the bottom was too fast to allow any significant separation. However, it did show that a properly designed device of this type may produce the desired separation..

ADSORPTION MECHANISMS

Generally, adsorption of a polymer is utilized in many applications, such as: dispersion of particles, flotation, flocculation processes, treatment of surfaces, etc. If a solvent is a poor solvent (i.e., the interaction energy between the polymer segment and the solvent molecules is unfavorable when compared to polymer-polymer or solvent-solvent molecular interaction energy), then the effective polymer-surface interaction can be strongly attractive and the polymer will seek any opportunity to minimize the contact points with the solvent. Hence, in cases where a poor solvent is used, adsorption will

increase on almost any surface, even the liquid-air interface. Adsorption is, therefore, always accentuated before precipitation will occur. The surfaces will act as a nucleation sites for polymer precipitation. This means, the poorer the solvent, the higher the adsorption and vice versa.

In addition to the solvent quality, there are other factors that can affect the polymer adsorption and change its conformation, including: polymer molecular weight, polymer concentration, pH, and ionic strength.

Previous studies of polymer adsorption suggest a number of qualitative trends that have been noticed in most polymer adsorption systems. The most important of them are as follows:

- Many polymers adsorb on a variety of surfaces, and
- Reach a plateau at few mg/m^2, which corresponds to 2-5 equivalent monolayers
- A sharp isotherm sometimes is obtained, and
- Molecular weight is a major factor, especially in a poor solvent.

As mentioned above, the polymer (PVA) is used as a membrane-forming agent to capture produced CO_2 gas on dolomite particles making them lighter than other particles leading to their flotation and separation from non-carbonate (apatite) particles.

To understand this process and to elucidate the mechanism of interaction between polyvinyl alcohol (PVA) and dolomite/apatite surfaces in the reactive flotation process, different techniques were used, such as: estimation of work of adhesion using surface tension and contact angle measurements, adsorption/ desorption isotherms, Zeta potential, and surfaces characterization using Fourier Transform InfraRed (FTIR), etc. The details of these techniques are discussed in this section.

Work of Adhesion

The strength of adhesion to a solid surface can be estimated from the value of the thermodynamic 'work of adhesion' or W_a, a concept first introduced by Harkins (1928). In a simple system where a liquid *L* adheres to a solid *S*, Figure 17, the work of adhesion is defined as:

$$W_a = \gamma_l + \gamma_s - \gamma_{sl} \qquad \text{(Equation 1)}$$

where γ_s , γ_l and γ_{sl} are the interfacial tensions of the solid/air, liquid/air and solid/liquid interfaces, respectively.

The problem with using Equation 1 is that, of the three interfacial tensions, only γ_l can be measured with fluid phases, in this case the liquid and air. Those tensions involving the solid cannot be measured independently. Another approach, then, is to combine Equation 1 with the Young-Dupre equation (Equation 2), to provide a more useful expression for the work of adhesion (Adamson and Gast 1997):

$$\gamma_s - \gamma_{sl} = \gamma_l \cos\theta \qquad \text{(Equation 2)}$$

where θ is the contact angle that the liquid makes with the solid surface. Provided that γ_l and θ can be measured experimentally, it is then possible to use Equation 3 to calculate the work of adhesion.

$$W_a = \gamma_l(1+\cos\theta) \qquad \text{(Equation 3)}$$

Therefore, the measurements of surface tension and contact angle are essential towards the calculation of the work of adhesion of the polymer (PVA) with solid surfaces, which will be discussed in the following sections.

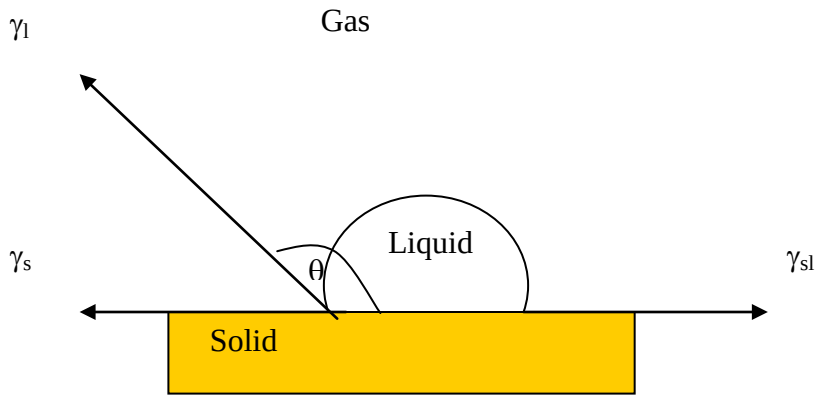

Figure 17. Contact Angle and Interfacial Surface Tension at Solid/Liquid/Gas Interface.

Surface Tension

The equilibrium surface tension values of fully hydrolyzed PVA solutions (average Mw = 150000) as a function of the initial bulk concentration at room temperature (23° C) are shown in Figure 18. The surface tension of PVA decreases with increasing concentration of PVA until it reaches a region where the surface tension (59-60 dyne/cm) no longer decreases with increasing the polymer concentration. The critical concentration at which the surface tension starts to be constant is 1% PVA in aqueous solution. These results coincide with the literature concerning the surface tension of fully hydrolyzed polyvinyl alcohol (PVA). The fully hydrolyzed polymer (as shown in Figure

18) has less effect on surface tension than partly hydrolyzed PVA (Biehn and Ernsberger 1948; Kim and Luckham 1991).

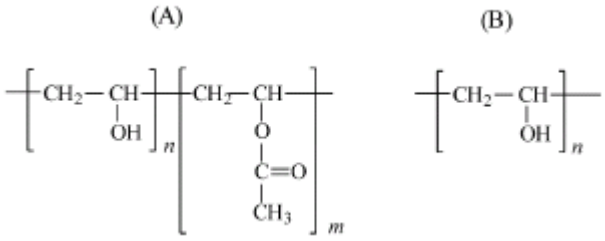

Figure 18. Structural Formula for PVA: (A) Partially Hydrolyzed; (B) Fully Hydrolyzed.

It is reported that the surface tension reaches a constant level at 1-3% PVA depending on the PVA molecular weight and degree of hydrolysis (Finch 1973, 1992). These results (shown in Figure 19) are similar to several findings reported in the literature regarding polymer systems; the stabilization of the surface tension of high-*Mw* PEO (> 100,000) solutions was associated with the saturation of the air/water interface by the polymer chains (Zeno and others 2004).

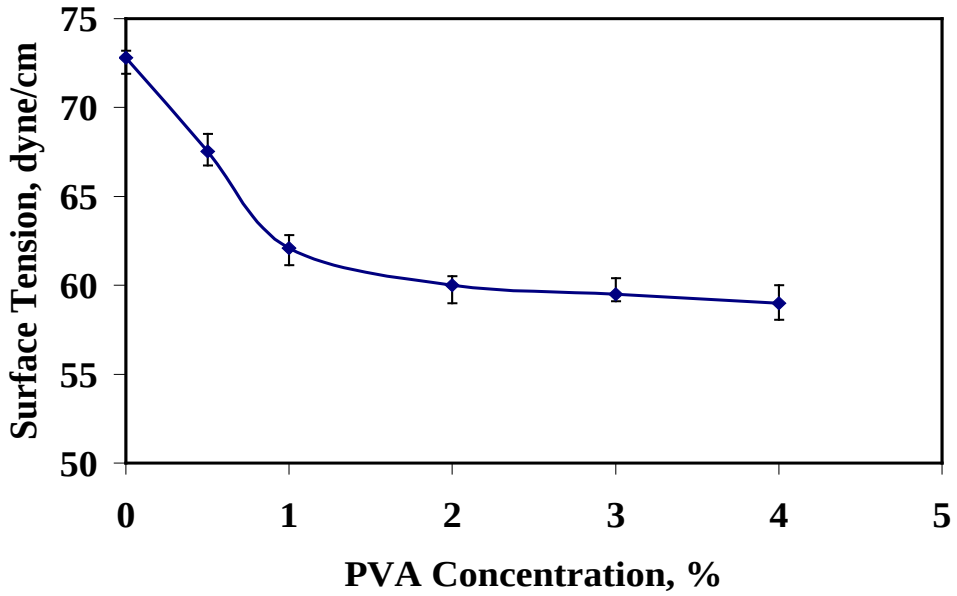

Figure 19. Equilibrium Surface Tension for Aqueous PVA Solutions at 23 °C.

An explanation of this phenomenon is that the surface activity of a polymer mainly relies on its conformation in the aqueous solution, whereas the conformation of macromolecule depends on its chemical structure and composition, etc. At low concentrations, the chains of macromolecule are stretched in the water due to the formation of hydrogen bonding with water molecules. These long chains lying on the liquid/air interface can dramatically decrease the surface tension of water, even though

the adsorbed amount on the liquid/air interface is very small. With the increase of concentration, the polymer's molecules that adsorb on the surface increase to form a tight macromolecular film, which makes the surface tension decrease. When the polymers occupy all the surface of solution, the adsorption reaches a level of saturation corresponding to the lowest value of surface tension. As this concentration further increases, the polymers in the solution begin to aggregate and form micelle-like clusters; at this point, the surface tension shows no more changes. In the case of PVA, it may also be related to degree of crystallinity due to formation of hydrogen bonding as indicated in Figure 20 (Finch 1973).

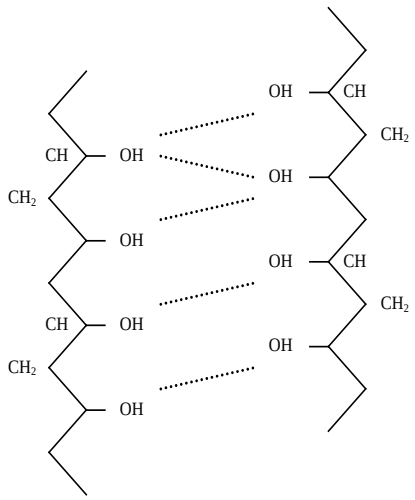

Figure 20. PVA Crystal Structure; the Dotted Lines Indicate Hydrogen Bonds.

It is expected that the surface tension will have higher values in the presence of the acidic media since the SO_4^{-2} ions increases the surface tension, affects the polymer solubility, and enhances the formation of polymer aggregates at even a slightly high acid concentration (Sun 1994).

Contact Angle

The phenomenon of wetting or non-wetting of solids by liquids is better understood by studying contact angle, which is the most universally applied method of quantifying wettability. Contact angle methods have been developed extensively over the past four decades. The contact angles of dolomite and apatite surfaces with PVA aqueous solutions at different concentrations are shown in Figure 21. From the figure, it can be seen that the contact angle increases with the increase of PVA concentration for both minerals' surfaces, which demonstrates that the hydrophobicity of both surfaces increases with the adsorption of PVA. This phenomenon can be explained by the structure of PVA in the solution shown in Figure 20. When a droplet of PVA placed on the surface of dolomite or apatite, the PVA adsorbs to the surface by hydrogen bonding.

As the PVA concentration increases, more and more hydrogen bonds form; as a result of hydrogen bonds among its molecules, the PVA begins to form clusters. These clusters result in a local viscosity increase, which controls the droplet shape as well as its tendency to spread. This, in turn, increases the contact angle accordingly. This phenomenon is observed for PVA and also for some modified PVA end groups (Finch 1992).

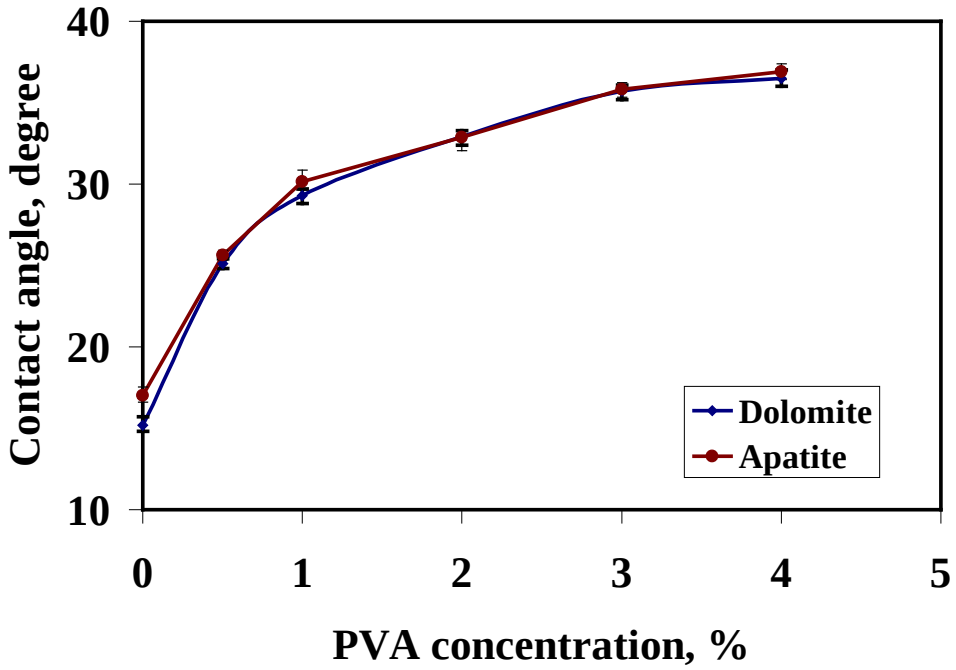

Figure 21. Static Contact Angle Variation with the PVA Concentration.

It should be mentioned that all measurements shown in Figure 21 were conducted immediately after application of the drop. Evaporation of water caused the drop to contract and a consequent change in the contact angle.

Work of Adhesion

Figure 22 shows the dependence of work of adhesion, W_a, on the PVA concentration. The work of adhesion decreases with increasing PVA concentration (increase in ΔG, where $W_a = - \Delta G$ (Lloyd 1994). The increase in ΔG reflects the formation of polymer clusters and increase in its crystallinity. This is due to the formation of OH-group bonds between PVA molecules causing them to favor adhesion to a solid surface. Additionally, the polymer's diffusivity decreases with higher concentrations.

With increasing PVA concentration, the PVA molecules not only adsorb to the surface but also form hydrogen bonds among themselves. This behavior affects the

conformation of the molecules at the solid-liquid interface till they reach the saturation stage, when the work of adhesion becomes constant. It appears that this saturation stage is the same region of PVA concentration, 1-3%, at which constant surface tension and contact angle are achieved.

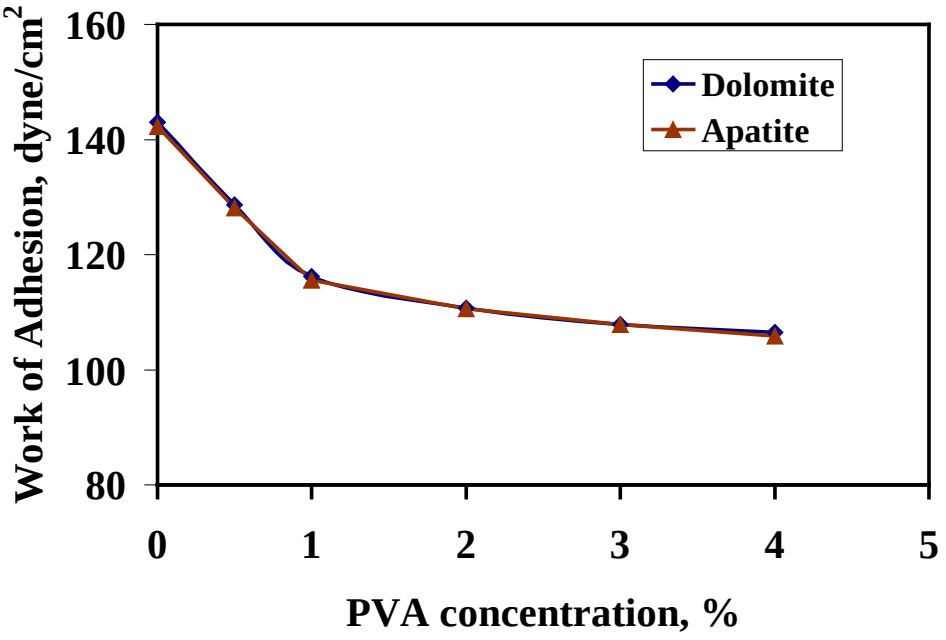

Figure 22. Work of Adhesion as a Function of PVA Concentration on Dolomite and Apatite Substrates.

Adsorption Study

Research grade samples were purchased from Wards Natural Science and used to conduct the adsorption study. These samples were chemically analyzed by the wet chemical method and the results are listed in Table 19.

Table 19. Chemical Analysis of the Samples Used in Adsorption Tests.

Mineral	MgO%	P_2O_5%	CaO%	Al_2O_3%	Fe_2O_3%	I.R.%	L.O.I. %
Dolomite	20.39	0.58	31.6	0.97	0.10	2.52	42.6
Apatite	-	31.73	49.50	2.64	1.04	4.95	5.0

Specific Surface Area Measurements (BET Method)

The specific surface area of dolomite and apatite particles was determined by the BET in order to be used in adsorption isotherm calculations (applied in the next section). Using nitrogen as the adsorbate, the measured surface areas for dolomite and apatite were 0.9 and 1.48 m^2/g, respectively.

Pore Size Distribution

The results of cumulative pore size distribution for apatite and dolomite are shown in Figures 23 and 24. It is clear that the apatite has a higher cumulative pore area, 9 m^2/g, than the 1.8 m^2/g for dolomite. Mean pore sizes for apatite and dolomite are 28 Å and 42.5 Å, respectively.

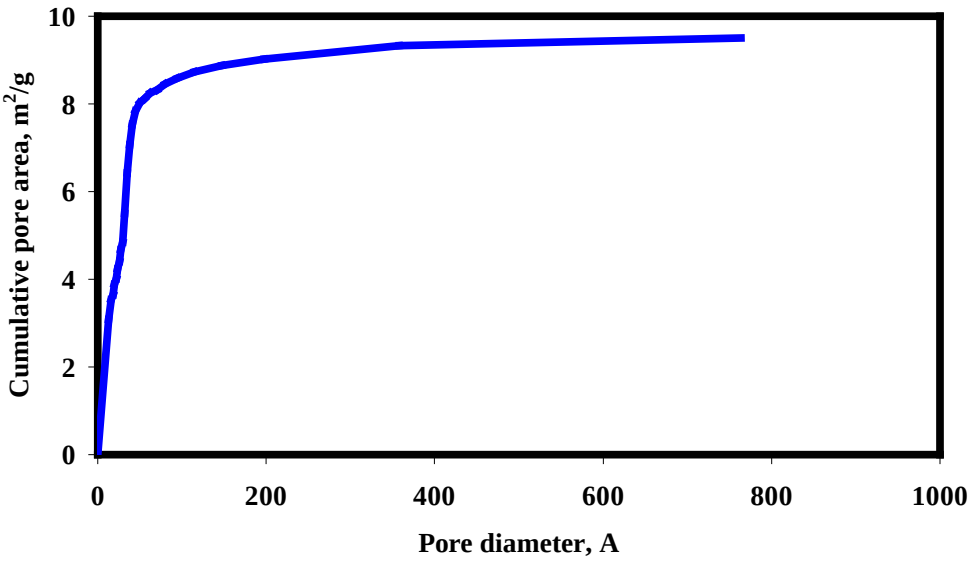

Figure 23. Cumulative Pore Size Distribution for Apatite Sample.

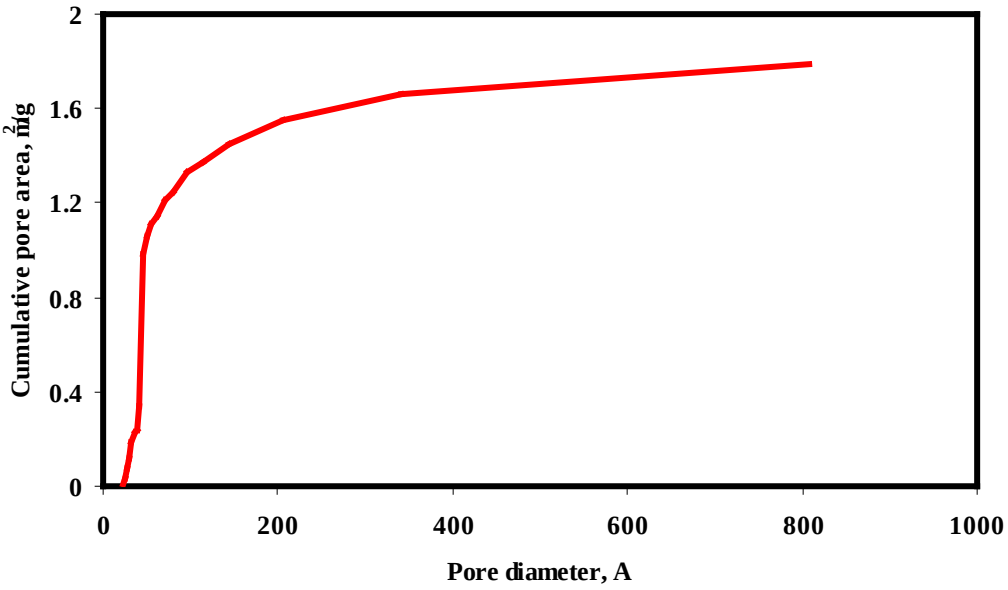

Figure 24. Cumulative Pore Size Distribution for Dolomite Sample.

Zeta Potential

In order to obtain a more detailed description of the adsorption and electrical properties of the solid-solution interface, measurements of the zeta potential were taken. The tendency of zeta potential to vary with nonionic polymer adsorption may be caused by one of two different factors: (1) the shift of the position of the shear plane, or (2) the blocking of the active sites on the surface by adsorbing polymer chains. The participation of these effects was estimated by the determining the difference in the values of the zeta potential with no polymer and with polymer present. The use of a KNO_3 solution (3×10^{-3} M) acted as a control in these experiments.

The zeta potential values of apatite and dolomite in 3×10^{-3} KNO_3 solution as function of pH are presented in Figure 25. It can be seen that the isoelectric points (IEP) of apatite and dolomite are about 6.8 and 9, respectively. This is in agreement with the results reported in the literature (Amankonah and Somasundaran 1985; Chander and Fuerstenau 1982; Pugh and Stenius 1985).

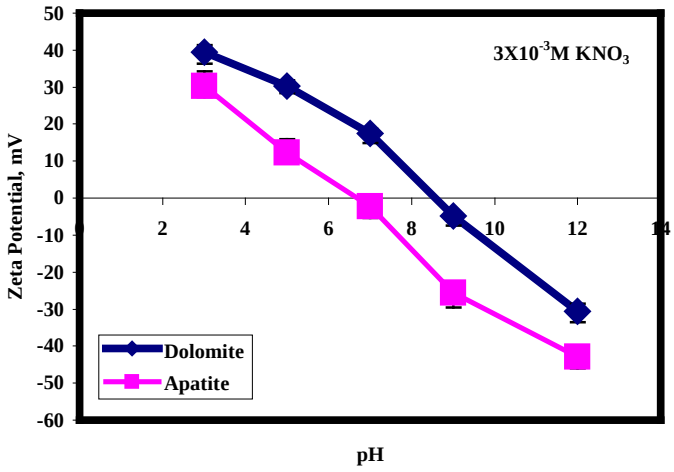

Figure 25. Zeta Potential of Dolomite and Apatite Samples.

Figures 26 and 27 show the results of the zeta potential measurements in PVA solution. It is evident that the presence of PVA does not change the IEP of the apatite or dolomite. It does, however, cause compression in the electrical double layer.

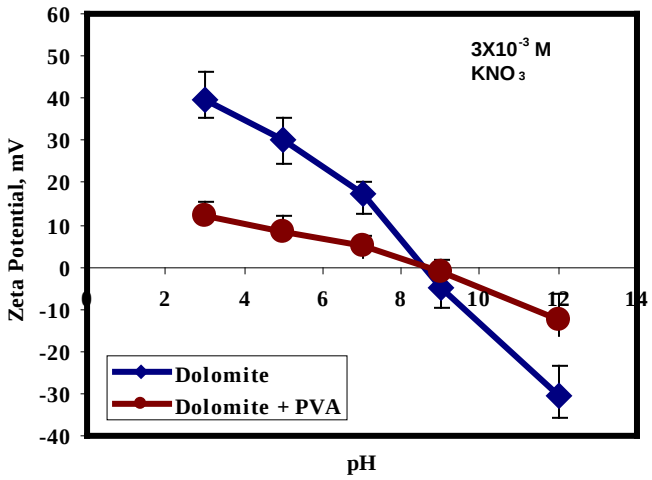

Figure 26. Zeta Potential of Dolomite in Absence and Presence of Polymer.

The results indicate that the surface sites remain accessible to potential determining ions (H^+ and OH^-) and the IEP remains unchanged during PVA adsorption, thus implying that the polymer does not alter the surface potential.

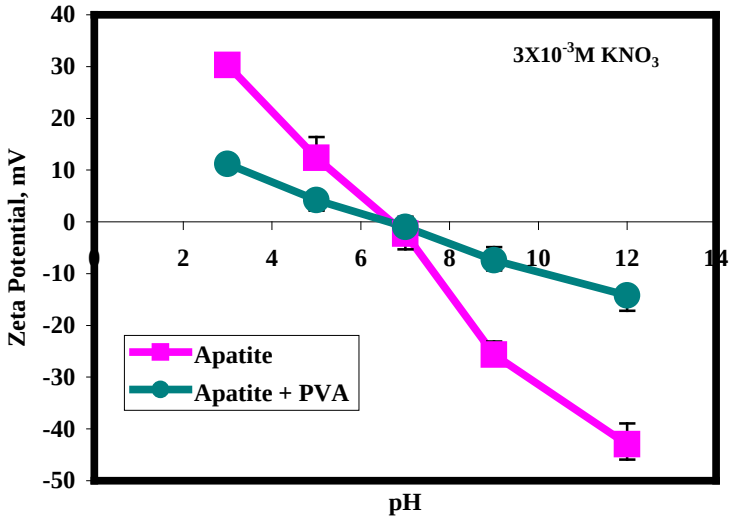

Figure 27. Zeta Potential of Dolomite in Absence and Presence of Polymer.

It may be considered, as other investigators asserted (Ottewill 1967; M'Pandou and Siffert 1987; Luckham and others 1983), that the decrease in zeta potential relating to adsorption of PVA is not due to a decrease in charge and surface potential, but rather to a shift of the shear plane (Figure 28).

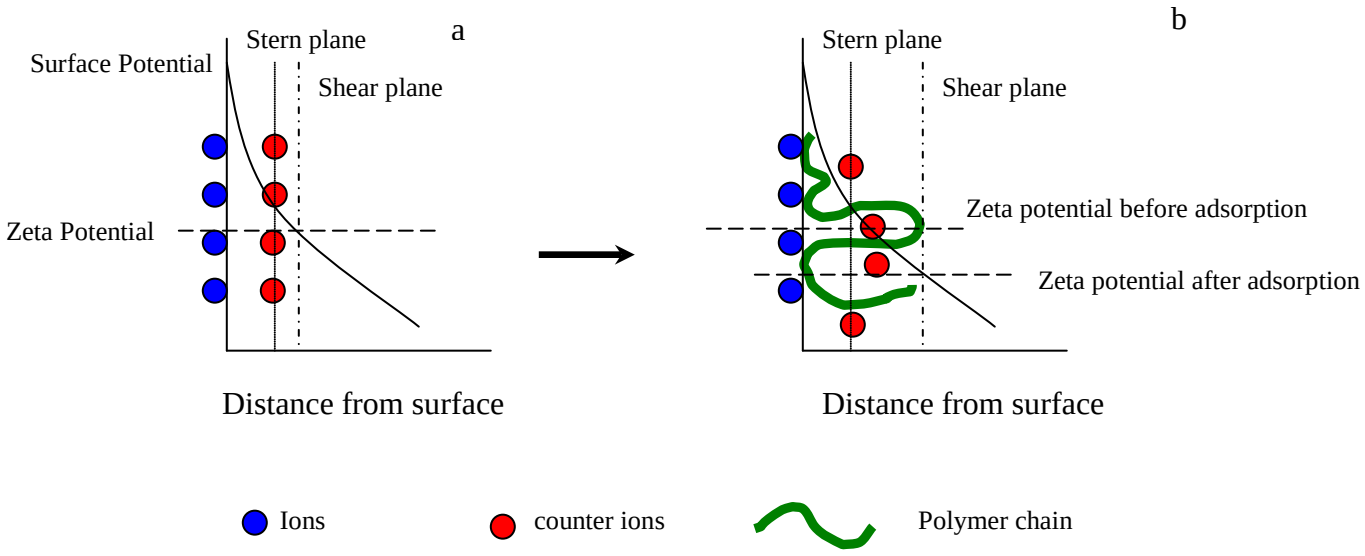

Figure 28. Effect of Polymer on the Shear Plane Position (a) Without Polymer, (b) After Polymer Adsorption.

Zeta Potential of Minerals in Supernatant Solutions

In natural ores, the dolomite and apatite form a mixture. Their presence together may affect the adsorption of the polymer on both of the minerals' surfaces. Therefore, the adsorption on the dolomite in presence of apatite supernatant and apatite in presence of dolomite supernatant were studied.

The effect of the supernatant of dolomite on the zeta potential of apatite is shown in Figure 29. The results show that the apatite surface becomes more positive over the entire pH range and that the IEP has shifted from 6.8 to 8.6. Both effects are hypothesized to be due to the presence of calcium and magnesium ions in the solution.

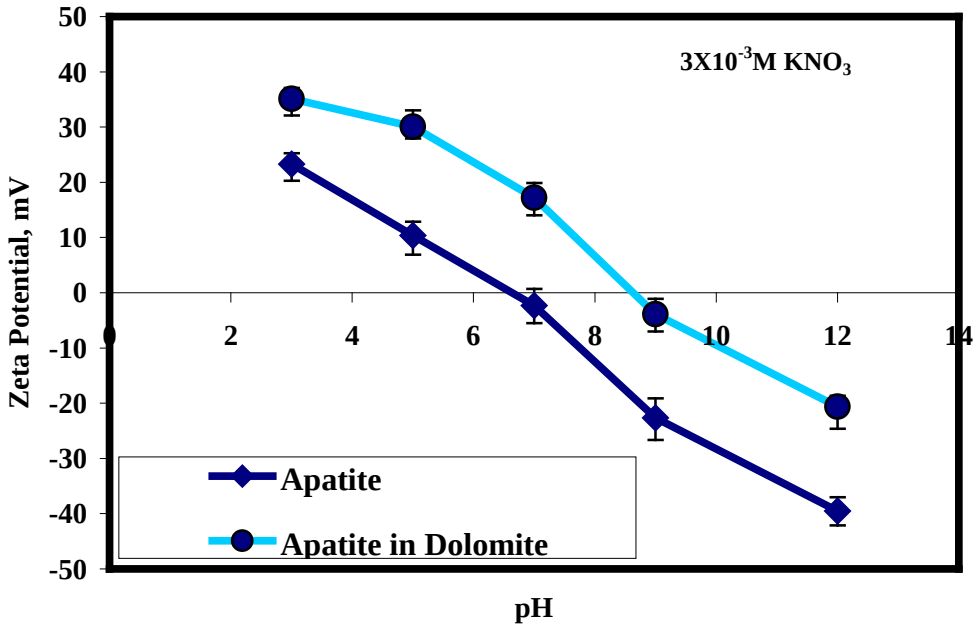

Figure 29. Zeta Potential of Apatite and Apatite in Dolomite Supernatant.

Similarly, the zeta potential of dolomite in an apatite supernatant was measured as a function of pH. The results, given in Figure 30, show the zeta potential of dolomite to be reduced drastically in presence of apatite supernatant. The IEP shifts from 9 to 6.5.

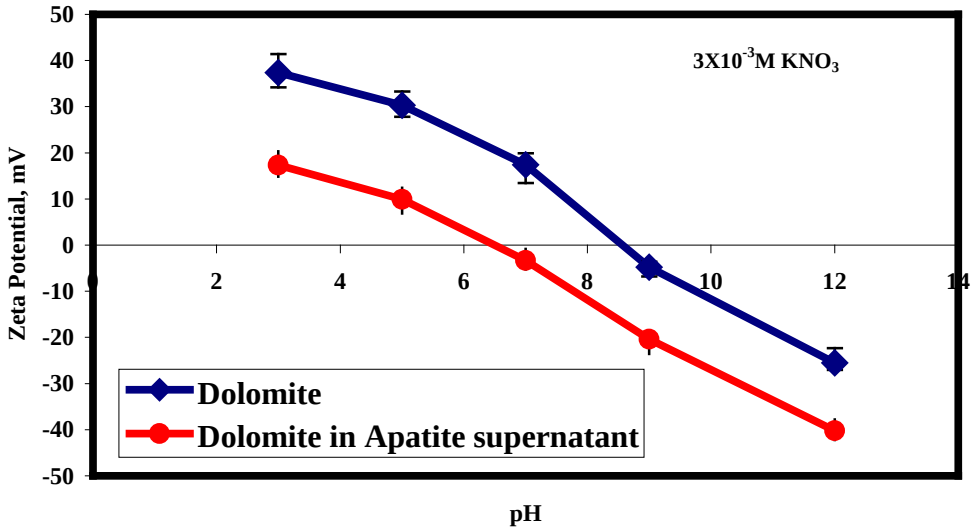

Figure 30. Zeta Potential of Dolomite and Dolomite in Apatite Supernatant.

Zeta Potential in the Presence of PVA

Moreover, the zeta potential of dolomite in apatite supernatant in presence of PVA was determined. The results in Figure 31 indicate that the PVA deals with surface of dolomite, when suspended in an apatite supernatant, as an apatite surface. This is due to the faster diffusion of small ions and molecules from the solution to the dolomite surface, which converts it to surface similar to apatite. As can be expected, the movement and diffusion of these ions is quite faster than that of polymer molecules. Consequently, the polymer's adsorption takes place after the surface has changed to be similar to the apatite surface.

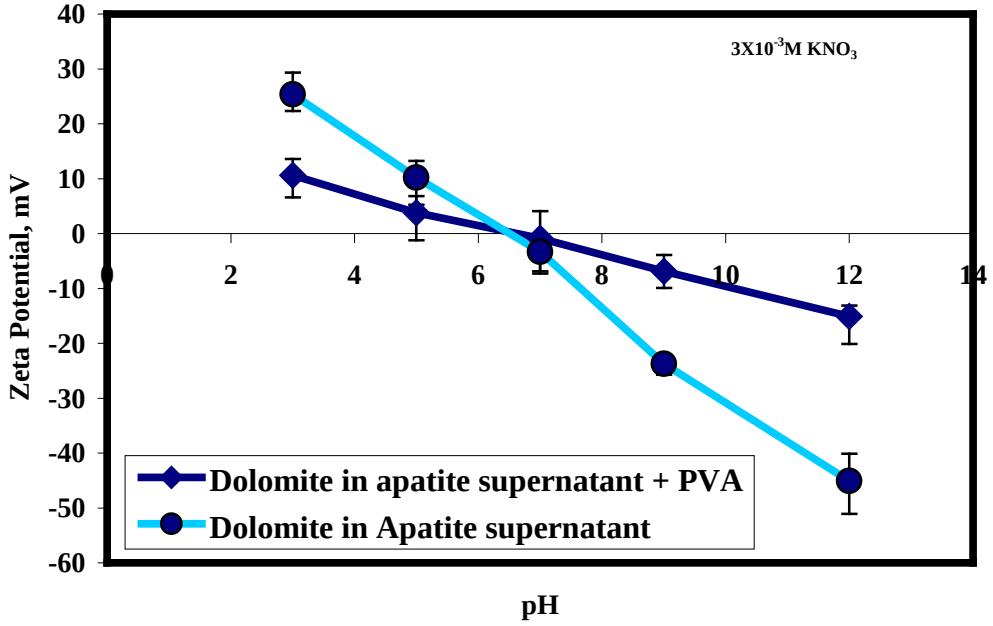

Figure 31. Zeta Potential of Dolomite in Apatite Supernatant Before and After PVA Adsorption.

The same argument mentioned in the previous paragraph can be applied to the adsorption of PVA on apatite in a dolomite supernatant. The results of the zeta potential of these systems are shown in Figure 32.

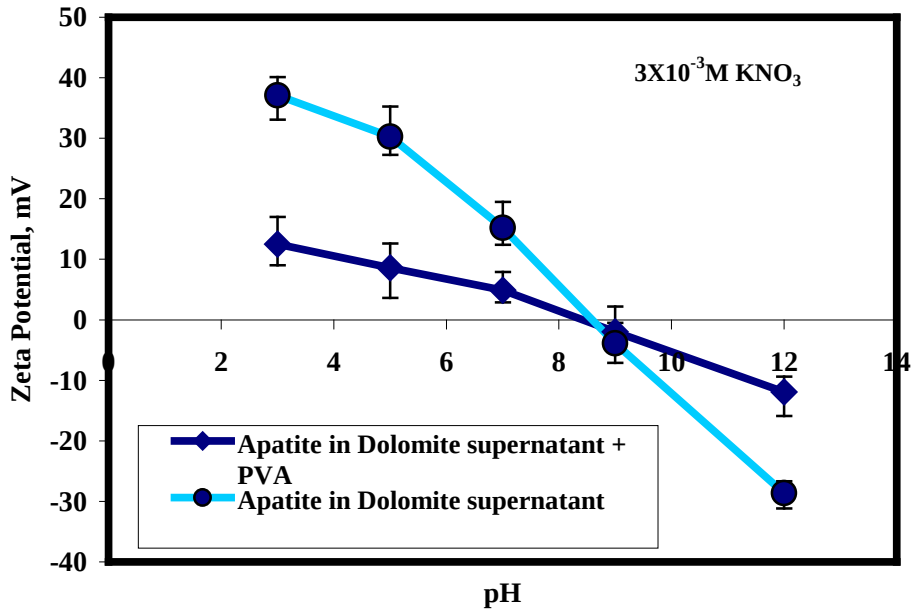

Figure 32. Zeta Potential of Apatite in Dolomite Supernatant Before and After PVA Adsorption.

Infrared (FTIR)

The FTIR spectra of the powders, both with and without polymer adsorbed to them, were compared in order to illustrate the mechanisms of adsorption of PVA on dolomite and apatite surfaces. This method was applied in previous studies (Kiselev and Lygin 1975; Pradip and Moudgil 1991; Howard and McConnel 1967a, b; Behl and Moudgil 1993; Bjelopavlic and others 2000; Zaman and others 2002; Mathur and Moudgil 1997; Moudgil and Prakash 1998) to explain polymer-solid interactions. The major peaks for dolomite and apatite are identified according to Ince and others (1991).

FTIR spectroscopic studies were carried out on the dolomite and apatite and polymer samples both before and after adsorption. The assignments of the various bands and peaks made in this study are in reasonable agreement with those reported in the literature for similar functional groups (Finch 1973; Chanchani 1986; Ince 1987).

The FTIR spectrum of PVA is shown in Figure 33. A broad band is displayed at 3450 cm^{-1}, which may be attributed to hydrogen-bonded surface hydroxyl groups. The sharp band at 2930 cm^{-1} is due to strong C-H stretching. The band at 2860 cm^{-1} is a result of shoulder C-H stretching. The transmission band at 1650 cm^{-1} is due to the presence of moisture in the sample. The band at 1460 cm^{-1} can be attributed to O–H and C-H bending. These results are in good agreement with the spectra of PVA reported by other workers (Finch 1973, 1992).

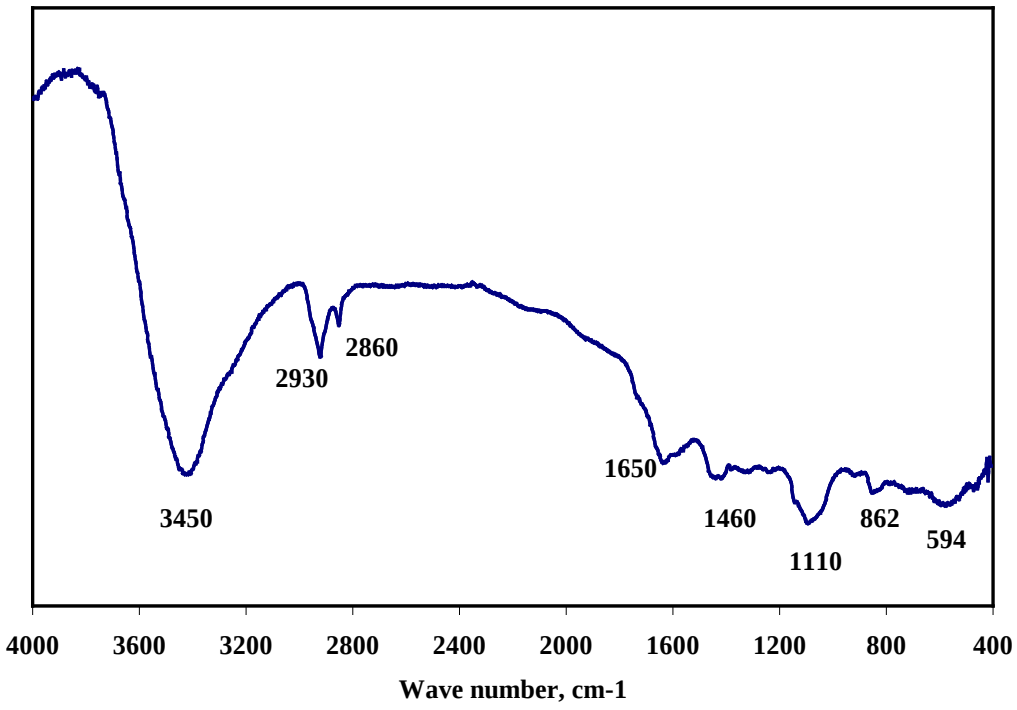

Figure 33. Infrared Spectra (FTIR) of Polyvinyl Alcohol (PVA).

The FTIR spectra of the bare dolomite sample as well as those that had previously interacted with PVA are shown in Figure 34. The isolated hydroxyl group peak is present in dolomite powder without polymer, but the spectrum of dolomite in presence of the polymer does not show this peak. Moreover, the peak intensity of the hydrogen-bonded hydroxyl groups is smaller in case of the powder with the polymer than without. These observations indicate that the adsorption of PVA on dolomite occurs by hydrogen bonding involving –OH groups of the polymer. This finding is in concurrence with earlier studies on silica-PEO (Rubio and Kitchener 1976; Cheng 1985) and silica-polyacrylic acid PAA (Tadros 1978), which showed that the presence of isolated OH-groups on the surface was responsible for the adsorption of polymer molecules by hydrogen bonding.

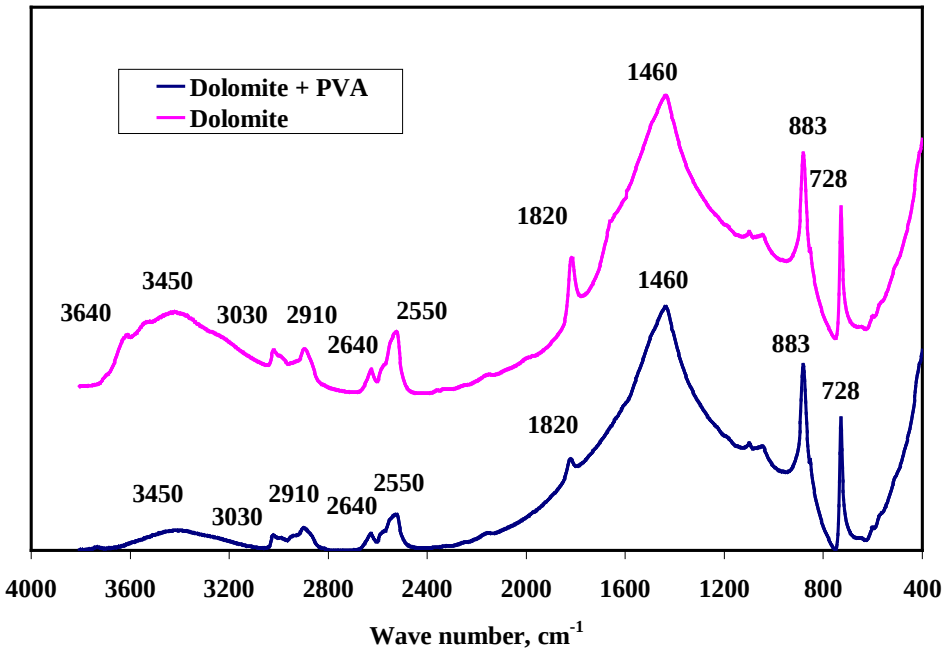

Figure 34. Infrared Spectra (FTIR) of (a) Dolomite Alone, and (b) Dolomite/PVA System.

The FTIR spectrum of the apatite sample after having interacted with PVA is shown in Figure 35. However, unlike the case of dolomite, this figure indicates that the adsorption mechanism of the polymer on apatite is not clarified by using FTIR—no change is shown in the bands' intensities or positions, either for bare apatite or apatite with polymer adsorbed on it. This finding is in agreement with the previous reports (Chanchani 1986; Ince 1987). It is pertinent to mention that FTIR spectroscopic studies on the dolomite-PVA and apatite-PVA systems revealed the presence of hydrogen bonding only.

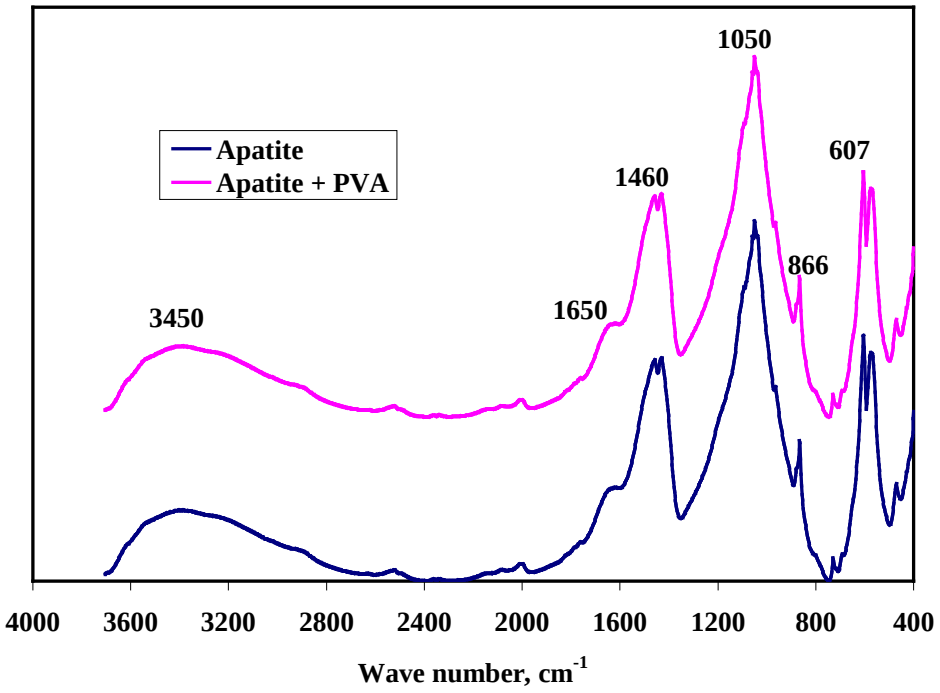

Figure 35. Infrared Spectra (FTIR) of (a) Apatite Alone, and (b) Apatite/PVA System.

Kinetics of Adsorption

A study of the kinetics of adsorption to determine the equilibrium time is fundamentally important for understanding its mechanism. The rate by which equilibrium is established during adsorption depends on the chemical nature of the polymer and its molecular weight, the solvent, and the type of adsorbent. In most cases, the kinetic curves indicate an increase in the amount of adsorbed polymer over time, with an asymptotic approximation of the equilibrium value (Lipatov and Sergeeva 1974).

The adsorption of polymers on solid surfaces may occur by a three-step mechanism (Dijt and others 1990; Somasundaran and Ramachandran 1988). First, the polymer is diffused from the bulk to the interface. Second, adsorption of the polymer molecules occurs on the initially bare solid surface. Finally, polymer conformation and orientation changes in the surface layer to accommodate the adsorption of more polymer molecules.

To ascertain the time required for the adsorption equilibrium to be attained, kinetic tests were carried out at the natural pH of 7 for 24 hours and using PVA at a concentration of 100 ppm (6.7×10^{-7} M). Figure 36 shows results of PVA adsorption onto dolomite and apatite as a function of time. It is evident that the equilibrium is attained at about one hour. The equilibrium values are 0.04×10^{-6} and 0.011×10^{-6}

mole/m^2 for dolomite and apatite respectively. Based on these findings, a 2-hour conditioning time was selected for the adsorption studies.

It was observed that the adsorption followed a typical second order adsorption process. The second order model predicts the behavior over the whole range of adsorption. The second order rate expression (Oezacar 2003) based on solid capacity is generally expressed as follows:

$$\frac{d\Gamma}{dt} = k(\Gamma eq - \Gamma)^2 \qquad \text{Equation (4)}$$

or, by integration

$$\Gamma = \frac{t}{\frac{1}{k\Gamma_{eq}^2} + \frac{t}{\Gamma_{eq}}} \qquad \text{Equation (5)}$$

where Γ is adsorption density (mole/m^2), Γ_{eq} is equilibrium adsorption density (mole/m^2), K is the second order adsorption rate constant (hr^{-1}), and t is time (hr).

By fitting the experimental data to Equation 5, the parameters Γ_{eq} and K were determined. These are listed in Table 20.

Table 20. Fitting Parameters of 2nd Order Kinetic Model.

Sample	$\Gamma_{eq} \times 10^{-6}$ mole/m^2	K, hr^{-1}
Dolomite	0.04	361.6
Apatite	0.011	200

It can be seen from Table 20 and Figure 36 that the equilibrium adsorption values Γ_{eq} for dolomite and apatite match the experimental data. Most importantly, the higher Γ_{eq} value for dolomite indicates the presence of more available sites for PVA adsorption than on apatite. Moreover, the K_{ad} for dolomite is higher than that for apatite, indicating a higher adsorption rate on dolomite. However, the plateau was reached at almost the same time for both minerals.

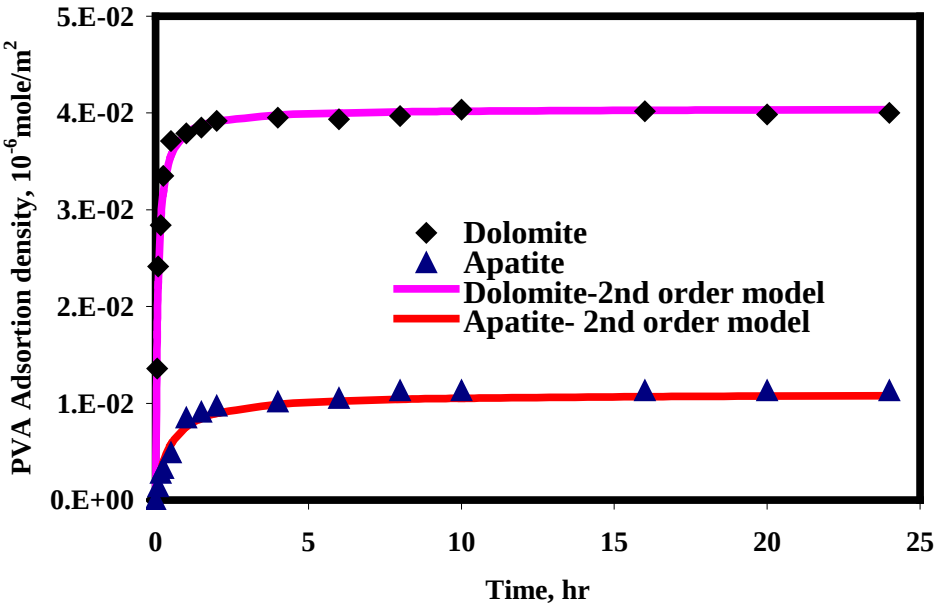

Figure 36. Kinetics of PVA Adsorption on Dolomite and Apatite (Initial PVA Concentration 6.7×10^{-7} M, pH 7, 2×10^{-3} M KNO_3 and 23° C).

Adsorption Isotherm

Most polymer adsorption isotherms from dilute solutions can be visually represented as curves that reach saturation at specific concentrations (Lipatov and Sergeeva 1974). It is important to note that polymers may adsorb on surfaces in various conformations depending on bulk (solvent) and surface chemical properties of the substrate, as well as other physical conditions of the system (Hong and others 2001).

At low concentrations, the polymer chains behave like isolated coils. If the polymer concentration in the solution is raised, the chains become close to each other, which allows polymer-polymer intermolecular interactions to influence the motion of the polymer chains. The effects may be expected to be cumulative until the concentration leads to chain-overlapping or close packing of the polymer coils in solution. Once the overlapping concentration has been reached, the polymer motion will be dominated by the presence of direct polymer-polymer interaction. As the polymer concentration is increased, the polymer diffusivity decreases. If the concentration increases even further, a pseudo-matrix-gel will be formed. The resulting viscosity is governed mainly by intermolecular interaction, which is related to the overlapping of the polymer chains (Izmailova and others 1975; Goetze and Sonntag 1987; Andreyeva and others 1973; Babayevskii and others 1986; Koopal and others 1988).

For PVA, –OH is the only functional group (Koopal and Lyklema 1979; Chibowski and Pazkiewicz 1995; Chibowski and others 2000). Increasing the degree of hydrolysis reduces acetate groups, which usually show preferential adsorption. Thus, the conformation of the polymer chain at the solid-polymer solution interface will depend on the number of acetate groups in a PVA macromolecule. The lower the degree of hydrolysis, the flatter the polymer chains will be on the solid surface. Conversely, at a high degree of hydrolysis, the polymer chains should be oriented perpendicularly to the surface (Santhiya and others 1999; Sjoberg and others 1999; Bajpai and Vishwakarma 2003; Koopal and Lyklema 1979). This conformation of the PVA macromolecule will favor the adsorption of the polymer on the surfaces of dolomite and apatite, which is shown in Figures 37 and 38. In a different system, Chibowski (1998) reported that the adsorption of PVA on alumina increased with an increase in the degree of hydrolysis. In this study, it was found that fully hydrolyzed PVA gave better results than PVA of a lower degree of hydrolysis.

The adsorption density (mol/m^2) of fully hydrolyzed PVA (acetate groups < 1%) on the minerals' surface as a function of the initial polymer concentration (0 to 4×10^{-6} mole) was determined at 23° C and a pH 7 for dolomite and apatite. The results obtained are presented in adsorption isotherm plots (Figures 37 and 38 for dolomite and apatite, respectively).

These adsorption isotherms show a plateau for both apatite and dolomite. This result suggests that the observed increase in PVA adsorption is caused mainly by the change in conformation of the polymer chain at the minerals' surface. Following this change, a number of active sites on the surface become available for further adsorption of polymer molecules. As mentioned previously, the greater porosity of apatite leads to a high number of available adsorption sites and subsequently to the horizontal stretching of the polymer to cover these sites. This, in turn, explains the lower adsorption layer thickness and higher parking area on apatite.

The shape of the adsorption isotherms shown in Figures 37 and 38 is typical for physical adsorption and is an acceptable shape for that range of polymer molecular weight (Adamson and Gast 1997).

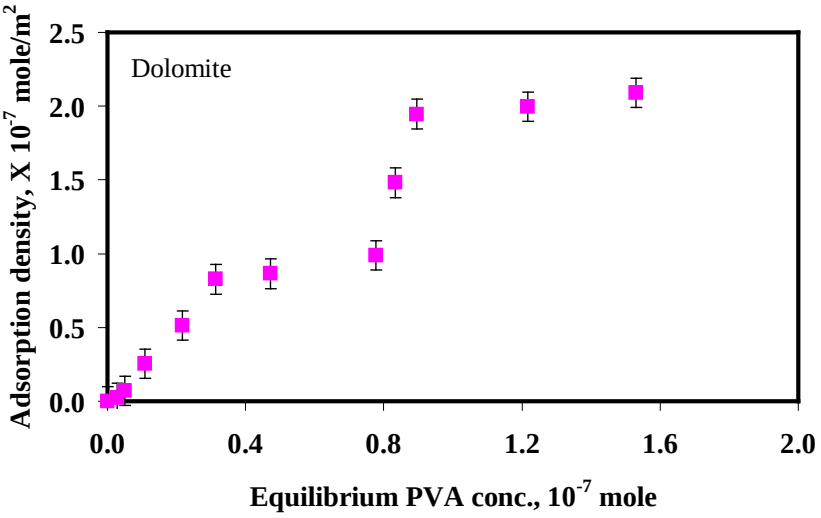

Figure 37. Adsorption Isotherm of PVA on Dolomite at 23° C.

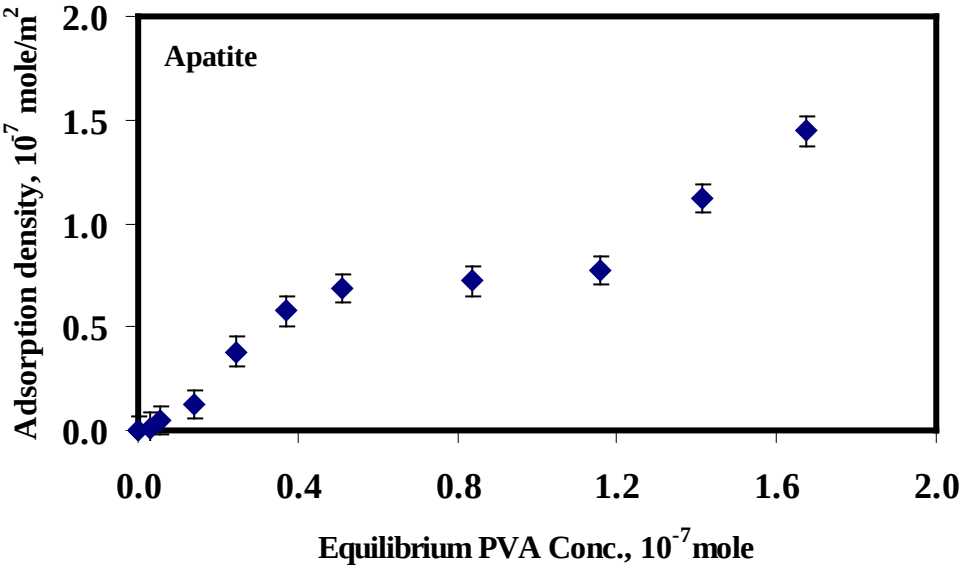

Figure 38. Adsorption Isotherm of PVA on Apatite at 23° C.

It is clear from the figures that the adsorption isotherm is S-shaped, which suggests physical adsorption of PVA onto the dolomite and apatite surfaces.

Calculation of PVA Adsorption and Parking Area

The amount of adsorbed PVA is calculated using the following formula:

$$\Gamma = \frac{(C_i - C_r) * V}{m * SA}$$

where Γ is the amount of PVA adsorption (mole/m^2), (C_i-C_r) is the PVA concentration on the particle (mole/ml), C_i is the initial PVA concentration, C_r is the residual PVA concentration, V is the volume of solution (ml), m is the mass of dolomite or apatite particles (g), and SA is the specific surface area of particles (dolomite 0.9 and apatite 1.48 m^2/g).

The parking area of PVA molecules is calculated using the following formula:

$$\text{Parking area} = \frac{\left(\frac{1 \times 10^{18} \times Mw}{\Gamma}\right)}{Av}$$

where MW = 150,000 g/mole, Av is Avogadro's number (6.023 × 10^{23} #/mol), and the parking area is nm^2/#. The calculated parking areas for dolomite and apatite at the first plateau are (23.72 nm^2) and (75.47 nm^2), respectively. Taking into account that the surface area per stretched molecule is 0.2 nm^2 (Koopal and Lyklema 1979), it was observed that the PVA molecule forms a wavy or zigzag shape on the solid particles with the higher thickness on the dolomite particles. Moreover, this conformation appears on dolomite at lower relative concentration range.

It is worth noting that in the case of dolomite the adsorption isotherm is both steeper and reaches a plateau at lower concentrations than in case of apatite. The observed results may be explained based on the following hypothesis, which is schematically illustrated in Figure 39: macromolecules are generally more tightly bound to surfaces due to the multiple points of attachment. The figure shows the conformation of a single polymer chain (39a) and/ or several chains (39b).

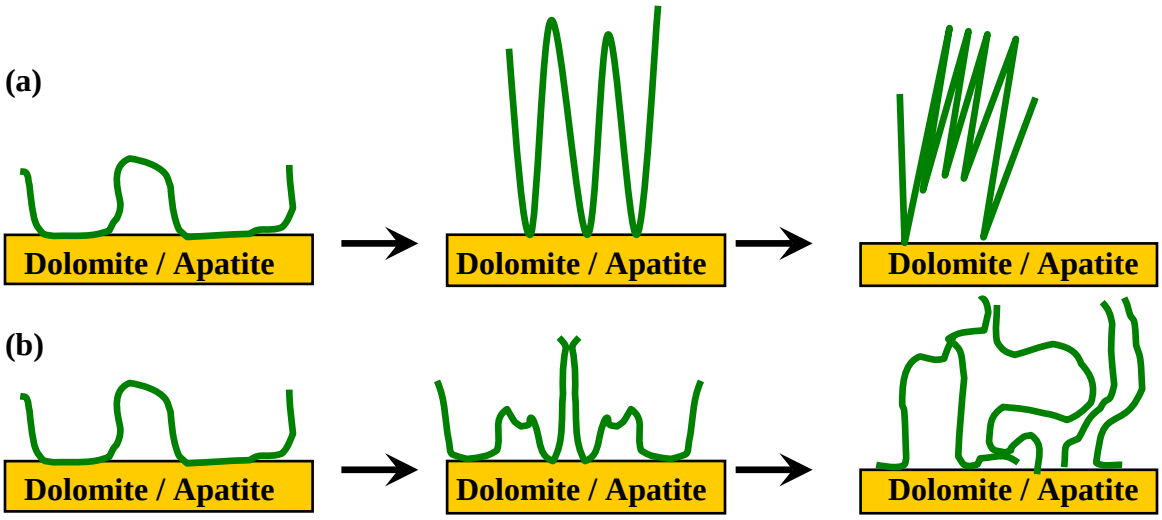

Figure 39. Polymer Conformation Change with Increasing Concentration: (a) Conformation of a Single Molecule; (b) Conformation of More than One Molecule.

It may be concluded that without intermolecular H-bonds, spiral conformations of PVA are favorable and zigzag conformations are expected when intermolecular H-bonds are present.

Adsorbed Layer Thickness

The thickness of PVA layer adsorbed on dolomite and/or apatite can be calculated from the adsorption isotherm by using the following relationship:

$$h = \frac{\Gamma}{\rho}$$

where h is the adsorbed layer thickness, m; Γ is adsorption density, g/m^2, and ρ is PVA density, g/m^3.

Using this relationship, the thickness of the adsorbed layer was found to be 27 nm on dolomite and 9 nm on apatite, which indicates that the vertical polymer chains are stretched three times longer in the case of the dolomite than in the case of the apatite. This explains the higher adsorption densities that were obtained on dolomite in comparison to apatite since, according to this conformation, the polymer chains occupy a smaller number of sites. In addition, more sites are available on dolomite than on apatite.

Note that the length of the PVA molecule of this molecular weight is about 600 nm, which indicates the polymer conformation would be like that shown in Figure 39b.

Factors Affecting Adsorption

The surface charges on salt-type minerals such as apatite and dolomite are generally controlled by the M^{+2}, MOH^{+}, $M(OH)_2$, and $MHCO_3^{+}$ sites at the surface. Specifically, for dolomite the surface sites are Mg^{++}, Ca^{++}, CO_3^{--}, HCO_3^{-}, OH^{-}, $MgHCO_3^{+}$, $MgOH^{+}$, $Mg(OH)_2$, $CaHCO_3^{+}$, $CaOH^{+}$, $Ca(OH)_2$ and those for apatite are Ca^{++}, HPO_4^{--}, $CaOH^{+}$, $Ca(OH)_2$, $H_2PO_4^{-}$, $CaH_2PO_4^{+}$. The nature of the mineral surface, pH, the presence of solutes, and the functional group of the polymer all affect the adsorption behavior. Previous studies on different minerals (i.e., alumina, silica, kaolin, clays) showed that the OH group of PVA is mainly responsible for adsorption on the surface of minerals (Santhiya and others 1999; Sjoberg and others 1999; Bajpai and Vishwakarma 2003).

Effects of pH

The effect of pH on the adsorption of PVA onto dolomite and apatite is shown in Figure 40. It can be seen that adsorption is pH-dependent in the studied range of 2 to 12.

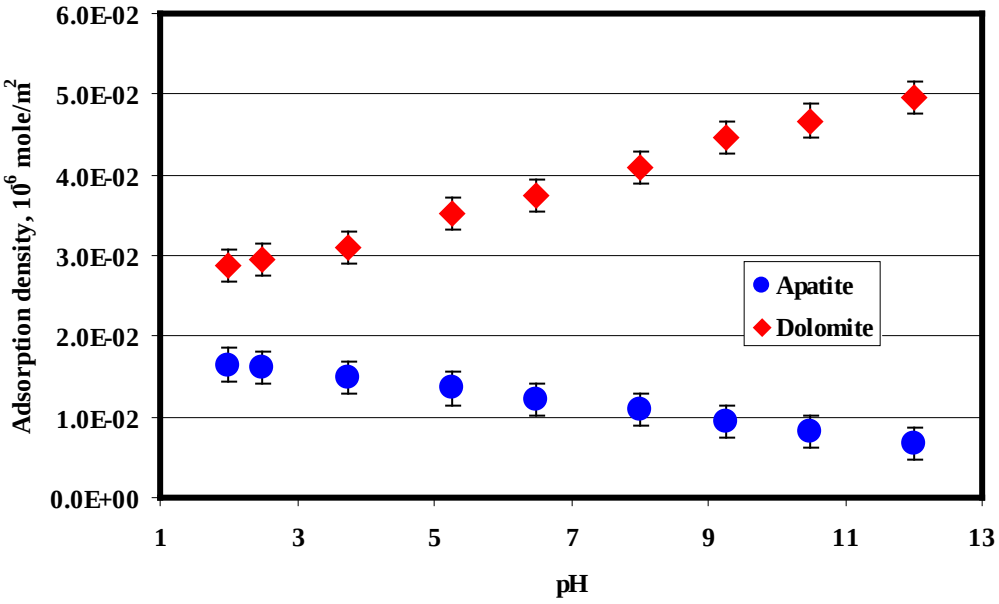

Figure 40. Effect of pH on Adsorption of PVA on Apatite and Dolomite.

Studying the adsorption of PVA on both minerals gives evidence that the adsorption is due to the formation of hydrogen bonding between the dolomite or apatite surface and the OH- polymer functional groups.

Effects of pH on Apatite

It is evident from Figure 40 that the adsorption density decreases with an increase in the pH. The decrease in the adsorption density as a function of pH may be explained by taking into consideration the surface charge of the apatite particles as well as the surface species, both of which are dependent on pH. It is interesting to note that the decrease of $CaH_2PO_4^+$ and $H_2PO_4^-$ species, according to the apatite activity chart (Attia and Fuerstenau 1989), in the whole pH range are responsible for formation of hydrogen bonding. Moreover, both the increase in the number of high negatively dissociated groups like PO_4^{-2}, CO_3^{-2}, HPO_4^{-2} and the increase in the repulsion among these species adversely affects the formation of hydrogen bonding (Rachas and others 2000).

Effects of pH on Dolomite

It can also be seen in Figure 40 that the adsorption density of dolomite increases with an increase in the pH. This increase of adsorption with pH can be attributed to the hydroxylation of the dolomite surface, which enhances its hydrogen-bonding capacity. Additionally, it has been reported in some cases that at the acidic pH, the decrease in PVA adsorption can be caused by some or all of the following factors: loss of the most active binding sites for PVA bonding, reduction of the affinity for nonionic compounds by a salting-out effect, the screening effect of hydrated counter-ions, or preferential adsorption of water molecules at those ionized sites (Barker and Garvey 1980; Bonekamp and others 1989; Platonov and others 1979; Zhang and others 1996; Hidber and others 1995; Santhiya and others 1998).

Desorption

To ascertain whether or not the adsorption process is reversible, desorption tests were carried out by interacting the sample containing the adsorbed polymer with distilled water for a specified period and analyzing the supernatant solution for residual polymer content. The results are shown in Figures 41 and 42. Comparing these data with the results shown in Figures 43 and 44, it is evident that about 20% of the polymer could be desorbed, confirming the relatively weaker nature of this particular interaction with dolomite and apatite.

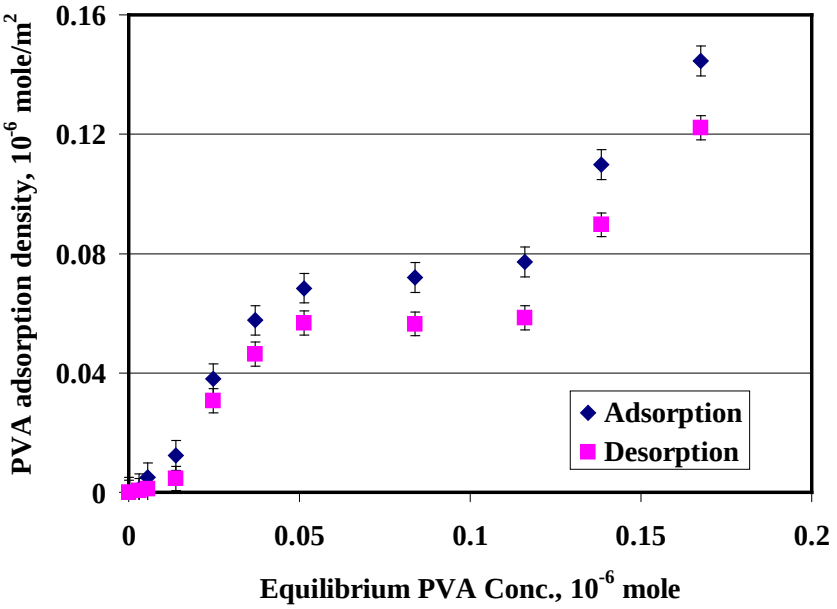

Figure 41. Desorption of PVA from the Apatite Surface.

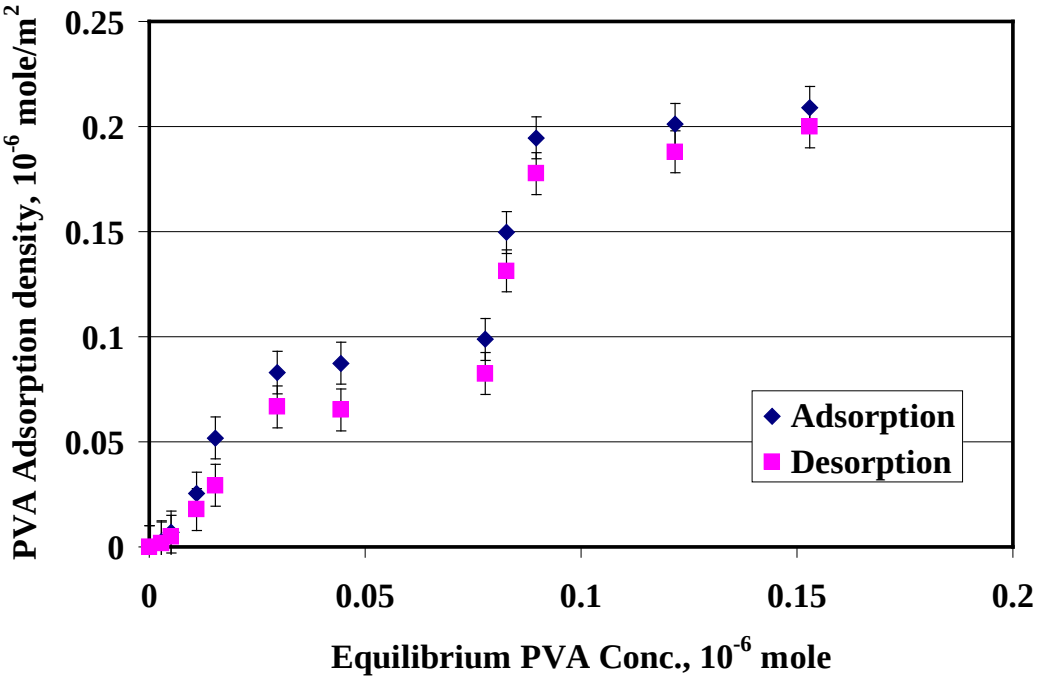

Figure 42. Desorption of PVA from the Dolomite Surface.

Desorption in Acidic Solution

Since the reactive flotation process requires adding PVA coated particles to an acidic medium, desorption of PVA in an acidic solution was studied to simulate the RF process. Desorption data show almost no desorption in both cases of dolomite and apatite. This behavior confirms that the formation of polymer cluster at the particle/solution interface is enhanced by the presence of SO_4^{-2} ions, which is one of the most ionic species leading to cross-linking of the polymer chains (Finch 1973, 1992; Yahya and others 1996).

Adsorption in Supernatants

The results of adsorption of PVA on apatite in a dolomite supernatant solution and dolomite in an apatite supernatant solution are given in Figure 43. The adsorption density is lower than that obtained in water, possibly due to the presence of several ionic species that may affect the polymer aggregation. The observed high adsorption density on dolomite, on the other hand, could be due to the presence of more sites, as mentioned previously.

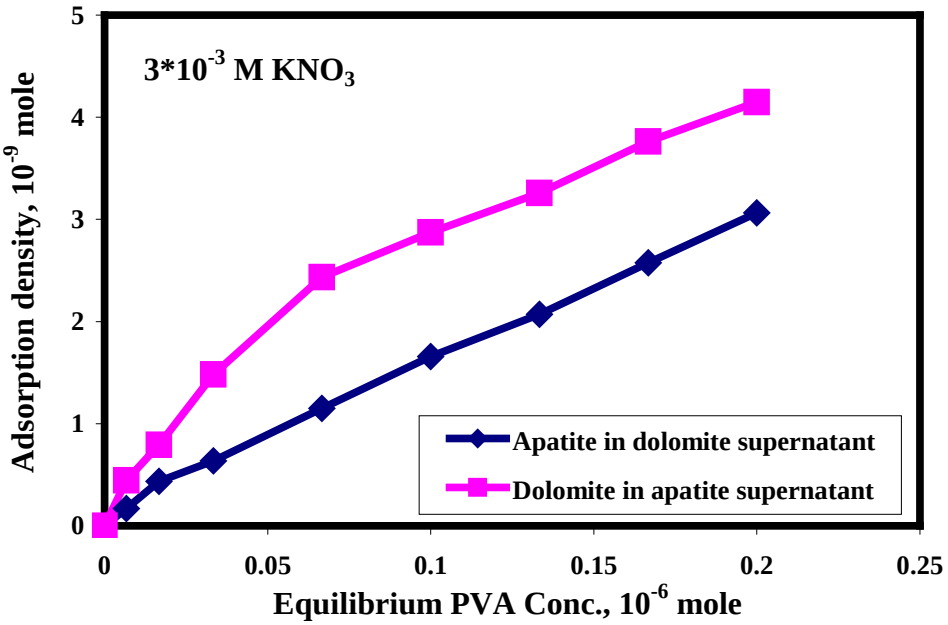

Figure 43. Adsorption Isotherm of Apatite in Dolomite Supernatant Solution, and Dolomite in Apatite Supernatant Solution.

Reactive Flotation Kinetics

The reactive flotation (RF) process, as mentioned earlier, includes two main steps: (1) the coating step, which was discussed in detail in the previous section, and (2) the

reaction step. In the second step, the sulfuric acid penetrates the polyvinyl alcohol (PVA) membrane and reacts with the dolomite surface. CO_2 gas is one of the reaction products according to the following reaction:

$$Ca\ Mg\ (CO_3)_2 + 2H_2SO_4 \rightarrow CaSO_4 + MgSO_4 + 2CO_2 + 2H_2O$$

Because PVA is known for its very low permeability to gases (Finch 1992), the CO_2 will accumulate between the particle and the membrane, causing the dolomite particles to be of lower density. A schematic illustration of the mechanism of bubble formation during the reaction and how the density changes is given in Figure 44.

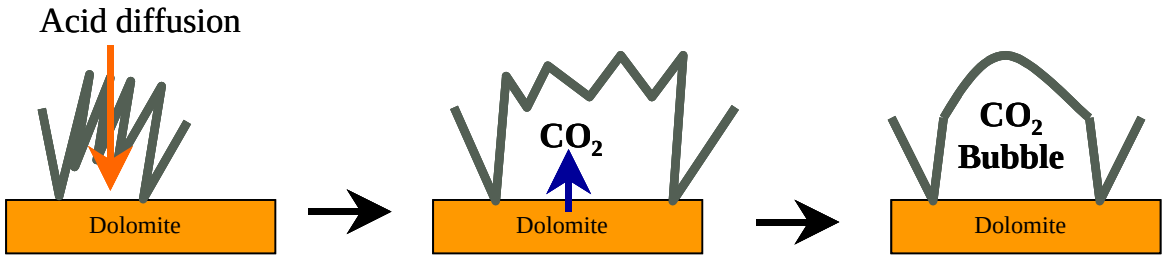

Figure 44. Bubble Formation Mechanism.

To predict the required amount of CO_2 to float the particle, the modeling of the acid reaction with the dolomite surface and bubble formation was essential. In this section, different modeling efforts are discussed and the CO_2 production rate and the amount of CO_2 required to float the particle are calculated. Furthermore, the results are correlated with dynamic surface tension (DST) measurements to predict the membrane elasticity at a certain CO_2 flow rate. Figure 45 shows a schematic diagram of the requirements to achieve flotation by the RF process.

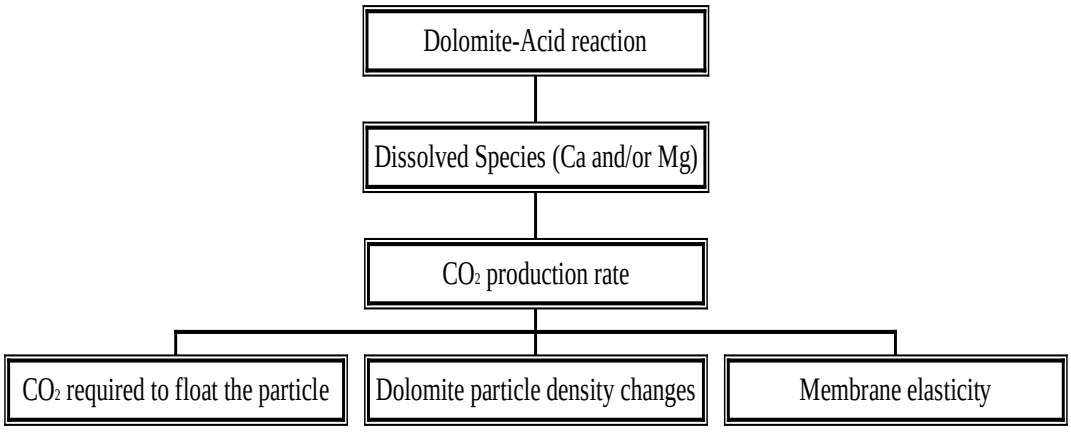

Figure 45. Schematic Diagram of Reaction Kinetics of the RF Process.

Chemical Analysis of Samples Used in the Kinetic Study

The experiments were carried out with two particle size fractions (0.2-0.3, and 1-2 mm). The chemical analyses of these two fractions are given in Table 21.

Table 21. Chemical Analysis of the Samples Used in Kinetic Tests.

Size, mm	MgO%	P_2O_5%	CaO%	Al_2O_3%	Fe_2O_3%	I.R.%	L.O.I. %
-2+1	14.48	2.82	32.6	1.02	1.56	11.2	32.12
-0.3+0.2	15.36	2.45	31.47	0.99	1.34	10.95	34.37

It can be seen from Table 21 that the analyses of the two samples are approximately the same. It is expected that the very small differences, as shown in the analyses, will have a negligible effect on the results of the kinetic tests.

Effect of the Particle Size

Different particle sizes were tested in solutions containing 3% sulfuric acid. The results of reacting uncoated particles with acid at room temperature (23 ± 1°C), are shown in Figures 46-47 in terms of dissolved Ca and Mg, respectively. In all of the experiments, the solid loading in the reactor was 10% by weight.

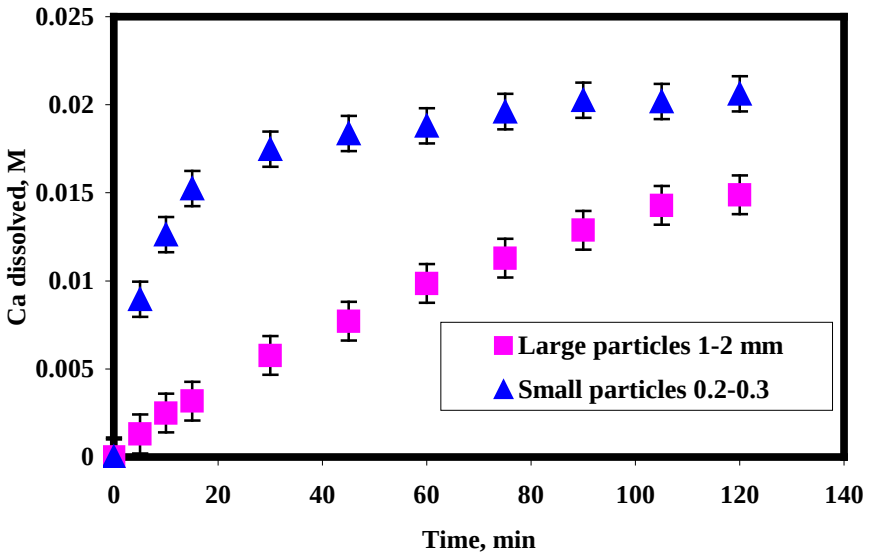

Figure 46. Dissolution Kinetics of Different Particle Sizes in Terms of Calcium Ions in a 3% Sulfuric Acid Solution at 23° C.

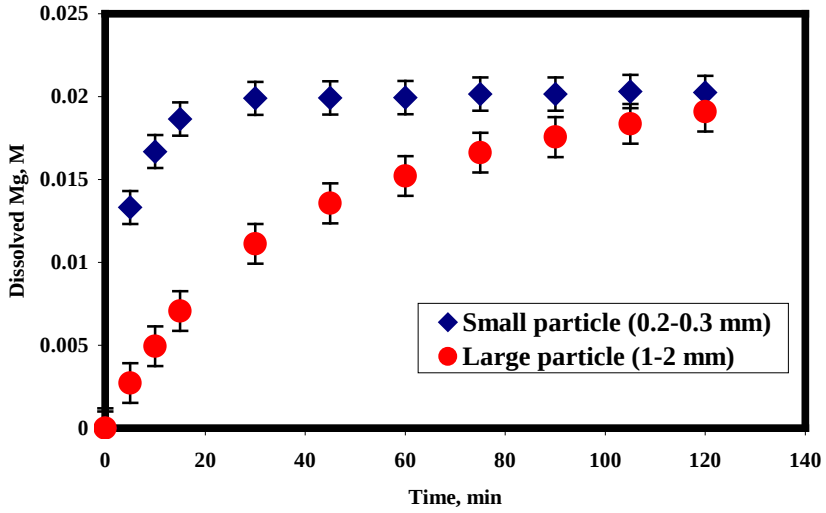

Figure 47. Dissolution Kinetics of Different Particle Sizes in Terms of Magnesium Ions in 3% Sulfuric Acid Solution at 23° C.

Formation of an Insulating Layer

The H^+ transport is perturbed by the presence of the reaction products and since the H^+ has a higher diffusivity, the reaction continued until it reached the point of equilibrium. At this point, the H^+ can no longer reach the surface due to the formation of an insulating layer of reaction products, most probably gypsum, $CaSO_4 \cdot 2H_2O$ and/or a CO_2 gas layer around the particle. This was especially true in the case of coated particles.

Effect of PVA Coating

The reaction was tested with the particles having been coated with PVA. Figure 48 shows the results of both coated and uncoated particles. The curve is steeper in the case of uncoated particles and the curves for both coated and uncoated reach a plateau after 30 and 40 minutes, respectively. This can be explained by the presence of a polymer that controls the transfer of ions to and from the boundary layer and then to the bulk solution. In addition, formation of the products occurs in a confined place (between the membrane and the particle surface), which also leads to a decrease in the saturation point and helps in rapid nucleation and growth of hydrated calcium sulfate ($CaSO_2 \cdot 2H_2O$), i.e., gypsum. Such a possibility exists in the case of a calcite-sulfuric acid system, providing that the solubility products are 2.5×10^{-5} M^2 for ($CaSO_4 \cdot 2H_2O$) (Culberson and others 1978) and 4.8×10^{-9} M^2 for ($CaCO_3$) (Stark and Wallace 1982). Moreover, the accumulation of CO_2 works as a diffusion barrier as well.

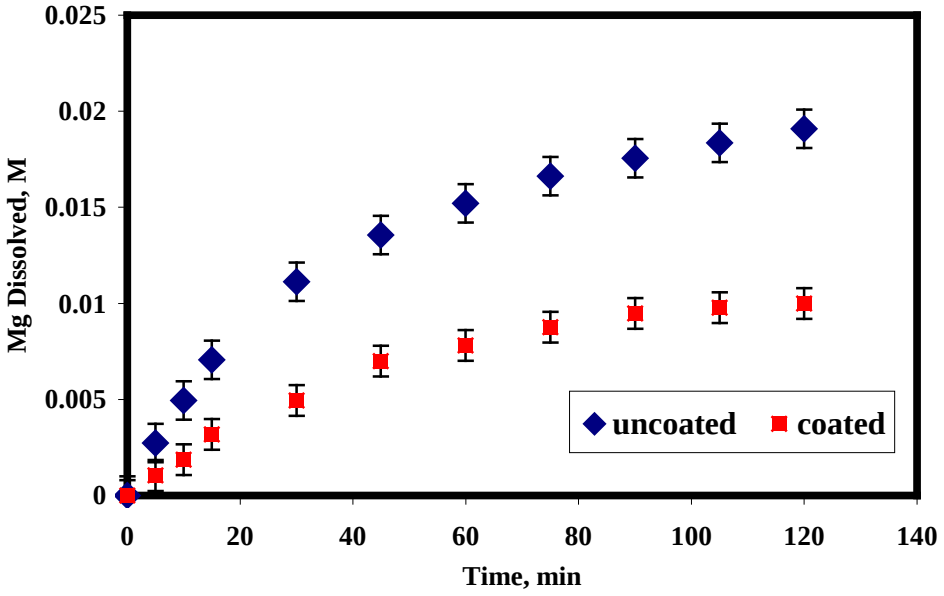

Figure 48. Dissolution Kinetics of Coated and Uncoated 0.2-0.3 mm Dolomite Particles in a 3% Sulfuric Acid Solution at 23° C.

Bubble Formation and Growth

Figure 49 (a-e) shows the growth of bubbles on the dolomite particle surface with time. The reaction starts immediately after adding the particles to the acidic solution. The bubbles then grow as a result of the evolution of CO_2, the impermeability of the PVA membrane, and the stretching of that membrane. If this membrane is not flexible enough, it will rupture and CO_2 gas will be released, leaving the particle without causing any flotation. It is also interesting to notice the rapid growth of bubbles within a few seconds.

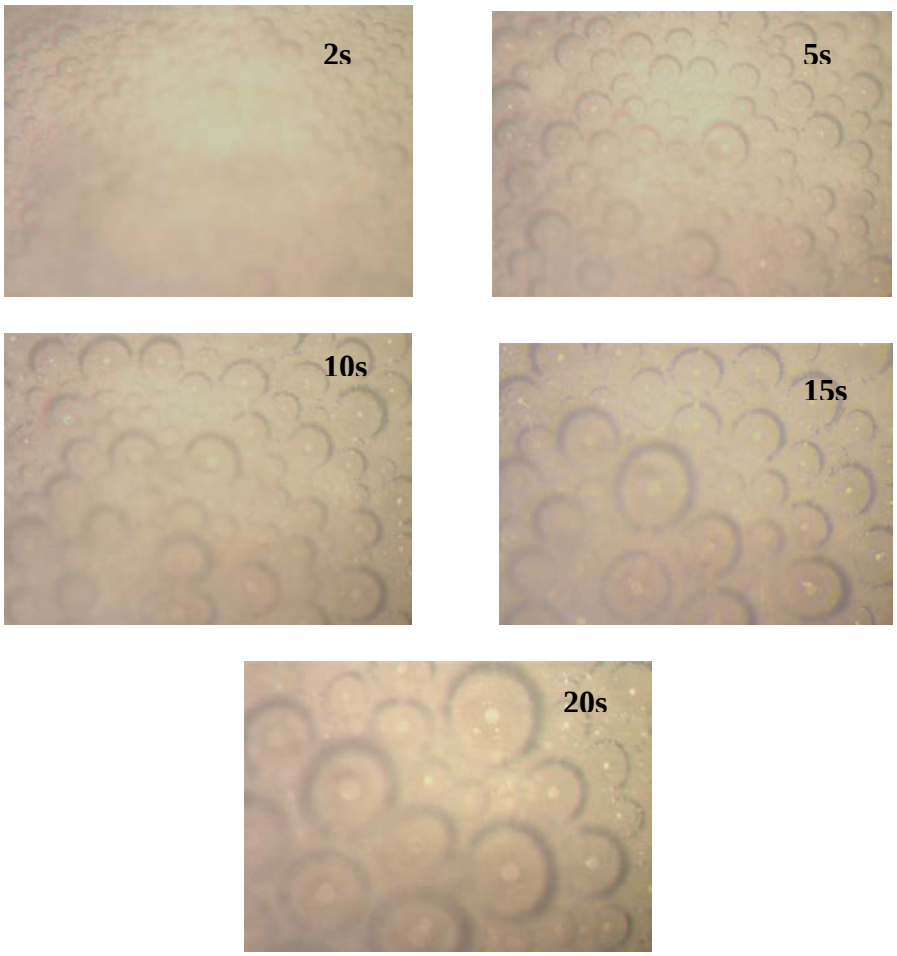

Figure 49. Growth of Bubbles with Time on the Dolomite Particle Surface (50 X).

Modeling of Bubble Formation and Dolomite-Particle Separation

In the present study, two models were developed to explain the phenomena associated with the RF process. These models depend on the mechanisms controlling the dissolution process. The two mechanisms studied are (a) blockage of acid and (b) depletion of the active sites. The main purpose of these models is to predict the amount of CO_2 evolved and the consequent density changes of the dolomite particles, which leads to its separation. The details of each model are explained in the following paragraphs.

Blockage of the Acid Model

In this model, the reaction depends on the transfer of the acid to the particle surface; the products of the reaction then diffuse out to the bulk solution. The formation of the reaction products, i.e. Ca-sulfate and/or CO_2 gas, prevents the acid's accessibility to the surface and stops the reaction.

For simplicity of calculations, the sphericity of the particle, homogeneity of the coating around the particle, and presence of a barrier to CO_2 gas transfer are assumed. The equations of this model are:

$$\frac{dC_{mi}}{dt} = K_r A C_{ai} + K_m A(C_{mi} - C_{mo})$$

$$\frac{dC_{ai}}{dt} = -K_r A C_{ai} + K_a A(C_{ao} - C_{ai})$$

$$\frac{dC_{mo}}{dt} = \gamma K_m A(C_{mi} - C_{mo})$$

$$\frac{dK_m}{dt} = -\alpha A C_{ai}$$

$$\frac{dK_a}{dt} = -\beta A C_{ai}$$

where:

C_{mi} :concentration of Mg at the surface, M
C_{mo} : concentration of Mg in the bulk, M
C_{ai} : concentration of acid at the surface, M
A : surface area, cm^2
K_r : reaction rate coefficient, $cm^{-2}\cdot min^{-1}$
K_a : transfer coefficient, $cm^{-2}\cdot min^{-1}$
K_m : transfer coefficient, $cm^{-2}\cdot min^{-1}$
α and β : coefficients, $M^{-1}\ cm^{-4}\cdot min^{-2}$
γ : ratio between the boundary layer volume to total solution volume (Vi/Vo)

Fitting of this model to the experimental data is given in Figures 50 and 51 for both size fractions. The fitting parameters are given in Table 22.

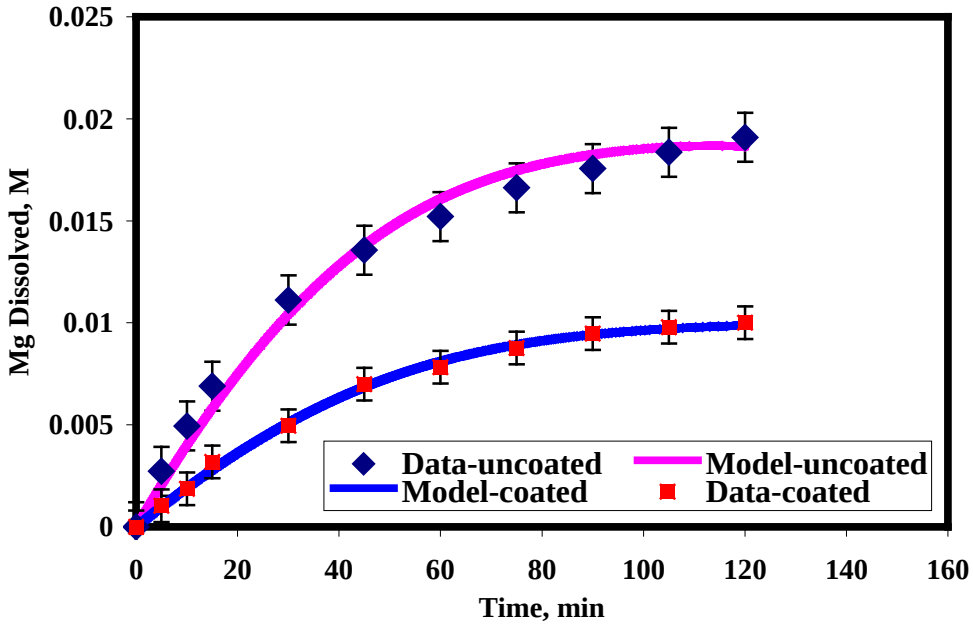

Figure 50. Acid Blockage Model Fitting to 1-2 mm Experimental Data.

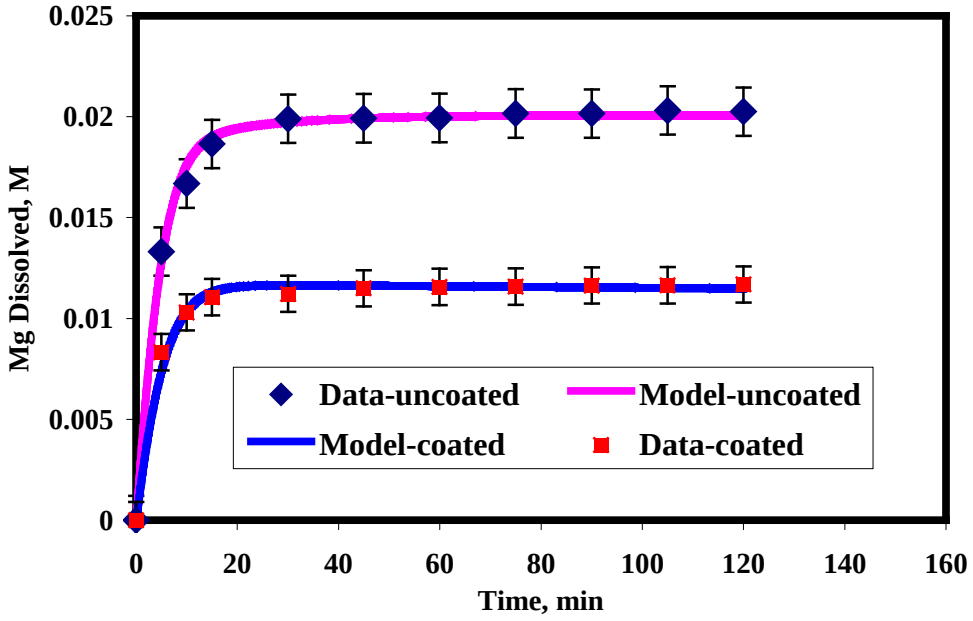

Figure 51. Acid Blockage Model Fitting to 0.25-0.35 mm Experimental Data.

Table 22. Acid-Blockage Model Parameters.

Parameter	Large		Small	
	Uncoated	Coated	Uncoated	Coated
*P-1	3	3	8.99	8.99
α	0.67	0.67	9	9
β	0.37	0.46	8.3	8.32
γ	0.00038	0.00085	0.0012	0.002
*K_m'	5.97	5.97	10.04	10.1
*K_a'	3.29	3.29	9.27	9.26

P-1 = $K_r A$ $K_m' = K_m A$ $K_a' = K_a A$

This model shows no difference in all its factors between coated and uncoated particles except γ, which increases in the case of coated particles. The γ increase can be explained by the swelling of the membrane due to the formation of CO_2 gas, which increases the internal boundary layer volume at constant external volume. The increase in P-1 for small particles is due to the increase in the number of sites with which the acid can react.

Disappearance of Active Sites Model

In this model, the reaction depends on the availability of the active sites at the particle surface. The depletion and disappearance of these sites will lead to cessation of the reaction. The disappearance of active sites may be due to formation of a passive layer from the reaction products, i.e., Ca-sulfate and/or CO_2 gas. In this way the acid is available to react, but there are no active sites to react with. Once again, for simplicity of calculations, the sphericity of the particle, absence of an acid barrier, constancy of acid concentration, homogeneity of the coating around the particle, and presence of a barrier to CO_2 gas transfer are assumed.

$$\frac{dC_{mi}}{dt} = K_r A C_{ao} + K_m A(C_{mo} - C_{mi})$$

$$\frac{dC_{mo}}{dt} = \gamma K_m A(C_{mi} - C_{mo})$$

$$\frac{dA}{dt} = -K_r A C_{ao}$$

where:

C_{mi} : concentration of Mg at the surface, M
C_{ao} : concentration of acid in the bulk, M (assuming C_i=C_o)

A : surface area, cm^2 concentration of Mg at the surface, M
C_{mo} : concentration in the bulk, M
K_m : transfer coefficient, $cm^{-2} \cdot min^{-1}$
K_r : reaction rate coefficient, $cm^{-2} \cdot min^{-1}$
γ : ratio of volume of boundary layer to the volume of the bulk (Vi/Vo)

Fitting of this model to the experimental data is given in Figures 52 and 53 for both size fractions. The fitting parameters are given in Table 23.

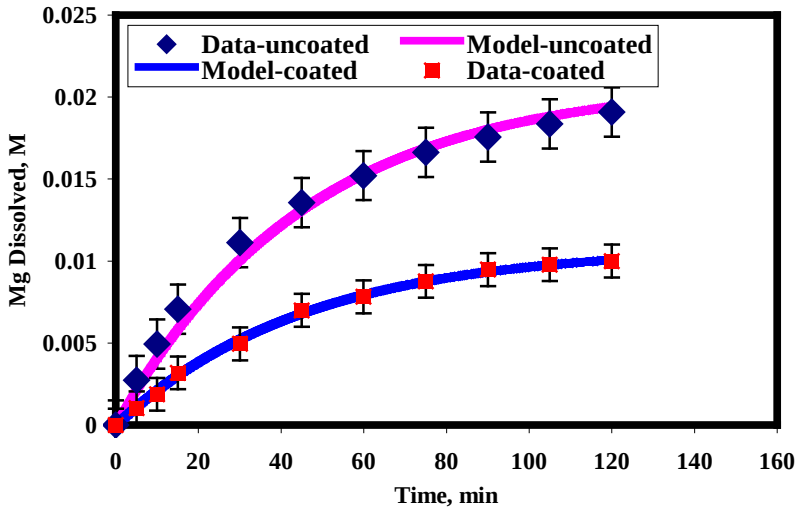

Figure 52. Active Sites Disappearance Model Fitting to 1-2 mm Data.

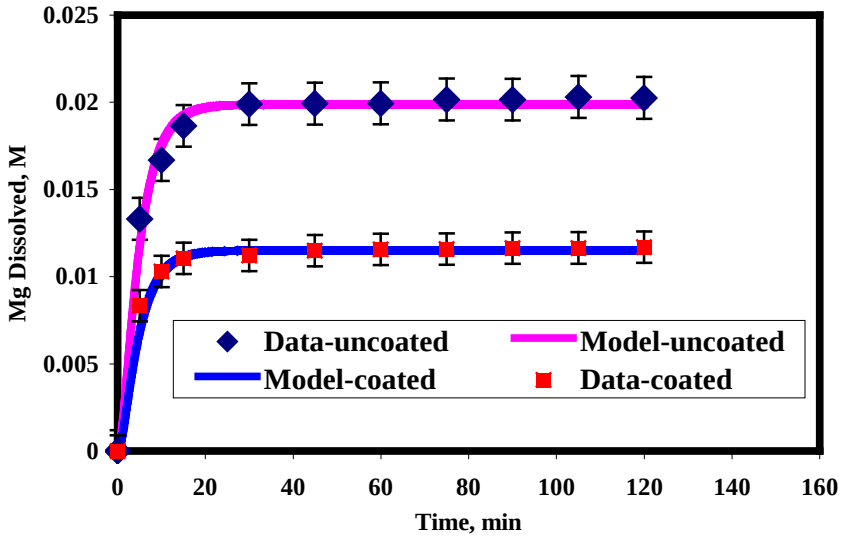

Figure 53. Active Sites Disappearance Model Fitting to 0.25-0.35 mm Data.

Table 23. Active Sites Disappearance Parameters.

Parameter	Large		Small	
	Uncoated	Coated	Uncoated	Coated
*P-1	3	3	8.99	8.99
γ	0.00038	0.00085	0.0012	0.002
*K_m'	5.97	5.97	10.04	10.1
K_a	3.29	3.29	9.27	9.26

P-1 = K_r A $K_m' = K_m$ A $K_a' = K_a$ A

In this case also, this model shows no difference in P-1, K_m, and K_a between coated and uncoated particles. The only difference is in the value of γ, which increases in the case of coated particles. The reason behind this increase is the constant external volume and increase of the internal volume since the polymer does not permeate the CO_2.

Estimation of CO_2 Required to Float the Dolomite Particles

Simple calculations were used to predict the size of the particle with its surrounding envelope of gas and to estimate the relation between the radius of the particle before and after the formation of the gas bubbles around the particles. For simplicity, the following conditions were assumed: spherical particle, uniform gas layer around the particle, and at equilibrium condition: The part of the particle dissolved in the reaction was also neglected in the calculations.

As a starting point, we assume that the particle starts to float when the density of the particle and the gas layer around it is less than the density of acidic solution. The calculations are as follows:

$$\text{density (Dolomite} + CO_2 \text{ gas)} < \text{density (acidic solution)}$$

$$\left(\frac{M_d + M_g}{V_d + V_g}\right) < \frac{M_w}{V_w} = 1\,\text{gm/cm}^3 \quad (M_g \cong 0)$$

$$M_d < V_d + V_g$$

$$\frac{2.9 * 4\pi}{3} r^3 < \frac{4\pi}{3} r^3 + \frac{4\pi}{3}(r_1^3 - r^3)$$

$$\frac{2.9 * 4\pi}{3} r^3 < \frac{4\pi}{3} r_1^3$$

$$(\sqrt[3]{2.9})r < r_1$$

$$r_1 > 1.4\,r$$

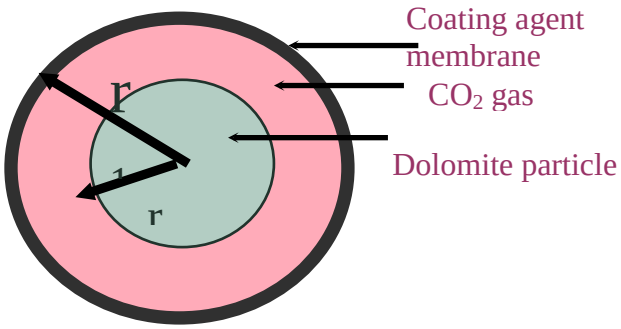

Where:
M_d : mass of dolomite particle
M_g : mass of CO_2 gas
M_w : mass of water
V_d : volume of particle
V_g : volume of CO_2 gas
V_w : volume of water
R: particle radius
R_1 : total radius (particle + gas)

In addition, the ratio between gas volume and particle volume and the ratio between the gas volume and particle surface area were calculated as follows:

Gas volume : particle volume

$$\frac{V_g}{V_d} = \frac{\frac{4\pi}{3}(r_1^3 - r^3)}{\frac{4\pi}{3}r^3} \quad and \quad r_1 \geq 1.4r$$

$$\frac{V_g}{V_d} = \frac{[(1.4)^3 r^3 - r^3]}{r^3}$$

$$\frac{V_g}{V_d} = (1.4)^3 - 1 = 1.75$$

$$V_g = 1.75 V_d$$

Gas volume : particle surface area

$$\frac{V_g}{S_d} = \frac{\frac{4\pi}{3}(r_1^3 - r^3)}{4\pi r^2}$$

$$\frac{V_g}{S_d} = \frac{((1.4)^3 r^3 - r^3)}{3r^2}$$

$$\frac{V_g}{S_d} = \frac{((1.4)^3 - 1)r}{3} = 0.58r$$

From the previous calculations, we can deduce that the total radius is 140% of the original radius of the particle (without taking the dissolved part of the particle and the pores volume into account). The volume of gas around the particle is approximately twice the original particle radius. A larger particle needs more volume of gas to float due to its lower surface area.

Change in Density

The density change can be calculated according to the sequence in Figure 53. The model will be used to calculate the number of moles of Mg, which consequently will give the number of moles of CO_2 through the equation of chemical reaction. Using the CO_2 density, the volume of CO_2 gas can be calculated. The volume generated in certain period of time can then be used to calculate the average flow rate of CO_2 as it evolves. This flow

rate can be used to calculate the change in the density as well as to correlate that change to membrane elasticity at different flow rates.

Figure 54 shows the change in dolomite particle density as a function of reaction time. It is very rapid due to the CO_2 build up in the RF process.

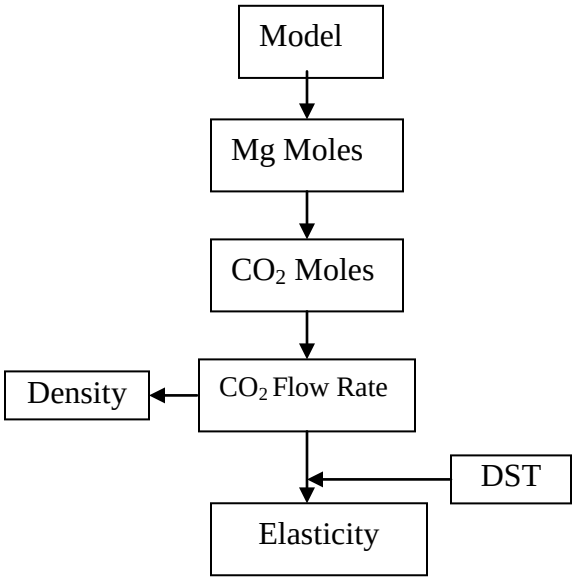

Figure 54. Sequence of Calculating the Particle Density and Membrane Elasticity.

The density of the dolomite particles changes rapidly due to intense reaction in the first 20-30 seconds; after that the rate of change decreases dramatically (Figure 55). The change is sharper in the case of the smaller particles due to their higher surface area and greater amount of CO_2 generated. The density can be calculated by:

$$\rho_f = \frac{\rho_p \times V_p}{V_p + V_g}$$

where:

ρ_f : floated particle density, g/cm^3,
ρ_p: particle density, g/cm^3,
V_p: particle volume, cm^3, and
V_g: gas volume, cm^3

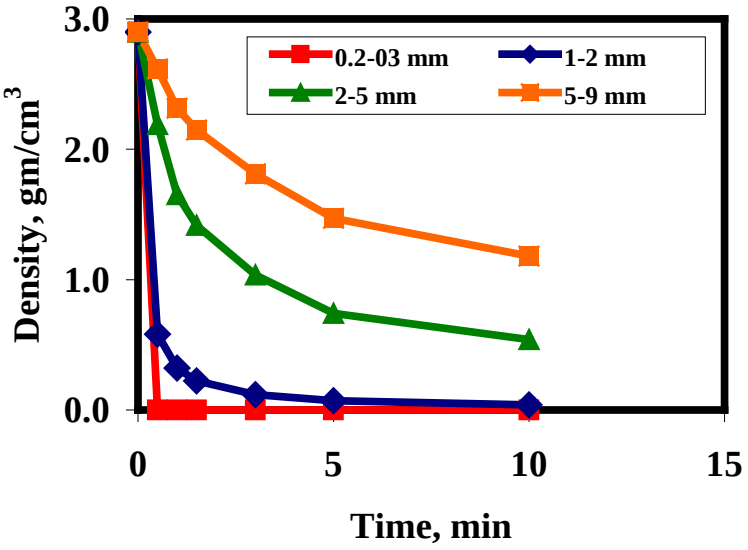

Figure 55. Density Changes for Different Particle Sizes.

Dynamic Surface Tension

As the reaction transpires at the dolomite particle surface, the CO_2 gas produced affects the growing bubbles in terms of their stability, i.e., the stretching and elasticity of the polymer due to gas-pressure on the adsorbed polymer layer. Presence of the surfactant or polymer adsorbed at either the gas-liquid or liquid-liquid interface leads to the viscoelastic properties of that interface. These properties may be characterized by the surface dilatational modulus, which is defined according to Gibbs's equation (Johnson and Stebe 1996; Lunkenheimer and others 1996; Pikhitsa and Tsargorodskaya 2000):

$$E = \frac{d\gamma}{d \ln A}$$

where γ is the dynamic surface tension (DST) and A is the geometric area of the surface.

For that reason, the Dynamic Surface Tension (DST) measurements using the Maximum Bubble Pressure Technique were determined at different gas flow rates: 0.23, 0.47, 0.78, and 1.55 cm^3/min. In Figure 56, the experimental DST data for PVA solutions of different concentrations are given. These results show the change in DST as a function of the increase in polymer concentration. Clearly, at PVA polymer concentrations of up to 1%, the surface tension significantly decreases as compared to the surface tension of water. Over the concentration range from to 1% to 3%, the surface

tension decreases gradually, but at greater concentration levels the surface tension remains nearly constant.

The decrease in surface tension can be described, according to the Ward and Tordai model (Pefferkorn and others 1985; Nahringbauer 1995; Fainerman and Miller 1996), as a diffusion controlled adsorption process. For a short time scale (from milliseconds to seconds) the equation can be written as

$$\Gamma(t) = 2c_0\left(\frac{Dt}{\pi}\right)^{1/2}.$$

where:

Γ the surface concentration at any time, (g m^{-2}),
C_o the bulk concentration, (g m^{-2}),
C_s the surface concentration, (g m^{-2}), and
D the monomer diffusion coefficient, (m^2 s^{-1}).
π: The commonly used value
t: time, (s)

It is interesting to note that the observed decrease in surface tension is more pronounced at lower flow rates—the greater the increase in the flow rate, the smaller the variation in the DST. This can be referred to as the time needed for the polymer to get onto the newly formed interfacial region. Therefore, at high flow rates, the bubbles' surfaces remain almost clean and the effect of the polymer as an active agent at the interfacial region will be less because the polymer molecules do not have enough time to adsorb onto it. The lower the flow rate, the higher the chance for the polymer molecules to adsorb onto the interface of the generated bubbles.

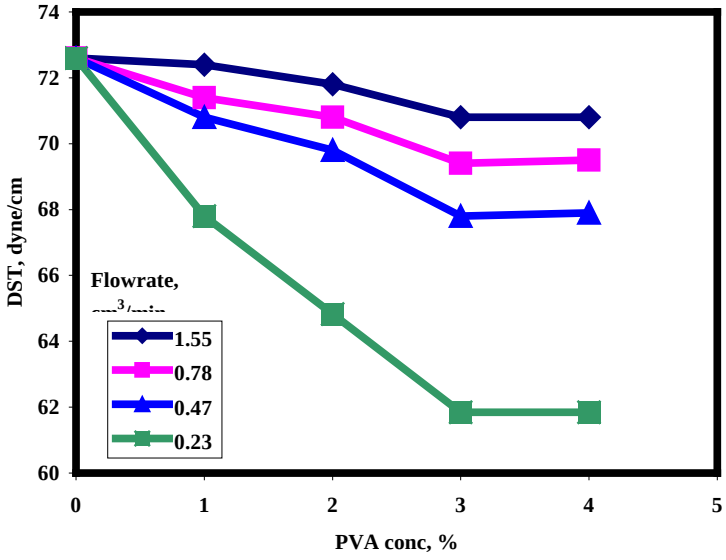

Figure 56. Dynamic Surface Tension of PVA Concentration at Different CO_2 Flow Rates.

Figure 57 shows the results of using Gibbs equation to determine the elasticity in terms of PVA concentration at a different CO_2 gas flow rate.

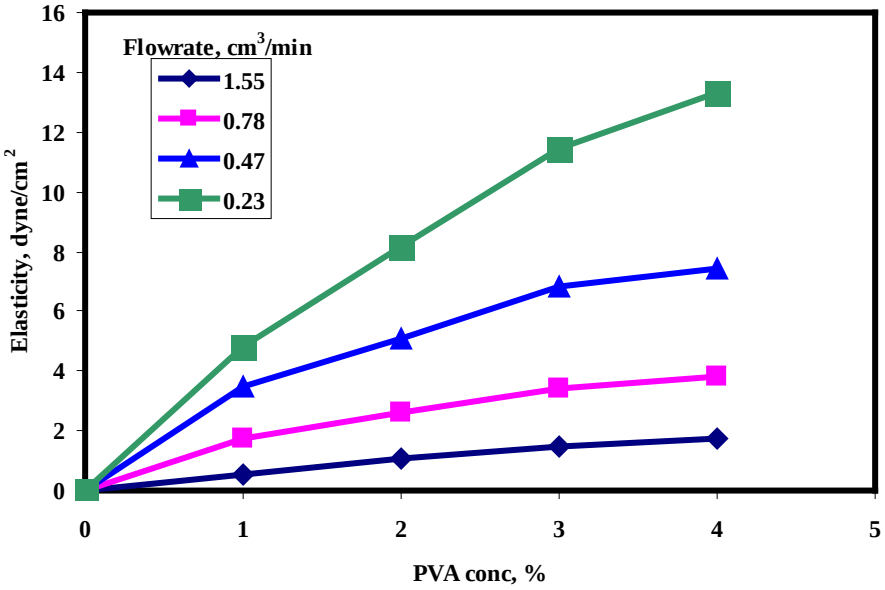

Figure 57. Elasticity of PVA Membrane in Terms of PVA Concentration at Different CO_2 Flow Rates.

It is interesting to note that the elasticity increases with PVA concentration. This is due to formation of a membrane as a result of increasing the polymer concentration, which is able to resist the pressure exerted by the CO_2 gas generated. However, the higher the bubble formation rate (gas flow rate), the lower the elasticity. This can be referred to as the lower diffusivity of the polymer to the bubble surface and, consequently, DST at high bubble speeds. The flow rate of CO_2 generation due to the reaction was found to be very low, which is closer to equilibrium conditions. This also indicates higher membrane elasticity.

PROCESS ECONOMICS

Although the RF process equipment is not totally defined, it is possible to give a ballpark estimate for at least the operating cost for processing high MgO rock. The process will consist of rock crushing (to 1-2 mm), spray-coating the crushed rock with PVA, and then separation of the rock in a sluice like device using 3% sulfuric acid. Chemical consumables will be sulfuric acid and PVA.

The minimum sulfuric acid consumption would be that required to generate a volume of CO_2 that is about twice the volume of dolomite in the rock. At high MgO (6%) this can be as much as 50% of the rock. At a dolomite density of 2.5, the volume of the dolomite would be about 6.5 cubic feet. Twice this would be 13 cubic feet or about 0.036

moles of CO_2 gas. This would require 0.036 moles of sulfuric acid or 3.6 pounds of sulfuric acid. At $25/ton, this would represent a cost of less than 5 cents per ton of rock feed. However, it is likely that more sulfuric acid will be lost as entrainment with the rock and dolomite streams. It will be assumed that a volume of the 3% sulfuric acid equal to the volume of the feed rock is lost. This would mean that 13 cubic feet of 3% sulfuric acid solution would be lost per ton of feed or 25 pounds of sulfuric acid per ton of feed. At $25/ton of sulfuric acid this is a cost of $0.32 per ton of feed.

PVA consumption has been demonstrated to be as low as 1 pound per ton of feed. However, this is under laboratory conditions. For commercial purposes, consumption will be assumed to be 1.5 pounds per ton. At $1.20 per pound for PVA, this is a cost of $1.80/ton of feed.

Electricity will be required for rock crushing, pumping of the 3% sulfuric acid solution, operation of the spray coating system, and conveying the rock to and from the sluice system. Without a detailed layout drawing, it is not possible to accurately estimate the total electrical consumption. However, it should be less than 15 KWH per ton, or less than $1.00/ton of feed for any practical system.

The total of chemical and electrical operating costs will then be less than $3.12/ton of feed. Of course, operating labor, maintenance, depreciation etc must still be added to come up with a total cost. These would not only be dependent on the details of the process equipment, but on the scale of the operation. At 10,000 tons/day of feed, these are not likely to exceed $2.50/ton.

CONCLUSIONS

- In this study, the reactive flotation (RF) process was developed with a high potential to separate dolomite from phosphate rock at high recoveries.

- A sluice or sluice like device gives the best separation of the dolomite and apatite. Typically the rock recovered contains over 90% of the phosphate with a MgO content of less than 1%.

- Consumption of PVA as low as 1 pound per ton can give good separation of the apatite and dolomite.

- The 3% sulfuric acid solution used for the reactive flotation can be reused even when saturated with calcium with no reduction in effectiveness.

- The PVA coating remaining on the processed rock does not inhibit the ability of the rock to react in the phosphoric acid reactors.

- While chemical plant pond water could be used instead of the 3% sulfuric acid solution, it is not quite as effective.

- Chemical consumption costs are estimated to be less than $2.15 per ton of feed.

- Electrical consumption costs re estimated to be less than $1.00 per ton of feed.

- Operating labor, maintenance, analytical, depreciation etc cost is estimated to be less than $2.50 per ton of feed for a 10,000 ton per day plant.

REFERENCES

Adamson A, Gast A. 1997. Physical chemistry of surfaces. 6th edition. New York: Wiley. 525 p.

Amankonah JO, Somasundaran P. 1985. Effects of dissolved mineral species on the electrokinetic behavior of calcite and apatite. Colloid and Surfaces 15(3-4): 335-53.

Andreyeva VM, Anikeyeva AA, Lirova BI, Tager AA. 1973. Investigation of PVA solutions. Polymer Science USSR 15(8): 1991-8.

Attia YA, Fuerstenau DW. 1989. The equilibrium composition of hydroxyapatite and fluorapatite-water interfaces. Colloids and Surfaces 34(3): 271-86.

Babayevskii PG, Kozlov NA, Trostyanskaya EB. 1986. Effect of water on physical transformations and viscoelastic properties of sparse-network polyvinyl alcohol. Polymer Science USSR 28(2): 475-82.

Bajpai AK, Vishwakarma N. 2003. Adsorption of polyvinyl alcohol onto Fuller's earth surfaces. Colloids and Surfaces A: Physicochemical and Engineering Aspects 220(1-3): 117-30.

Barker MC, Garvey MJ. 1980. The effect of solvency on the adsorption of poly(vinyl alcohol) onto polystyrene latex. Journal of Colloid and Interface Science 74(2): 331-40.

Behl S, Moudgil BM. 1993. Mechanisms of poly(ethylene oxide) interactions with dolomite and apatite. Journal of Colloid and Interface Science 161(2): 443-9.

Biehn GF, Ernsberger ML. 1948. Polyvinyl alcohol as an emulsifying agent. Journal of Industrial and Engineering Chemistry 40: 1449-53.

Bjelopavlic M, Singh P, El-Shall H, Moudgil BM. 2000. Role of surface molecular architecture and energetics of hydrogen bonding sites in adsorption of polymers and surfactants. Journal of Colloid and Interface Science 226(1): 159-165.

Bonekamp BC, van't Veen WH, Schoute MJ, Veringa HJ. 1989. Deflocculation of aqueous α-Al_2O_3 suspensions in the presence of adsorbing polymer and polyelectrolyte. In: de With G, Terpstra RA, Metselaar R, editors. Euro-ceramics (Proceedings of the First European Ceramic Society Conference), Vol. 1, Processing of ceramics; 1989 Jun 18-23; Maastricht, The Netherlands. London: Elsevier Science. p 145.

Burt RO. 1984. Gravity concentration technology. Developments in mineral processing. Volume 5. Amsterdam: Elsevier Science Publishers. p 605.

Chanchani R. 1984. Selective flotation of dolomite from apatite using sodium oleate as collector [DPhil thesis]. Gainesville (FL): University of Florida. 272 p.

Chander S, Fuerstenau DW. 1982. On the dissolution and interfacial properties of hydroxyapatite. Colloids and Surfaces 4(2): 101-20.

Cheng YC. 1985. The effect of surface hydration on the adsorption and flocculation of a model silica suspension using polyethylene oxide [MS thesis]. Gainesville (FL): University of Florida.

Chibowski S. 1996. Investigation of the mechanism of polymer adsorption on metal oxide - water solution interface. Adsorption Science and Technology, 14: 179-188.

Chibowski S, Paszkiewicz M. 1995. Studies of the effect of acetate groups in the molecule of poly(vinyl alcohol) on its adsorption on TiO_2. Polish Journal of Chemistry 69(3): 461-6.

Chibowski S, Paszkiewicz M, Krupa M. 2000. Investigation of the influence of the polyvinyl alcohol adsorption on the electrical properties of Al_2O_3-solution interface and thickness of the adsorption layers of PVA. Powder Technology 107(3): 251-5.

Culberson CH, Latham G, Bates RG. 1978. Solubilities and activity coefficients of calcium and strontium sulfates in synthetic seawater at 0.5 and 25º C. Journal of Physical Chemistry 82(25): 2693-9.

Deurbrouck AW, Agey WW. Wet concentrating tables. Chapter 5, Section 4: Gravity concentration. In: Weiss NL, editor. SME Mineral Processing Handbook, Vol. 1. New York: Society of Mining Engineers. p 4-32 to 4-39.

Dijt JC, Stuart MA, Hofman JE, Fleer GJ. 1990. Kinetics of polymer adsorption in stagnation point flow. Colloids and Surfaces 51: 141-58.

El-Shall HE. 1994. Evaluation of dolomite separation techniques: final report. Bartow (FL): Florida Institute of Phosphate Research. FIPR publication nr 02-094-108.

Fainerman VB, Miller R, Joos P. 1994. The measurement of dynamic surface tension by the maximum bubble pressure method. Colloid and Polymer Science 272(6): 731-39.

Fainerman VB, Miller R. 1996. Adsorption kinetics of short-chain alcohols at the water/air interface: diffusion-controlled adsorption under the conditions of a nonequilibrium surface layer. Journal of Colloid and Interface Science 178(1): 168-75.

Finch CA. 1973. Polyvinyl alcohol; properties and applications. New York: John Wiley and Sons. 622 p.

Finch CA. 1992. Polyvinyl alcohol—developments. New York: John Wiley and Sons. 850 p.

Garrett PR, Ward DR. 1989. A reexamination of the measurement of dynamic surface tensions using the maximum bubble pressure method. Journal of Colloid and Interface Science 132(2): 475-90.

Goetze T, Sonntag H. 1987. The effect of solvent quality on the interaction between two layers of adsorbed polyvinyl alcohol (PVA). Colloids and Surfaces 25(1): 77-90.

Hanna J, Anazia I. 1990. Selective flotation of dolomitic limestone impurities from Florida phosphates: final report. Bartow (FL): Florida Institute of Phosphate Research. FIPR publication nr 02-066-089.

Harkins WD. 1928. Surface energy and the orientation of molecules in surfaces as revealed by surface energy relations. Surface relations reveal surface energy and orientation of the molecules in surfaces. Z. Physik. Chem. 139 (Abt. A): 647-91.

Hidber PC, Graule TJ, Gauckler LJ. 1995. Competitive adsorption of citric acid and poly(vinyl alcohol) onto alumina and its influence on the binder migration during drying. Journal of American Ceramic Society 78(7): 1775-80.

Hong P-D, Chou C-M, He C-H. 2001. Solvent effects on aggregation behavior of polyvinyl alcohol solutions. Polymer 42(14): 6105-12.

Howard G, McConnel P. 1967a. Adsorption of polymers at the solution-solid interface. I. Polyethers on silica. Journal of Physical Chemistry 71(9): 2974-81.

Howard G, McConnel P. 1967b. Adsorption of polymers at the solution-solid interface. II. Polyethers on carbon. Journal of Physical Chemistry 71(9): 2981-90.

Ince DE. 1987. Effect of sodium chloride on the selective flotation of dolomite from apatite [DPhil thesis]. Gainesville (FL): University of Florida.

Ince DE, Johnston CT, Moudgil BM. 1991. Fourier transform infrared spectroscopic study of adsorption of oleic acid/oleate on surfaces of apatite and dolomite. Langmuir 7(7): 1453-7.

Izmailova VN, Alekseeva IG, Tulovskaya ZD. 1975. Rheological properties of interfacial adsorption layers of poly(vinyl alcohol) on liquid boundaries. Vysokomolekulyarnye Soedineniya, Seriya A [Polymer Science USSR] 17(9): 2098-103.

Jacobs [Jacobs Engineering Group, Inc.]. 1995. Phosphate rock treatment for waste reduction. Bartow (FL): Florida Institute of Phosphate Research. FIPR publication nr 01-112-125.

Johnson DO, Stebe KJ. 1996. An oscillating bubble technique to determine surfactant mass transfer kinetics. Colloids and Surfaces, A: Physicochemical and Engineering Aspects 114: 41-52.

Kelvin Lord [Thomson W]. 1871. Hydrokinetic solutions and observations. Phil. Mag. 42: 362-77.

Kim IT, Luckham PF. 1991. The viscoelastic properties of polystyrene latex-particles bearing an adsorbed layer of poly(vinyl alcohol). Journal of Colloid and Interface Science 144(1): 174-84.

Kiselev AV, Lygin VI. 1975. Infrared spectra of surface compounds. New York: John Wiley. 384 p.

Koopal LK, Hlady V, Lyklema J. 1988. Electrophoretic study of polymer adsorption: dextran, polyethylene oxide and polyvinyl alcohol on silver iodide. Journal of Colloid and Interface Science 121(1), 49-62.

Koopal LK, Lyklema J. 1979. Characterization of adsorbed polymers from double layer experiments. The effect of acetate groups in poly(vinyl alcohol) on its adsorption on silver iodide. Journal of Electroanalytical Chemistry and Interfacial Electrochemistry 100: 895-912.

Laird DH, Hanson WK. 1997. Magnesium separation from dolomitic phosphate by acid leaching: final report, Phase III investigation. Bartow (FL): Florida Institute of Phosphate Research. FIPR publication nr 01-113-138.

Lipatov Y, Sergeeva L. 1974. Adsorption of polymers. New York: John Wiley and Sons. 177 p.

Lloyd TB. 1994. Experimental procedures to characterize acid-base and dispersion force contributions to solid wettability. Colloids and Surfaces, A: Physicochemical and Engineering Aspects 93: 25-37.

Luckham PF, Vincent B, Tadros TF. 1983. The controlled flocculation of particulate dispersions using small particles of opposite charge. IV. Effect of surface coverage of adsorbed polymer on heteroflocculation. Colloids and Surfaces 6(2): 119-33.

Lunkenheimer K, Winsel K, Fruhner H, Fang J, Wantke K-D, Siegler K. 1996. Dynamic surface tension and surface area elasticity of adsorbed pulmonary surfactant layers. Colloids and Surfaces, A: Physicochemical and Engineering Aspects 114: 199-210.

MacLeod CA, Radke CJ. 1993. A growing drop technique for measuring dynamic interfacial tension. Journal of Colloid and Interface Science 160(2): 435-48.

Mathur S, Moudgil BM. 1997. Adsorption mechanism(s) of poly(ethylene oxide) on oxide surfaces. Journal of Colloid and Interface Science 196(1): 92-98.

Miller R, Sedev R, Schano K-H, Neumann AW. 1993. Relaxation of adsorption layers at solution/air interfaces using axisymmetric drop-shaped analysis. Colloids and Surfaces 69(4): 209-16.

Moudgil BM, Prakash TS. 1998. Competitive adsorption of polymer and surfactants on solid substrates. Colloids and Surfaces, A: Physicochemical and Engineering Aspects 133(1/2): 93-7.

M'Pandou A, Siffert B. 1987. Polyethleneglycol adsorption at the titania-water interface: distortion of ionic structure and shear plane position. Colloids and Surfaces 24(2-3): 159-72.

Mysels KJ. 1986. Improvements in the maximum-bubble-pressure method of measuring surface tension. Langmuir 2(4): 428-32.

Nahringbauer I. 1995. Dynamic surface tension as aqueous polymer solutions, I: ethyl(hydroxyethyl)cellulose (BERMOCOLL cst-103). Journal of Colloid and Interface Science 176(2): 318-28.

Oezacar M. 2003. Equilibrium and kinetic modeling of adsorption of phosphorus on calcined alunite. Adsorption 9(2): 125-32.

Ottewill RH. 1967. Effect of nonionic surfactants on the stability of dispersions. In: Schick MJ, editor. Nonionic surfactants. New York: Marcel Dekker. p 627-82.

Pefferkorn E, Carroy A, Varoqui R. 1985. Adsorption of polyacrylamide on solid surfaces. Kinetics of the establishment of adsorption equilibrium. Macromolecules 18(11): 2252-8.

Pikhitsa P, Tsargorodskaya A. 2000. Possible mechanism for multistage coalescence of a floating droplet on the air/liquid interface. Colloids and Surfaces, A: Physicochemical and Engineering Aspects 167(3): 287-91.

Platonov BE, Baran AA, Polishchuk TA. 1979. Adsorption of poly(vinyl alcohol) and its effect on the electrosurface characteristics of some oxides. Acta Physica et Chemica 25(3-4): 201-8.

Pradip, Moudgil BM. 1991. Selective flocculation of tribasic calcium phosphate from mixtures with quartz using polyacrylic acid flocculant. International Journal of Mineral Processing 32(3-4): 271-81.

Pugh R, Stenius P. 1985. Solution chemistry studies and flotation behavior of apatite, calcite and fluorite minerals with sodium oleate collector. International Journal of Mineral Processing 15(3): 193-218.

Rachas I, Tadros TF, Taylor P. 2000. The displacement of adsorbed polymer from silica surfaces by the addition of a nonionic surfactant. Colloids and Surfaces, A: Physicochemical and Engineering Aspects 161(2): 307-19.

Ross JL, Bruce WD, Janna WS. 1992. Surface ternsion measurements of benzyl benzoate using the Sugden maximum bubble pressure method. Langmuir 8(11): 2644-8.

Rubio J, Kitchener JA. 1976. The mechanism of adsorption of poly(ethylene oxide) flocculant on silica. Journal of Colloid and Interface Science 57(1): 132-42.

Santhiya D, Subramanian S, Natarajan KA, Malghan SG. 1999. Surface chemical studies on the competitive adsorption of poly(acrylic acid) and poly(vinyl alcohol) onto alumina. Journal of Colloid and Interface Science 216(1): 143-53.

Santhiya D, Nandini G, Subramanian S, Natarajan KA, Malghan SG. 1998. Effect of polymer molecular weight on the adsorption of polyacrylic acid at the alumina-water interface. Colloids and Surfaces, A: Physicochemical and Engineering Aspects 133(1/2): 157-163.

Sjoberg M, Bergstrom L, Larsson A, Sjostrom E. 1999. The effect of polymer and surfactant adsorption on the colloidal stability and rheology of kaolin dispersions. Colloids and Surfaces, A: Physicochemical and Engineering Aspects 159(1): 197-208.

Smith RW, Misra M, Mehta RK, Zheng X. 1997. Bacteria as flotation reagents for flotation of a dolomitic phosphate rock: final report. Bartow (FL): Florida Institute of Phosphate Research. FIPR publication nr 02-106-131.

Somasundaran P, Ramachandran R. 1989. Innovative approaches to elucidate floc structures and polymer conformations at interfaces. In: Moudgil BM, Scheiner BJ, editors. Flocculation and dewatering. Proceedings of the Engineering Foundation Conference; 1988 Jan 10-15; Palm Coast, FL. New York: Engineering Foundation. p 21-41.

Stana RR. 1997. Tomorrow's technology, today's challenges in mining and fertilizer production. Presented at 12th Annual Regional Phosphate Conference; 1997 Oct; Lakeland, FL [unpublished].

Stark JG, Wallace HG. 1982. Chemistry data book. 2nd edition. London: John Murray. 112 p.

Sun SF. 1994. Physical chemistry of macromolecules: basic principles and issues. New York: John Wiley and Sons. 469 p.

Tadros TF. 1978. Adsorption of poly(vinyl alcohol) on silica at various pH values and its effect on the flocculation of the dispersion. Journal of Colloid and Interface Science 64(1): 36-47.

Tamura T, Kaneko Y, Ohyama M. 1995. Dynamic surface tension and foaming properties of aqueous polyoxyethylene n-dodecyl ether solutions. Journal of Colloid and Interface Science 173(2): 493-9.

Thomas WDE, Hall DJ. 1975. Solution/air interfaces. II. Adsorption of surfactants in dilute aqueous solutions. Anomalous oscillating jet phenomena. Journal of Colloid and Interface Science 51(2): 328-34.

Venkatraman P, Kow W, Sadowski J, Anthraper A. 2000. Application of Floatex/spiral circuit in processing silica sand. Presented at SME Annual Meeting; 2000 Feb 28-Mar 1; Salt Lake City, UT. SME Preprint nr 00-162.

Wills BA. 1992. Mineral processing technology. 5th ed. Oxford, England: Pergamon Press. Chapter 10. Gravity concentration. p 407-50.

Yahya GO, Ali SKA, Hamad EZ. 1996. Surface and interfacial activities of hydrophobically modified poly(vinyl alcohol) (PVA). Polymer 37(7): 1183-8.

Zaman A, Tsuchiya R, Moudgil BM. 2002. Adsorption of a low-molecular-weight polyacrylic acid on silica, alumina, and kaolin. Journal of Colloid and Interface Science 256(1): 73-78.

Zeno E, Beneventi D, Carre B. 2004. Interactions between poly(ethylene oxide) and fatty acids sodium salts studied by surface tension measurements. Journal of Colloid and Interface Science 277(1): 215-20.

Zhang Y, Suga T, Kawasaki M, Tang X-X, Uchida N, Uematsu K. 1996. Effect of poly(vinyl alcohol) adsorption on binder segregation during drying. Journal of the American Ceramic Society 79(2): 435-40.

FOR ADDITIONAL READING

Blancarte-Zurita MA, Branion RM, Lawrence RW. 1987. Application of a shrinking particle model to the kinetics of microbiological leaching. In: Lawrence RW, Branion RMR, Ebner HG, editors. Fundamental and applied biohydrometallurgy. Amsterdam: Elsevier Science Publishers. p 243-53.

Booth J, Hong O, Compton R, Prout K, Payne R. 1997. Gypsum overgrowths passivate calcite to acid attack. Journal of Colloid and Interface Science 192: 207-14.

Cameselle C, Nunez MJ, Lema JM. 1997. Leaching of kaolin iron oxides with organic acids. Journal of Chemical Technology and Biotechnology 70(4): 349-54.

Compton RG, Pritchard KL, Unwin PR, Grigg G, Silvester P, Lees M, House WA. 1989. The effect of carboxylic acids on the dissolution of calcite in aqueous solution. 1. Maleic and fumaric acids. Journal of Chemical Society, Faraday Transactions 1: Physical Chemistry in Condensed Phases 85(12): 4335-67.

Farmer VC. 1974. The layer silicate. The Mineral Society, London.

Froment GF, Bischoff KB. 1979. Chemical reactor analysis and design. New York: John Wiley and Sons. 800 p.

Jho C, Burke R. 1983. Drop weight technique for the measurement of dynamic surface tension. Journal of Colloid and Interface Science 95(1): 61-71.

Lund K, Fogler HS, McCune CC. 1973. Acidization. I: Dissolution of dolomite in hydrochloric acid. Chemical Engineering Science 28(3): 691-700.

Sjöberg EL, Rickard DT. 1984. Calcite dissolution kinetics: surface speciation and the origin of the variable pH dependence. Chemical Geology 42(1-4): 119-36.

Sjöberg EL. 1979. Kinetics and mechanism of calcite dissolution in aqueous solutions at low temperatures. Stockholm Contributions in Geology 32: 1-92.